NAVAL POSTGRADUATE SCHOOL

MONTEREY, CALIFORNIA

THESIS

CHARACTERISTIC ERRORS IN 120-H TROPICAL CYCLONE TRACK FORECASTS IN THE WESTERN NORTH PACIFIC

by

Ryan M. Kehoe

March 2005

Thesis Advisor:	Russell L. Elsberry
Second Reader:	Mark A. Boothe

Approved for public release; distribution is unlimited

THIS PAGE INTENTIONALLY LEFT BLANK

REPORT DOCUMENTATION PAGE			Form Approved OMB No. 0704-0188
Public reporting burden for this collection of information is estimated to average 1 hour per response, including the time for reviewing instruction, searching existing data sources, gathering and maintaining the data needed, and completing and reviewing the collection of information. Send comments regarding this burden estimate or any other aspect of this collection of information, including suggestions for reducing this burden, to Washington headquarters Services, Directorate for Information Operations and Reports, 1215 Jefferson Davis Highway, Suite 1204, Arlington, VA 22202-4302, and to the Office of Management and Budget, Paperwork Reduction Project (0704-0188) Washington DC 20503.			
1. AGENCY USE ONLY *(Leave blank)*	**2. REPORT DATE** March 2005	**3. REPORT TYPE AND DATES COVERED** Master's Thesis	
4. TITLE AND SUBTITLE: Characteristic Errors in 120-h Tropical Cyclone Track Forecasts in the Western North Pacific		**5. FUNDING NUMBERS**	
6. AUTHOR(S) Ryan M Kehoe			
7. PERFORMING ORGANIZATION NAME(S) AND ADDRESS(ES) Naval Postgraduate School Monterey, CA 93943-5000		**8. PERFORMING ORGANIZATION REPORT NUMBER**	
9. SPONSORING /MONITORING AGENCY NAME(S) AND ADDRESS(ES) N/A		**10. SPONSORING/MONITORING AGENCY REPORT NUMBER**	
11. SUPPLEMENTARY NOTES The views expressed in this thesis are those of the author and do not reflect the official policy or position of the Department of Defense or the U.S. Government.			
12a. DISTRIBUTION / AVAILABILITY STATEMENT Approved for public release; distribution is unlimited		**12b. DISTRIBUTION CODE**	

13. ABSTRACT (maximum 200 words)
All large (>400 n mi at 96 h, >500 n mi at 120 h) Navy Operational Global Atmospheric Prediction System (NOGAPS) and U.S. Navy version of the Geophysical Fluid Dynamics Laboratory Model (GFDN) tropical cyclone track forecast errors in the western North Pacific during the 2004 typhoon season are examined. Responsible error mechanisms are described by conceptual models that are related to known tropical cyclone motion processes being misrepresented in the dynamical models. Of the 162 (135) cases of large NOGAPS (GFDN) forecast errors, 39 were due to tropical influences with excessive direct cyclone - tropics (E-DCI) interaction occurring most frequently. For the 217 large-error cases due to midlatitude influences, the most frequent error mechanisms were E-DCI (midlatitude), excessive response to vertical wind shear, excessive midlatitude cyclogenesis (E-MCG), insufficient midlatitude cyclogenesis (I-MCG), excessive midlatitude cyclolysis (E-MCL) and excessive midlatitude anticyclogenesis (E-MAG), which accounted for 68% of all large errors occurring in both NOGAPS and GFDN. Characteristics and symptoms of the erroneous forecast tracks and model fields are documented and illustrative case studies are presented. Proper identification and removal of the track forecast displaying an error mechanism could form a selective consensus that will be more accurate than a non-selective consensus.

14. SUBJECT TERMS Tropical cyclone track forecasting, Systematic Approach, conceptual model error mechanisms, Dynamical model track errors, 96-h and 120 h tropical cyclone track forecasting, Joint Typhoon Warning Center, Navy Operational Global Atmospheric Prediction System (NOGAPS), U.S. Navy version of the Geophysical Fluid Dynamics Laboratory Model (GFDN), tropical cyclone motion, western North Pacific typhoons	**15. NUMBER OF PAGES** 111
	16. PRICE CODE

17. SECURITY CLASSIFICATION OF REPORT	**18. SECURITY CLASSIFICATION OF THIS PAGE**	**19. SECURITY CLASSIFICATION OF ABSTRACT**	**20. LIMITATION OF ABSTRACT**
Unclassified	Unclassified	Unclassified	UL

NSN 7540-01-280-5500

Standard Form 298 (Rev. 2-89)
Prescribed by ANSI Std. 239-18

THIS PAGE INTENTIONALLY LEFT BLANK

Approved for public release; distribution is unlimited

CHARACTERISTIC ERRORS IN 120-H TROPICAL CYCLONE TRACK FORECASTS IN THE WESTERN NORTH PACIFIC

Ryan M. Kehoe
Captain, United States Air Force
B.S., University of Oklahoma, 2000

Submitted in partial fulfillment of the
requirements for the degree of

MASTER OF SCIENCE IN METEOROLOGY

from the

NAVAL POSTGRADUATE SCHOOL
March 2005

Author: Ryan M. Kehoe

Approved by: Russell L. Elsberry
Thesis Advisor

Mark A. Boothe
Second Reader

Philip A. Durkee
Chairman, Department of Meteorology

THIS PAGE INTENTIONALLY LEFT BLANK

ABSTRACT

All large (>400 n mi at 96 h, >500 n mi at 120 h) Navy Operational Global Atmospheric Prediction System (NOGAPS) and U.S. Navy version of the Geophysical Fluid Dynamics Laboratory Model (GFDN) tropical cyclone track forecast errors in the western North Pacific during the 2004 typhoon season are examined. Responsible error mechanisms are described by conceptual models that are related to known tropical cyclone motion processes being misrepresented in the dynamical models. Of the 162 (135) cases of large NOGAPS (GFDN) forecast errors, 39 were due to tropical influences with excessive direct cyclone - tropics (E-DCI) interaction occurring most frequently. For the 217 large-error cases due to midlatitude influences, the most frequent error mechanisms were E-DCI (midlatitude), excessive response to vertical wind shear, excessive midlatitude cyclogenesis (E-MCG), insufficient midlatitude cyclogenesis (I-MCG), excessive midlatitude cyclolysis (E-MCL) and excessive midlatitude anticyclogenesis (E-MAG), which accounted for 68% of all large errors occurring in both NOGAPS and GFDN. Characteristics and symptoms of the erroneous forecast tracks and model fields are documented and illustrative case studies are presented. Proper identification and removal of the track forecast displaying an error mechanism could form a selective consensus that will be more accurate than a non-selective consensus.

THIS PAGE INTENTIONALLY LEFT BLANK

TABLE OF CONTENTS

THIS PAGE INTENTIONALLY LEFT BLANK

LIST OF FIGURES

LIST OF TABLES

THIS PAGE INTENTIONALLY LEFT BLANK

ACKNOWLEDGMENTS

To my advisor, Dr. Russell Elsberry, and second reader, Mark Boothe, I would like to extend a sincere thank you for your guidance and expertise in preparing this thesis. You were vital from start to finish and have passed on skills that will help me at my next assignment and beyond. To my wife, Sharmell, I am forever indebted for your endless support and for shouldering the lion's share of the responsibility of caring for Emalyn while I strove to complete this thesis.

Without the help from all three of you, writing this thesis and earning a Master's Degree would not have been possible. Thank you.

THIS PAGE INTENTIONALLY LEFT BLANK

I. INTRODUCTION

A. MOTIVATION

Since the early 1990's, the quality of tropical cyclone (TC) track forecasts for both regional and global numerical weather prediction models has increased significantly. As a result, these track forecasts have become heavily relied upon by forecasters at both the National Hurricane Center (NHC) and the Joint Typhoon Warning Center (JTWC) (Goerss 2000). However, the plethora of available dynamic models combined with their independent variations of forecast TC center positions can create a real dilemma for forecasters at NHC or JTWC. This dilemma was remedied with the successful employment of the Systematic Approach Forecasting Aid to Tropical Cyclone Track Forecasting (SAFA) at JTWC. Since the 2000 implementation of SAFA by JTWC, they have seen an overall decrease in their 72-h official forecast track error (Figure 1).

Based on lessons learned with SAFA during the 2000-2001 typhoon seasons, JTWC implemented a testing period to create 96-h and 120-h forecasts using the non-selective consensus (explained in next section) step of SAFA to create a non-selective consensus forecast produced by all available dynamic models (CONU[1]). During the trial of CONU, JTWC was able to achieve a 31% decrease in the average of their 120-h forecast error for the western North Pacific TCs between the 2001 and 2002 seasons and were able to maintain about the same error average during the 2003 season (Figure 1) (Jeffries and Fukada 2002). Based on these results, JTWC implemented official 96-h and 120-h forecasts starting in May 2003. Later in the summer of 2003, JTWC changed their consensus of choice from CONU to CONW[2], which is comprised of the

[1] CONU is an ensemble of nine global and regional models. Of these models, only four have forecasts available to 120 h. These are interpolations of the Navy Operational Global Atmospheric Prediction System (NOGAPS), the Geophysical Fluid Dynamics Lab – Navy version (GFDN), the NCEP Global Forecast System (GFS), and the United Kingdom Met Office (UKMO).

[2] As of summer 2004, CONW is an ensemble of ten global and regional models. Of these models, only four have forecasts available to 120 h. These are interpolations of the Navy Operational Global Atmospheric Prediction System (NOGAPS), the Geophysical Fluid Dynamics Lab – Navy version (GFDN), the NCEP Global Forecast System (GFS), and the United Kingdom Met Office (EGRI).

same models in CONU but substitutes manually entered coordinates for the interpolated UKMO model track (EGRI) for automated coordinates (UKMI[3]) and also includes the Weber Barotropic Tropical Cyclone Track Prediction System (WBAR). They found the addition of WBAR to the model suite demonstrated skill over CONU (S. Gruber, JTWC, personal communication). Since WBAR is only integrated to 72 h, CONU and CONW are comprised of the same four models[4] at 96 h and 120 h. Therefore, CONU track statistics will be used in this study but will be referred to as CONW to remain consistent with current operational nomenclature at JTWC. Since their first official year of 120-h track forecasting, they have been able to maintain a consistent 120-h yearly average track error of approximately 300 n mi (Figure 1).

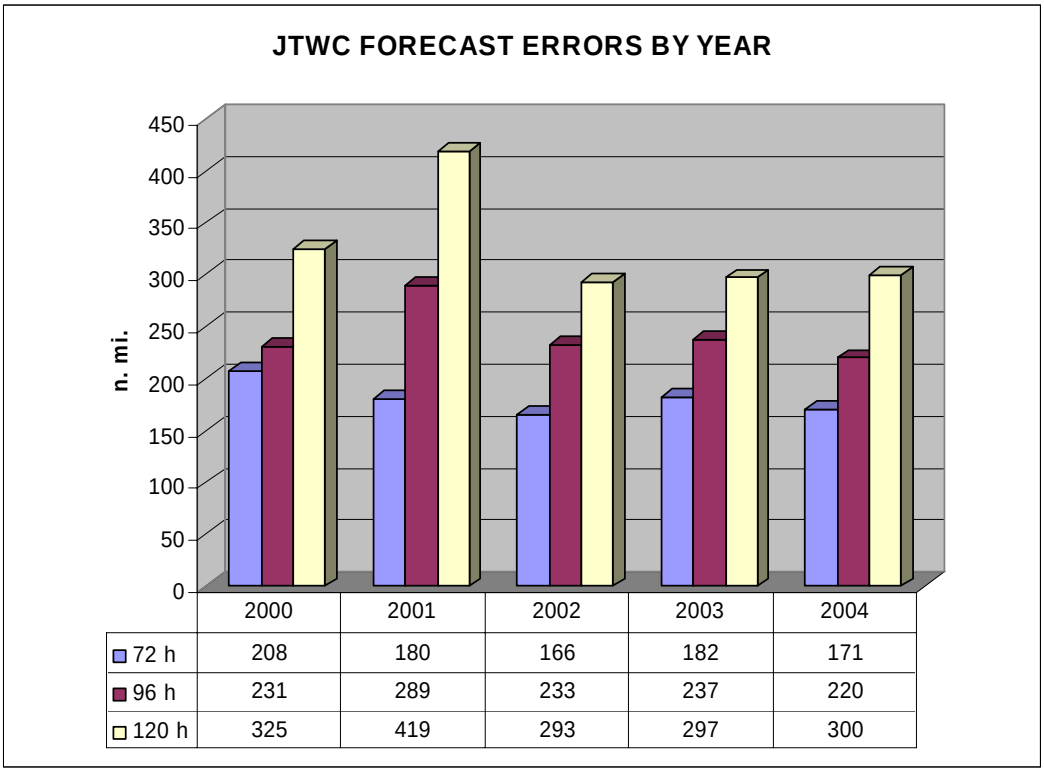

	2000	2001	2002	2003	2004
72 h	208	180	166	182	171
96 h	231	289	233	237	220
120 h	325	419	293	297	300

Figure 1. Average track errors (n mi) of JTWC official forecasts. The averages for 2000-2002 are referenced from Jeffries and Fukada (2002).

[3] After the summer of 2004, it was found EGRI showed skill over UKMI and JTWC re-substituted EGRI for UKMI in CONW (S. Gruber, JTWC personal communication).

[4] Since the UKMI and EGRI are track variations from the same model (UKMO), they will be treated as equal since this study will examine errors in excess of 500 n mi at 120 h.

In previous years, the skill of the official 72-h forecast was measured by comparing the 72-h forecast error to that of the Climatology and Persistence (CLIPER) model. However, CLIPER is only available to 72 h and updating CLIPER to 120 h is outside the realm of this project. To measure the accuracy of the JTWC 120-h official forecasts then, they are compared to four other track forecasts in a homogenous sample. This homogeneous sample is comprised of JTWC official track forecasts, CONW, and interpolated NOGAPS (NGPI), GFS (AVNI), and UKMO (EGRI) track forecasts. The fourth 120-h model (GFDN) was not included in this sample because it is integrated only at 0600 UTC and 1800 UTC while the other three are integrated at 0000 UTC and 1200 UTC (at a minimum). The JTWC CONU ensemble was included in this homogeneous group because it was the consensus of choice at JTWC prior to the summer of 2003 and no CONW stats were available. Interpolated track forecasts were used because these are the track forecasts the JTWC official forecast is based upon, due to the lag created by the run time and the operational forecasting schedule. The comparison of the homogenous errors in this group indicates that JTWC errors were in the middle of the various model 120-h track errors in both 2003 and 2004 (Table 1).

HOMOGENEOUS TRACK ERRORS (n mi)				
	Year	72 h	96 h	120 h
AVNI	2003	158	240	387
	2004	177	202	250
NGPI	2003	188	256	328
	2004	188	246	327
EGRI	2003	229	333	454
	2004	226	286	362
CONU	2003	156	247	337
	2004	157	201	248
JTWC	2003	152	240	350
	2004	157	211	261
#CASES	2003	87	64	51
	2004	292	195	132

Table 1. Homogeneous track errors comparison for 2003 and 2004 seasons for the various models, the consensus, and JTWC (calculated from JTWC aids and best-track files).

At first one would expect this result since the premise of using a non-selective consensus is that the consensus forecast will not be the worst forecast, but it will not be the best forecast either. When comparing the 72-h homogeneous comparison for the same group though, one finds that the JTWC official forecast errors were the smallest of the group during the 2003 and 2004 seasons.

Another measure of the progress of JTWC 120-h track forecasts since 2003 is to take a homogeneous comparison of the JTWC official forecasts and CONW 120-h forecast track errors (Figure 2). This comparison found the number of 120-h forecast errors exceeding 500 n mi by CONW (JTWC) in 2003 was 20 (20) and in 2004 was 29 (27), which implies that when CONW provides poor guidance, the JTWC errors will be large. This is corroborated by an almost one-for-one correlation between CONW and JTWC errors at 120 h (Figure 2). Indeed the Pearson correlation coefficient for these errors was 0.93 (0.94) in 2003 (2004).

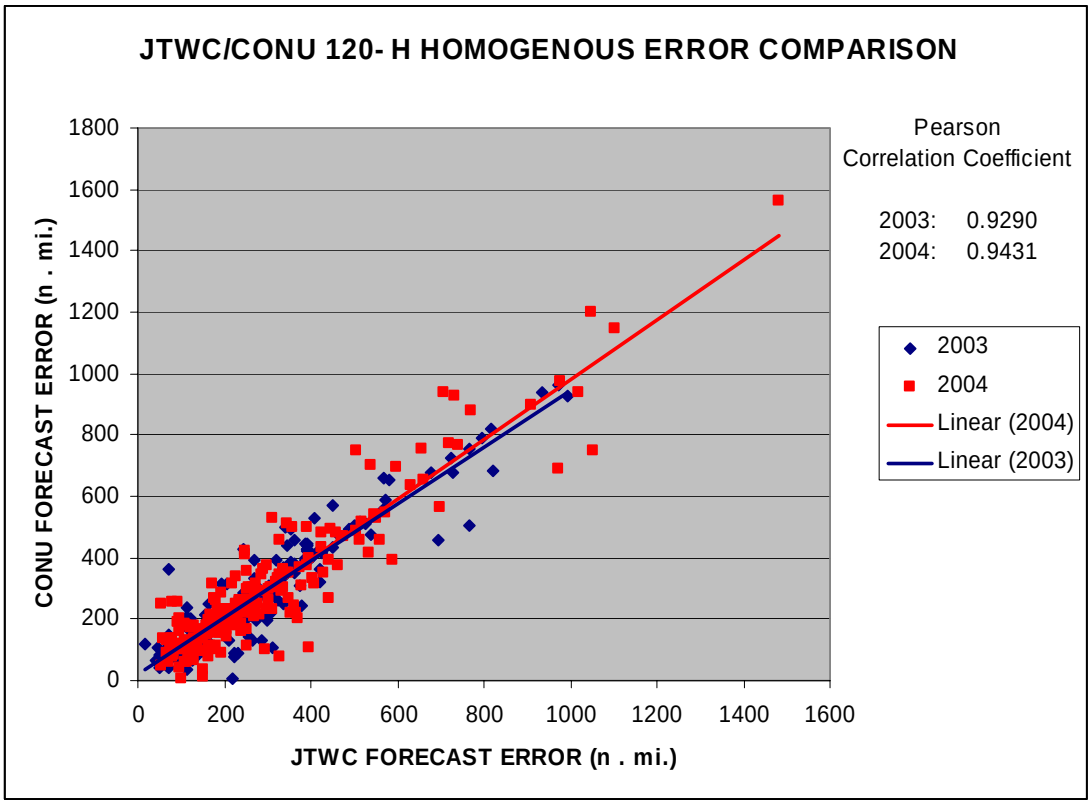

Figure 2. Homogeneous comparison of 120-h track forecast errors between JTWC and CONW during 2003 and 2004. The high correlations between errors for these years are given in the upper right.

This analysis suggests that 120-h forecasting accuracy has reached a plateau and there has been a slight upward trend in 120-h errors since the initial decrease in 2002. With this in mind, the question is raised of whether any steps can be taken to produce an improvement in 120-h track forecasting.

In a 2002 report from JTWC, it is noted that the consensus forecast was more accurate if more than three track forecasts were available (Jeffries and Fukada 2002). To apply this logic to 120-h track forecasting, all four 120-h models are needed to create an accurate consensus forecast. A dilemma with CONW occurs when one of the four 120-h models has a highly erroneous track, which may cause the consensus to be seriously degraded.

It is hypothesized that the elimination of the erroneous track and reduction of the number of members in the consensus to three (called a selective consensus) would still lead to a more accurate forecast. To confidently remove this track, the lessons learned with the selective consensus utilized in SAFA may be applied to 120-h track forecasts. The issue that occurs is that the model traits knowledge base of SAFA is rooted in research of model error characteristics for 72-h track forecasts. To employ the SAFA concept to 120 h, the relationship between 72-h and 120-h forecast errors and applicability of 72-h error mechanisms has to be explored.

B. BACKGROUND ON SAFA

SAFA was established and tested by Carr et al. (2001) to assist the forecaster in information management, visualization, and proactive investigation of frequently occurring track error mechanisms. The desired result of SAFA is the quantitative reduction in the number of official track forecasts with large errors, also known as “busts.” SAFA reduces busts by facilitating the forecaster’s development of an official track forecast through a meteorological knowledge basis of error mechanisms. This meteorological knowledge basis may be useful if the forecaster consistently utilizes: (i) the knowledge base of dynamically sound conceptual models that classify various TC-environment situations; (ii) a

knowledge base of recurring TC track forecast errors attributed to various combinations of TC structure and environment structure, and the anticipated changes; and (iii) an implementing methodology or strategy for applying these two knowledge bases to particular TC forecast situations (Boothe et al. 2000).

A key element of SAFA is to recognize how the TC will interact with its environment that is characterized as a synoptic pattern/region (Appendix A). The forecaster must comprehend when the TC will play a passive role and merely respond to the environmental steering flow versus when the TC will actively participate in the transformation of the environment through TC-environment interactions. Because each synoptic pattern is associated with a characteristic TC track, it is important that the forecaster be equipped to recognize when a transition between patterns will occur. Teaching forecasters to consistently recognize these changes in environmental structure is an ultimate goal of the SAFA.

C. OBJECTIVES OF THESIS

The objective is the extension of the error mechanism conceptual models (Carr and Elsberry 2000a,b) from 72 h to 120 h for NOGAPS and GFDN. Extension will be achieved through an in-depth retrospective analysis of tropical cyclone track forecasts over the western North Pacific Ocean to identify characteristic tropical and midlatitude wind, sea-level pressure, and geopotential height patterns that are associated with large 120-h model track errors. Conceptual models of these 120-h model error characteristics will be incorporated with known 72-h error mechanisms, any new mechanisms will be defined, and then both will be presented for incorporation into SAFA.

II. APPROACH

The approach has been to identify and analyze cases in which large track errors (300 n mi at 72, 400 n mi at 96 h, or 500 n mi at 120 h) occurred in NOGAPS and GFDN in the western North Pacific during 2004 (Figures 3 and 4). Of the four dynamical models available to 120 h, only these two model analyses and forecasts were available in entirety to search for explanations of large track errors. Only the tracks and a largely incomplete set of analysis and forecast fields were available for the other two models (GFS and UKMO).

To maximize the number of 120-h forecast verifications for both NOGAPS and GFDN, the best-track positions were manually extended beyond the point of extratropical declaration using mean sea-level pressure (MSLP) analyses. This extension is considered valid since the hazards associated with the wind, precipitation, and waves accompanying a TC do not suddenly diminish at the time it is declared extratropical. One obstacle that had to be overcome when extending the best-track was when the MSLP center had tracked outside of the forecast grid even though the forecast center was still well inside this grid. When the MSLP center tracked outside the forecast grid, the last location inside the grid was annotated and used as the verifying position for calculating all subsequent errors out to 120 h. This is considered a valid approach because the error calculated would be even less than the actual error. Sources of the errors were sought if they exceeded the prescribed error thresholds. This best-track extension was necessary whenever the 72-h (96-h) forecast error was above their respective threshold, but the 120-h forecast had not been verified because the storm was declared to be extratropical. This procedure was also used when the model had 72-, 96-, or 120-h errors above their respective large-error thresholds for successive integrations but then no error was calculated for all remaining integrations. This omission indicated the forecasts preceding the sudden void of error calculations continued beyond the JTWC best track

date/time group. When this sudden cessation of large track errors occurred, subsequent model tracks were analyzed until the model no longer had the errors exceeding the thresholds.

Consequently, the error summaries in this thesis will not match the JTWC summaries and will in fact be larger. By following these procedures to maximize verifications of 120-h forecasts, an increase of nearly 28% (24%) in large forecast errors was realized for NOGAPS (GFDN) (Table 2). One reason that the GFDN increase was lower than NOGAPS was because 26 of the 135 large error cases in GFDN did not have forecast fields archived to 120 h. Notice in Figures 3 and 4 that the number of large forecast errors for NOGAPS and GFDN is larger than for UKMO, GFS, and CONW because the latter three have not been extended.

Model	Year	No. Storms	No. 96-h forecast*	No. 120-h forecast*
NOGAPS	2004	32	367(422)	277(354)
GFDN	2004	32	286(318)	211(262)

Table 2. Number of cases of large forecast errors at 96 h and 120 h for 2004. *First total indicates number of verifying forecast positions from best track data. Second total, in parentheses, indicates verifying positions extended beyond declared extratropical transition to maximize 96-h and 120-h model verifications.

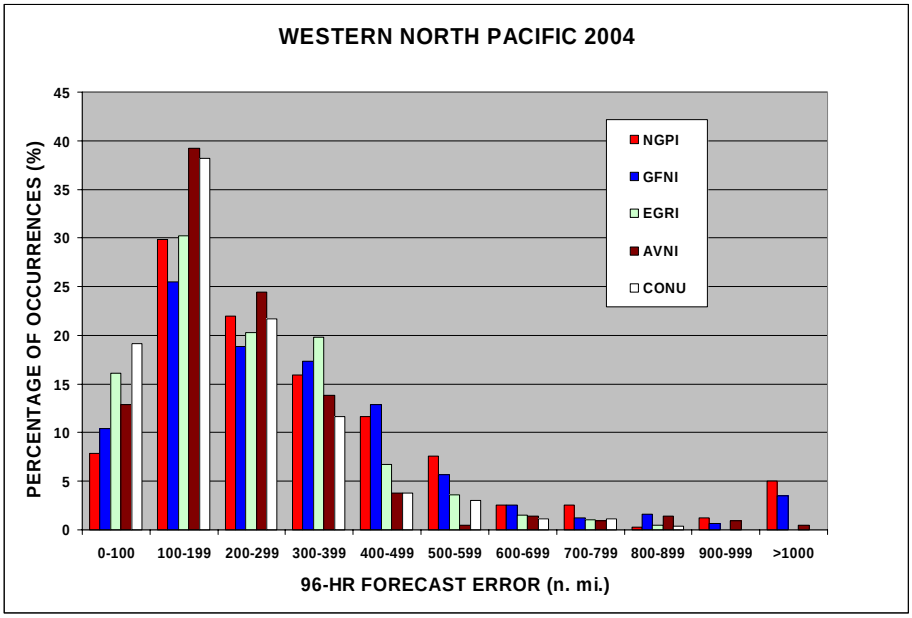

Figure 3. Frequency of occurrence of 96-h track forecast errors for the western North Pacific during 2004. Note: AVNI represents the GFS model.

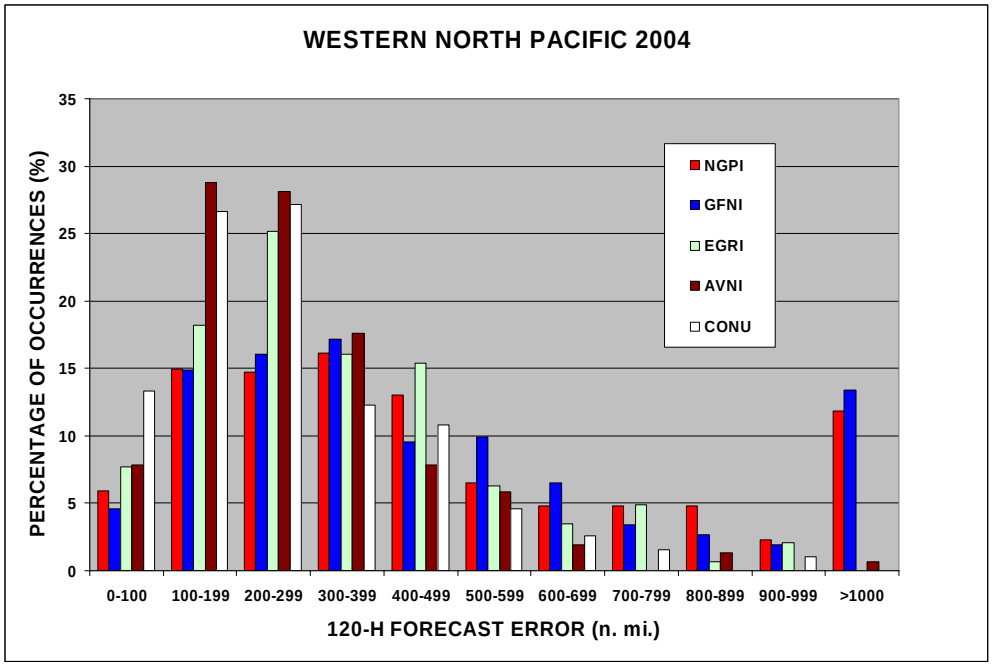

Figure 4. Frequency of occurrence of 120-h track forecast errors for the western North Pacific during 2004. Note: AVNI represents the GFS model.

In the identification of these large errors, NOGAPS had track errors at 0600 UTC and 1800 UTC for which no archived fields were available from the Navy Master Environmental Library. To still incorporate these forecasts in the summary, if the 0600 UTC (1800 UTC) error was between 0000 UTC and 1200 UTC (1200 UTC and 0000 UTC) forecasts that had large errors, and these adjacent forecasts had the same error mechanism, then the 0600 UTC or 1800 UTC error was assigned the same error mechanism. If the 0600 UTC or 1800 UTC error had a large error only on one side, and the error values and the track forecasts of the two times were similar, it too was assigned the same error mechanism. If a large 0600 UTC or 1800 UTC error did not have a large error at either adjacent time, it was listed as “no fields available” and included in the error summary. By applying this procedure, the NOGAPS (GFDN) sample included all 83 (65 of 72) 0600 UTC or 1800 UTC large forecast errors.

In 2004, a total of 354 (422) 120-h (96-h) NOGAPS forecasts were made for the western North Pacific TCs. For GFDN in the same year, 262 (318) 120-h (96-h) forecasts were available for the same basin (Table 2). Of those forecasts,

162 (135) cases for NOGAPS (GFDN) had a large forecast error at 72, 96, and/or 120 h. To identify the causes of these large errors, both the predicted and verifying analysis fields of the winds and geopotential heights at 200, 500, 700, and 850 mb and the mean sea-level pressures were utilized. The geopotential heights from 850 through 500 mb were found to be most beneficial in diagnosing the cause of the large track forecast error when midlatitude synoptic features were affecting the steering current for the TC. If vertical wind shear effects were suspected of causing the error, the vector difference in winds between 500 mb and 850 mb as well as the 200 mb level was vital. When a large TC was actively contributing to its propagation, the mean sea-level pressure fields were found to be most effective in detecting the cause of the error.

To extend the SAFA concept to 120 h, the relationship between 72-h and 120-h forecast errors, in addition to the applicability of 72-h error mechanisms, had to be explored. The relationship between an excellent (<150 n mi), good (<200 n mi) or fair (<300 n mi) forecast at 72 h was compared to the corresponding forecast error at 120 h. It was found that of the 354 NOGAPS 120-h forecasts, 126 had errors greater than 500 n mi. Of these 126 NOGAPS large errors, 13% occurred when the 72 h error was less than 150 n mi, 25% occurred when the 72 h error was less than 200 n mi, and 39% occurred when 72 h error was less than 300 n mi. A similar examination of the 262 GFDN 120-h forecasts found 108 forecasts greater than 500 n mi. Of these 108 GFDN large-error cases, 5% occurred when the 72 h error was less than 150 n mi, 21% occurred when the 72 h error was less than 200 n mi, and 45% occurred when 72 h error was less than 300 n mi. These statistics indicated that an excellent to fair forecast at 72 h does not guarantee even a fair forecast (less than 500 n mi) at 120 h.

III. ANALYSIS OF LARGE TRACK ERROR CASES

A. CONCEPTUAL MODEL ERROR MECHANISMS

A hypothesis in this analysis is that the large track error is due to an improper representation by the model of the TC interaction with the environmental flow. The intent of the analysis was therefore to diagnose when and where the model was not properly predicting the correct interaction that ultimately would steer the TC. If the intensity or horizontal scale of a synoptic feature was found to be incorrectly forecast, or if the timing of a transition between synoptic features was found to be incorrect, the track errors were directly related to that incorrect prediction and assigned a specific error mechanism.

Following Carr and Elsberry (2000a, b) who defined 72-h error conceptual models, large track errors at 120 h can also be attributed to misrepresentations by the dynamical model of physical processes known to be important to TC motion. The conceptual error mechanisms that affect tropical cyclone 120-h track forecasts can be classified into two categories: i) large track errors due to tropical influences; and ii) large track errors due to midlatitude influences. Large track error mechanisms due to tropical influences were Direct Cyclone Interaction – tropical (DCI-t), Reverse-oriented monsoon Trough Formation (RTF), and Beta Effect Propagation (BEP). Those error mechanisms due to midlatitude influences were Direct Cyclone Interaction – midlatitude (DCI-m), Response to Vertical Wind Shear (RVS), Baroclinic Cyclone Interaction (BCI), Midlatitude Cyclogenesis (MCG), Midlatitude Cyclolysis (MCL), Midlatitude Anticyclogenesis (MAG), and Midlatitude Anticyclolysis (MAL). One departure from the conceptual error mechanisms outlined in Carr and Elsberry (2000a, b) is to distinguish DCI occurring in the tropics from that occurring in the midlatitudes. While the physical process was the same, the large track errors associated with E-DCI-m were significantly larger than those associated with E-DCI-t, which will be discussed further in the case studies presented for each.

The NOGAPS (GFDN) model was affected by tropical influences in 25 of 162 or 15% (14 of 135 or 10%) of its large-error cases, and by midlatitude influences in 121 of 162 or 75% (95 of 135 or 70%) of its large-error cases (Table 3). As might have been expected, these percentages indicate that the proper prediction of amplitude, scales, and transition of midlatitude synoptic features is a critical component to 120-h TC track forecasting.

2004 96-h and 120-h Error Mechanisms			
Phenomenon name	**Acronym**	**No. of NOGAPS forecasts***	**No. of GFDN forecasts***
Large Errors due to Tropical Influences			
Direct cyclone interaction (tropical)	**DCI-t**	**20-0**	**11-0**
Reverse trough formation	**RTF**	**0-0**	**3-0**
Beta effect propagation	**BEP**	**0-5**	**0-0**
Large Errors due to Midlatitude Influences			
Direct cyclone interaction (midlatitude)	**DCI-m**	**6-0**	**5-0**
Response to vertical wind sheer	**RVS**	**26-0**	**0-0**
Baroclinic cyclone interaction	**BCI**	**6-0**	**0-0**
Midlatitude cyclogenesis	**MCG**	**6-53**	**28-46**
Midlatitude cyclolysis	**MCL**	**12-0**	**2-0**
Midlatitude anticyclogenesis	**MAG**	**6-0**	**9-6**
Midlatitude anticyclolysis	**MAL**	**2-4**	**0-0**
False Alarm		**6**	**4**
Tracker Error		**8**	**4**
Fields not available		**2**	**16**
Total of all large-error forecasts		**162**	**135**
***The first (second) number listed is the number of times the phenomenon occurred excessively (insufficiently)**			

Table 3. 96-h and 120-h error mechanisms for NOGAPS and GFDN occurring in 2004. *The first (second) number listed is the number of times the phenomenon occurred excessively (insufficiently).

Not all large track errors could be assigned a conceptual error mechanism. In 8 (4) cases for NOGAPS (GFDN), the model field accuracy was acceptable, but an undiagnosed problem with the tracking function caused the large error. In 6 (4) cases for NOGAPS (GFDN), the TC decayed to the point where it was no longer discernable in the verifying analysis fields but the model still predicted a circulation (false alarm). Since the best track stops when no circulation is present, there was no way to calculate a 120-h error. The last

group that was not assigned an error mechanism were 2 (16) cases when no fields were available for NOGAPS (GFDN), so no error mechanism could be assigned (Table 3). For convenience, error mechanisms will henceforth be referred to by their three letter acronym given in Table 3 with a prefix of E (excessively) or I (insufficiently), e.g., excessive-direct cyclone interaction is abbreviated E-DCI.

In the following sections, conceptual models of the error mechanisms leading to the large track errors will be presented and described along with the frequency of their occurrence based on the 2004 typhoon season.

B. TROPICAL INTERACTIONS

Tropical interactions generally occurred when the TC was south of the subtropical ridge axis and the environmental flow had either an easterly or southerly component or a combination of the two. This pattern/region is classified as Standard/Tropical Easterlies (S/TE) or Standard/Poleward Flow (S/PF) (Appendix A). Because the TC is south of the subtropical ridge axis, its motion is not directly affected by midlatitude synoptic features. Therefore, the poorly predicted interaction of the TC was typically with another warm-core circulation, (e.g., monsoon depression), or with the subtropical ridge. Large track error mechanisms due to tropical influences were DCI-t, RTF, and BEP. These conceptual error mechanisms will be described in detail along with their frequency and characteristics, and a case study from the 2004 season will be described below.

1. Direct Cyclone Interaction – Tropical (DCI-t)

a. Description

The conceptual model of DCI in Figure 5 illustrates the mutual cyclonic rotation of two cyclones and a potential merger into one circulation that is usually larger in size than the analyzed TC. In the analysis of the 2004 forecasts, the track of the larger circulation was found to be less affected than the

track of the smaller circulation in E-DCI-t. The smaller circulation usually accelerated rapidly as it rotated counterclockwise (CCW) around the larger circulation, whereas the larger circulation displayed little CCW rotation, and usually had only a slowing of its westward track. The two circulations did not always merge into one circulation. Direct cyclone interactions in the tropics for the 2004 season were found to always be excessively predicted by both NOGAPS or GFDN, i.e., no insufficient cases are shown in Table 3. As Carr and Elsberry (2000a) summarized, E-DCI errors (tropical or midlatitude) occurred when the TC circulation was forecast to directly interact with an adjacent cyclonic circulation such that the predicted interaction is either false or is significantly more vigorous than in reality. The adjacent cyclonic circulation in the E-DCI-t cases in this study was always either a developing tropical disturbance, a named TC, or a remnant of such a circulation. The two cyclones involved in E-DCI-t would often then become aligned in such a manner that their peripheral anticyclones formed a reverse-oriented monsoon trough (outlined in Section B.2). The flow in the reverse-oriented monsoon trough would then become dominant and overpower the influence the two cyclones had on each other during DCI. Thus, both cyclones would then track to the northeast. Since it was the E-DCI that lead to the reverse-oriented monsoon trough error mechanism, E-DCI was the conceptual error mechanism assigned. An example of E-DCI-t leading to a reverse-oriented monsoon trough will be presented in Section III.B.1.c.

As Carr and Elsberry (2000a) explained, the reasons for E-DCI with another real cyclonic circulation in the tropics include: (i) too large a horizontal extent and associated outer wind strength of the TC and/or other cyclone in the initial analysis or forecast (Figure 5); (ii) misplaced TC and/or other cyclone in the initial analysis or forecast, such that the separation of the two cyclones is smaller than in reality; and (iii) the 2004 analysis of NOGAPS and GFDN indicated that an improper intensification of a TC (weaker than reality) caused the larger circulation to the west to dominate the steering flow of the smaller TC as they came in close proximity.

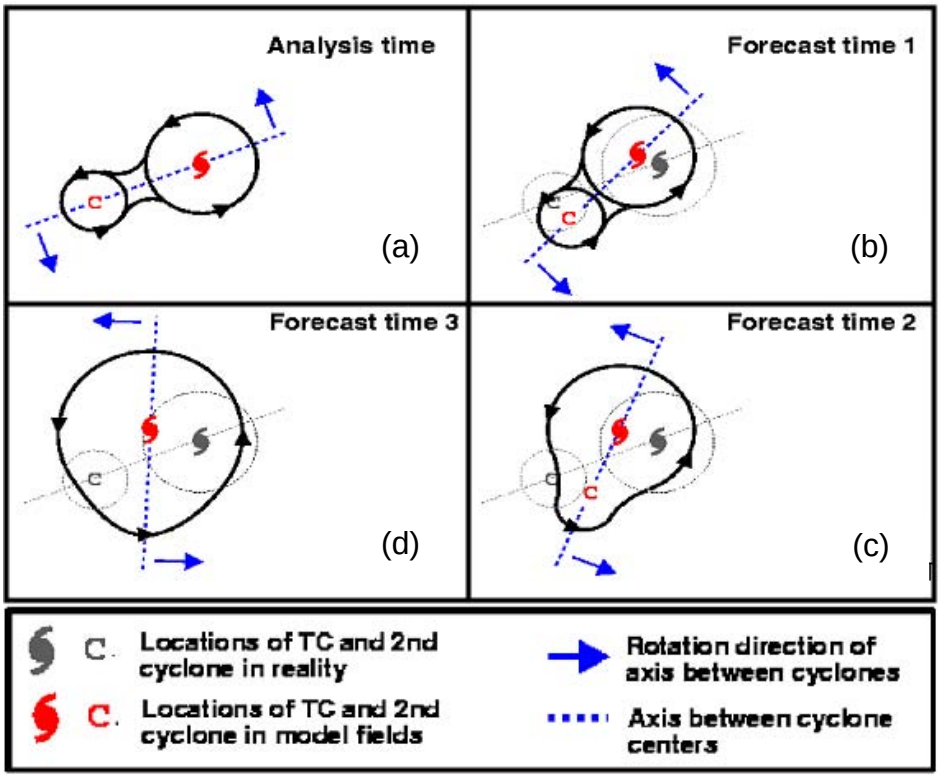

Figure 5. Conceptual model of DCI in which a TC circulation interacts with another cyclone © to cause a counterclockwise rotation of the axis between the cyclone centers (heavy dashed line) and a possible merger of the two cyclones in which the combined circulation becomes larger with time [(c) and (d)]. The TC may also be the smaller of the two cyclones, or the model may be applied to two TCs of similar sizes in which the tracks of both TCs will be affected (from Carr and Elsberry 2000a).

b. Frequency and Characteristics

In the 2004 sample of NOGAPS and GFDN track forecasts, 31 model integrations involved E-DCI-t (Table 4). The range of consecutive integrations affected ranged from as few as one by NOGAPS in TC Talas (TC number 31W) to as many as nine by GFDN in TC Chaba (19W). In NOGAPS, other periods of consecutive model-predicted E-DCI in the tropics included two occurrences in TC Chanthu (08W), two in TC Mindulle (10W), seven in TC Chaba (19W), and eight in TC Aere (20W). Consecutive E-DCI predictions by GFDN in addition to Chaba included two consecutive occurrences in TC Aere. It should be noted that while fewer E-DCI-t events were predicted by GFDN in the tropics, E-DCI was more common in the midlatitudes for GFDN than for NOGAPS. Although the environmental structure of all TCs during the period of

E-DCI in the tropics was classified as S/TE, the incidence of E-DCI then resulted in a shift from S/TE to S/PF. In 17 (55%) of the 31 cases, the TC was less than typhoon strength (64kt) during the period of E-DCI.

TC No.	Start time of affected model runs	No. iterations: NOGAPS (GFDN)	Synoptic environment of affected TC	Intensity during interaction	Nature of second cyclone	Location of second cyclone
08W	1800 UTC 08JUN - 0600 UTC 09JUN	2	S/TE	35-40	WP07	NNW
10W	1800 UTC 23JUN - 0000 UTC 24JUN	2	S/TE	35-45	Pre-WP11	E
19W	1800 UTC 19AUG - 1200 UTC 21AUG	7 (9)	S/TE	45-90	Pre-WP20 → WP20	W
20W	1800 UTC 19AUG - 1200 UTC 21AUG	8 (2)	S/TE	30-65	WP19	E
31W	0000 UTC 09DEC	1	S/TE	30	FTC	E

Table 4. Cases of model-predicted E-DCI-t in the western North Pacific in 2004. A total of 31 cases of E-DCI-t occurred in five TCs during 2004. Intensity is measured in knots. A Probable tropical circulation is indicated by “PTC”.

A more intriguing revelation was how often incorrect intensity forecasts lead to E-DCI in the tropics. While attempting to depict the western TC (07W) and the eastern TC (08W), NOGAPS mislocated 07W too close to 08W. While this mislocation alone could have lead to E-DCI, NOGPAS also under forecast the intensity of 08W, which exasperated the E-DCI, and a merger of 07W and 08W resulted. It is expected that the too weak TC intensity forecast would lead to a larger impact on the track of the weaker TC due to the stronger adjacent circulation that was predicted in NOGAPS. The insufficient intensification by NOGAPS (measured via mean sea-level pressures, and geopotential height contours at 850, 700, and 500 mb) of a circulation located to the east of TCs 10W and 20W also lead to E-DCI. For 20W, the eastern circulation was 19W, which was also degraded by this erroneous interaction. These cases of insufficient intensification of the eastern TC occurred when the two TCs were oriented east to west and both were in S/TE south of the

subtropical ridge. The E-DCI of the two TCs would then lead to the formation of a reverse-oriented monsoon trough, and both TCs subsequently were erroneously predicted to track to the NE.

In GFDN model integrations that were centered on either 19W or 20W, the intensity of the non-bogused TC was always under-forecast, and while the target TC intensity was either accurate or predicted too strong, the horizontal extent of the target TC was too small (to be discussed in Chapter III.B.1.c.). This predicted interaction resulted in the CCW rotation of the eastern TC (19W) and slowed the westward motion of the western TC (20W) that ultimately led to the formation of a reverse-oriented trough. In GFDN, it is inferred that the model is over-forecasting the horizontal extent and outer wind strength of 20W regardless of which TC is the target on which the model is centered.

Only one occurrence of a probable tropical circulation (PTC) falsely caused E-DCI in the tropics, and this occurred in NOGAPS. For this integration, NOGAPS did not develop 31W into an organized system, but rather it overdeveloped the PTC to the west. This overdevelopment caused 31W to begin a CCW rotation around the now fully developed PTC during the last 48 h of the forecast period. Whereas NOGAPS developed this system into an organized system, infrared satellite imagery verifies that this PTC was present at the start of the forecast period but then quickly decayed.

At first glance, it could be argued that the number of E-DCI incidences involving 19W and 20W (to be discussed in Chapter III.B.1.c.) has largely skewed the occurrences of E-DCI events in the tropics. If each typhoon is looked at as a single occurrence, a pattern of under-intensification of the eastern TC leading to CCW rotation around the western TC can be inferred. As in the Carr and Elsberry (2000a) study of the 1997 typhoon season in the western North Pacific, every case of E-DCI in the tropics was deemed to have falsely occurred. That is, there were no occurrences of a model exaggeration of an actual DCI in the tropics. If the analyses of the 2004 and 1997 seasons are taken to be representative, the models are biased towards E-DCI rather than real

DCI. The 2004 analysis reinforces the assertion made by Carr and Elsberry (2000a) that if the forecaster in real time can discern the occurrence of DCI in a dynamical model, the probability is high that the event is excessive. The forecaster would therefore be justified in removing the model track from CONW and forming a selective CONW forecast track that would be more accurate. The case studies that follow will outline how the forecaster can easily identify the key features that lead to the occurrence of E-DCI in the models.

c. Case Studies

This case study of Typhoons Chaba (19W) and Aere (20W) will demonstrate how the forecaster can detect E-DCI due to under-intensification of the eastern TC via the NOGAPS and GFDN forecast mean sea-level pressure fields for 19W and/or the 850 mb wind and streamline fields for 20W. The 120-h track errors associated with the E-DCI between these two TCs were 736 n mi (997 n mi) for 19W (20W) in NOGAPS and 1168 n mi (1167 n mi) for 19W (20W) in GFDN.

(1) Typhoon Chaba (19W). Both the NOGAPS and GFDN forecasts of Typhoon Chaba experienced E-DCI problems for a total of 16 model integrations. The E-DCI first emerged in the 1800 UTC 19 August 2004 model integration of NOGAPS and in the 1200 UTC 19 August 2004 integration of GFDN (Table 4, row 3). The inspection of NOGAPS and GFDN mean sea-level pressure fields for Chaba on the forecast period of 0600 UTC 21 August 2004 reveals a classic case of E-DCI. In Figure 6, it is evident that the forecast tracks for 19W by both NOGAPS (N) and GFDN (G) are fast, and they are eastern outliers of all the models and, in hindsight, of the TC best track.

Note that in the following model field comparisons, the forecast integrations of NOGAPS and GFDN are usually not equal. While the NOGAPS is run four times a day, GFDN is only run twice and the latest available GFDN fields can be six hours older than NOGAPS. This difference requires the examination of GFDN fields that are six hours older than that of NOGAPS when comparing fields with the same verifying time.

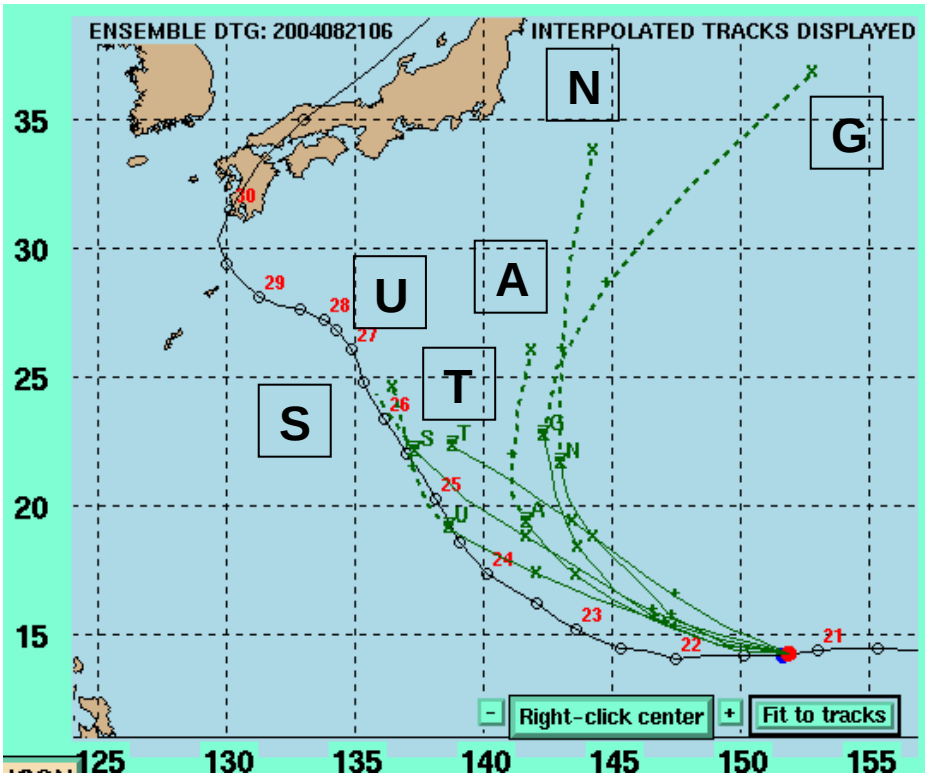

Figure 6. Interpolated forecast tracks for 19W by NOGAPS (N), GFDN (G), UKMO (U), the Global Spectral Model (S) and Typhoon Model (T) of the Japan Meteorological Agency, and GFS (A) for the forecast period of 0600 UTC 21 August 2004. The solid sections of the forecast tracks represent the 00-h through 72-h forecast while the dashed section represents the 72-h through 120-h forecast. The solid line with circles and corresponding dates represents the TC best track.

Comparing the 78-h forecast mean sea-level pressure fields of GFDN (Figure 7, row 1, column 2) to that of the verifying NOGAPS analysis (Figure 7, row 3, column 2), the strength (estimated from the number of contours) of Chaba (the eastern TC) in the two panels is similar, but Chaba has a much smaller horizontal scale in the GFDN fields. At the same time, GFDN portrays Aere (the western TC) as a much broader and less organized circulation. Despite the similar intensity forecasts for Chaba by GFDN, it is believed that the falsely forecast large horizontal scale of Aere lead to the direct interaction between the two. The 72-h forecast fields for NOGAPS (Figure 7, row 2, column 2) have the eastern TC (Chaba) being much weaker and has been predicted to rotate CCW around the slowing western TC (Aere). The verifying analyses fields for the same time (Figure 7, row 3, column 2) illustrates that Chaba has instead

intensified and both Chaba and Aere have remained on a west-northwest track. The slowing and southward deflection in the forecast track for Aere combined with the CCW rotation of Chaba around Aere are evidence that both GFDN and NOGAPS are predicting a mutual interaction of TCs Chaba and Aere.

By 102 h, the GFDN (Figure 8, row 1, column 1) is predicting an end of the E-DCI as Chaba and Aere have aligned such that their peripheral anticyclones have merged with the subtropical ridge to form a reverse-oriented trough, and Chaba is now tracking to the north-northeast. In the NOGAPS forecast (Figure 8, row 2, column 1) verifying at the same time, E-DCI is most likely ending as the track is now more poleward than westerly. This scenario is also hinting at the formation of a reverse-oriented trough, but TC Aere and its peripheral anticyclone need to move slightly more south of Chaba for their peripheral anticyclones to merge with the subtropical high. Twenty-four hours later, it is now apparent in both the GFDN (Figure 8, row 1, column 2) and NOGAPS (Figure 8, row 2, column 2) predictions that a reverse-oriented monsoon trough is forming, as is evident from the southwestern extension of the subtropical ridge to the east of Chaba and Aere. The resulting tracks at 120 h of both Chaba and Aere also indicate they are influenced by a reverse-oriented monsoon trough environment in that they are tracking to the northeast while still south of the primary subtropical ridge axis. The following analysis of the track forecast for TC Aere will further corroborate the mutual E-DCI between Chaba and Aere.

The track forecast of Chaba may not conclusively indicate E-DCI is occurring. However, the inspection of the forecast fields reveals an adjacent circulation to the TC. The motion of this adjacent circulation viewed in conjunction with the motion of the TC being forecast should be a clue for the forecaster that a mutual interaction between the two circulations is occurring.

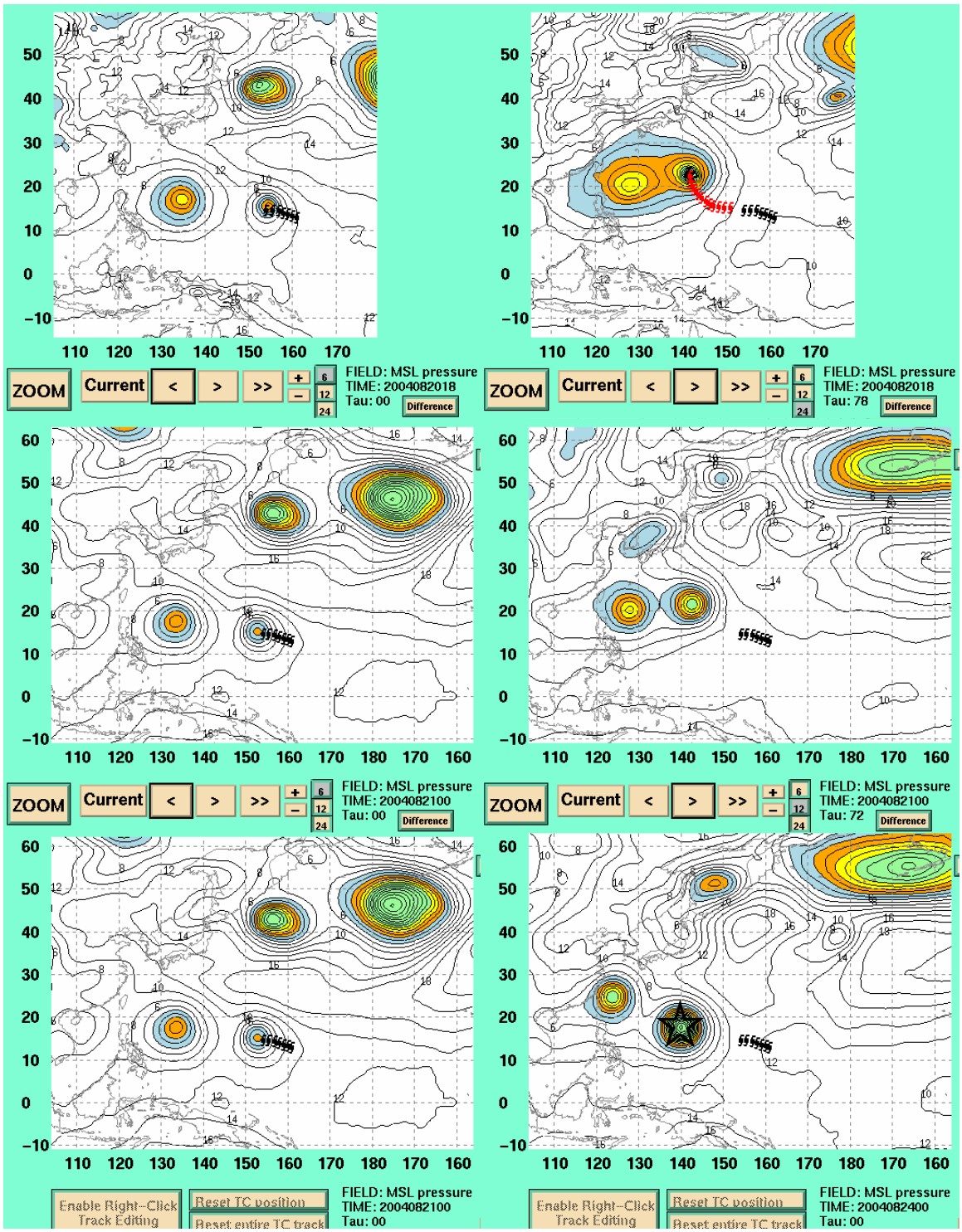

Figure 7. Mean sea-level pressure (mb) fields for 19W predicted by GFDN (row 1) and NOGAPS (row 2) and verifying 00-h NOGAPS analysis (row 3) for 1800 UTC 20 Aug 04 (0000 UTC 21 Aug 04) for GFDN (NOGAPS). First (second) column illustrates the 00-h analysis fields (78-h (72-h) forecast fields for GFDN (NOGAPS)). Verifying TC position indicated by star.

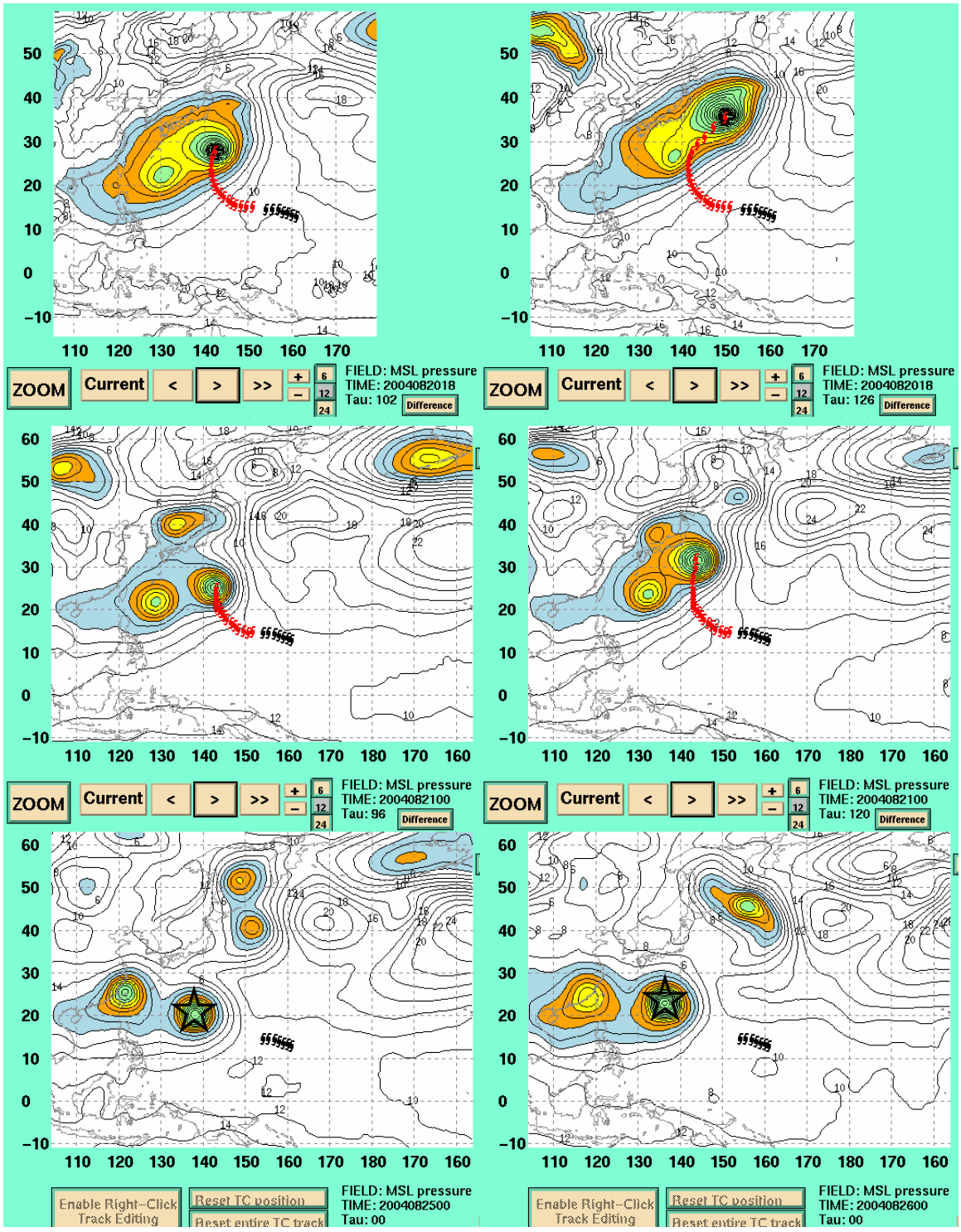

Figure 8. Mean sea-level pressure (mb) fields for 19W predicted by GFDN (row 1) and NOGAPS (row 2) and verifying 00-h NOGAPS analysis (row 3) for the forecast tau of 1800 UTC 20 August 2004 (0000 UTC 21 August 2004) for GFDN (NOGAPS). First column illustrates the 102-h (96-h) forecast fields and the second column illustrates 126-h (120-h) forecast fields for GFDN (NOGAPS). Verifying TC position indicated by star.

(2) Typhoon Aere (20W). Both the NOGAPS and GFDN forecasts of Typhoon Aere experienced E-DCI problems for a total of 10 model integrations. The E-DCI first emerged in the 1800 UTC 19 August 2004 model integration of NOGAPS and in the 0000 UTC 21 August 2004 integration of GFDN (Table 4, row 4). The forecast tracks for 20W by both NOGAPS and GFDN in Figure 9 are slow and south of the best track data by 72 h, and from 72 h through 120 h the track has changed from westerly to northeasterly.

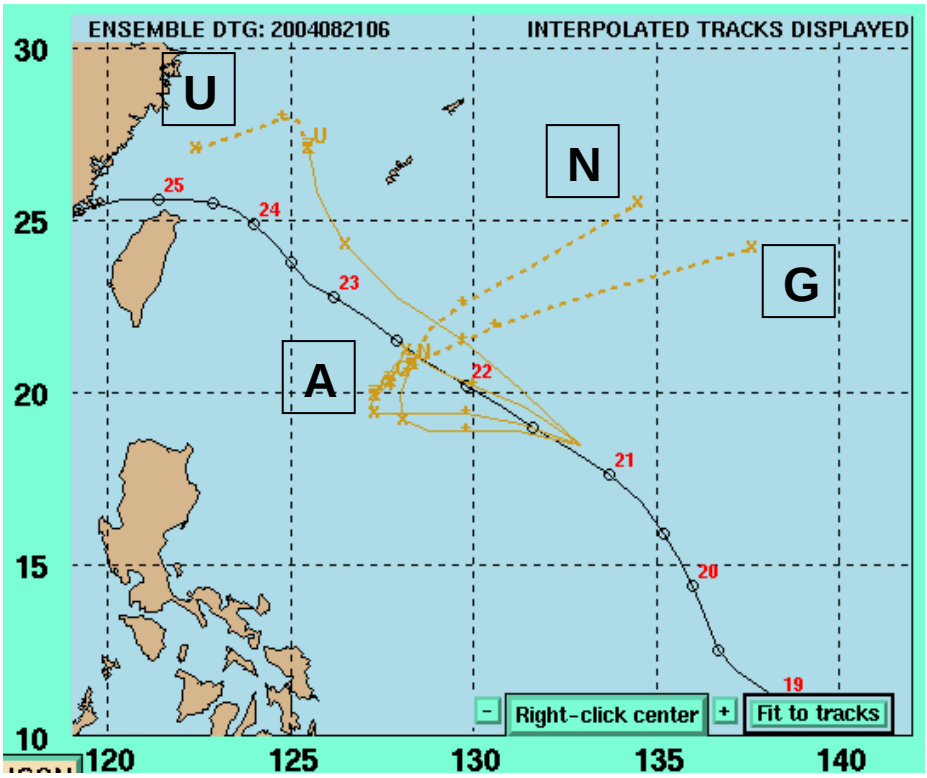

Figure 9. Interpolated forecast tracks for 20W predicted by NOGAPS (N), GFDN (G), UKMO (U), and GFS (A) for the forecast period of 0600 UTC 21 August 2004. The solid sections of the forecast tracks represent the 00-h through 72-h forecast while the dashed sections represent the 72-h through 120-h forecast. The solid line with circles and corresponding dates represents the TC best track.

The inspection of NOGAPS and GFDN 850 mb wind and streamline fields (Figure 10) for Aere for the forecast period of 0600 UTC 21 August 2004 for 20W reveal the corresponding effect of E-DCI on the western TC. The 78-h 850-mb wind/streamline forecast field for GFDN (Figure 10, row 1,

column 2) and corresponding 72-h forecast fields for NOGAPS (Figure 10, row 2, column 2) illustrate that the eastern TC (Chaba) is weak and has started to rotate CCW around the too slowly moving western TC (Aere). The analysis for the verification time (Figure 10, row 3) illustrate that Chaba has instead intensified and both Chaba and Aere have remained on a west-northwest track. The slowing and southward deflection in the forecast track of Aere, combined with the CCW rotation of Chaba around Aere, are evidence that the models are predicting that Aere and Chaba are involved in a direct cyclone interaction.

By 102/96 h, both the GFDN (Figure 11, row 1, column 1) and NOGAPS (Figure 11, row 2, column 1) forecast fields and resultant track forecasts (Figure 9) illustrate that a reverse-oriented monsoon trough is forming, as is evident from the southwesterly extension of the subtropical ridge to the east of Chaba and Aere. This erroneously predicted reverse-oriented monsoon trough is causing the track of TC Aere to diverge wildly from its initial direction at the beginning of the forecast. By 126/120 h (Figure 11, column 2), both GFDN and NOGAPS predict Aere will be nearly 600 n mi east of Taiwan, when in reality it is making landfall in China due west of Taiwan (Figure 9).

It is further acknowledged that two separate error mechanisms lead to the final forecast errors of Chaba and Aere for the 0600 UTC 21 August 2004 forecast by both NOGAPS and GFDN. Because it is the E-DCI through the first 72 h that leads to the reverse-oriented monsoon trough formation from 72-120 h, the error mechanism assigned to this date/time group was E-DCI. If the forecaster at JTWC was able to detect the mutual interaction of two TCs in close proximity, the potential exists for the accuracy of CONW to be improved if the erroneous tracks were removed from the consensus to create a selective CONW.

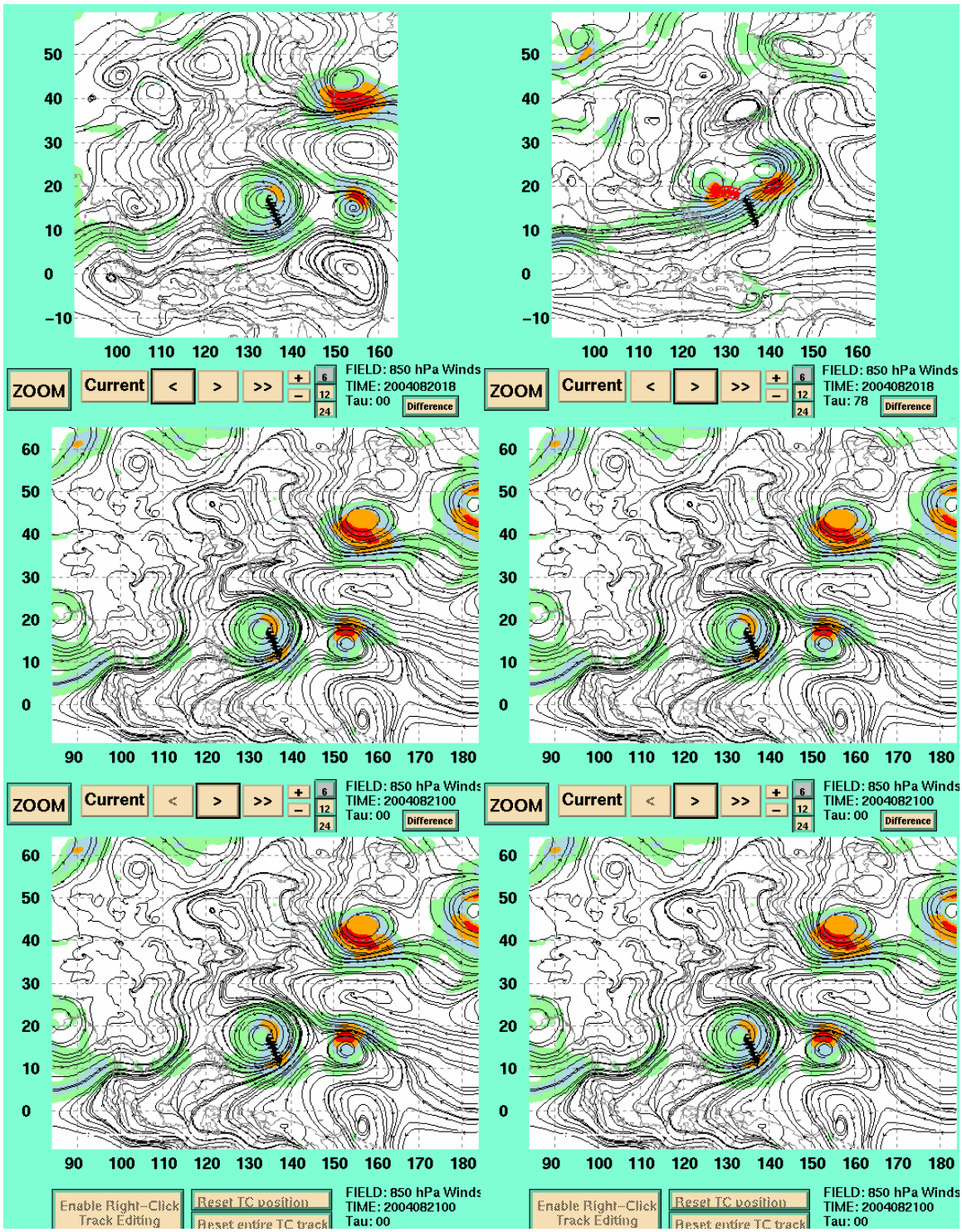

Figure 10. 850-mb streamline and isotach forecast fields for 20W by GFDN (row 1) and NOGAPS (row 2) and verifying 00-h NOGAPS analysis (row 3) for the forecast tau of 1800 UTC 20 August 2004 (0000 UTC 21 August 2004) for GFDN (NOGAPS). First column illustrates the 00-h analysis fields and the second column illustrates 78-h (72-h) forecast fields for GFDN (NOGAPS).

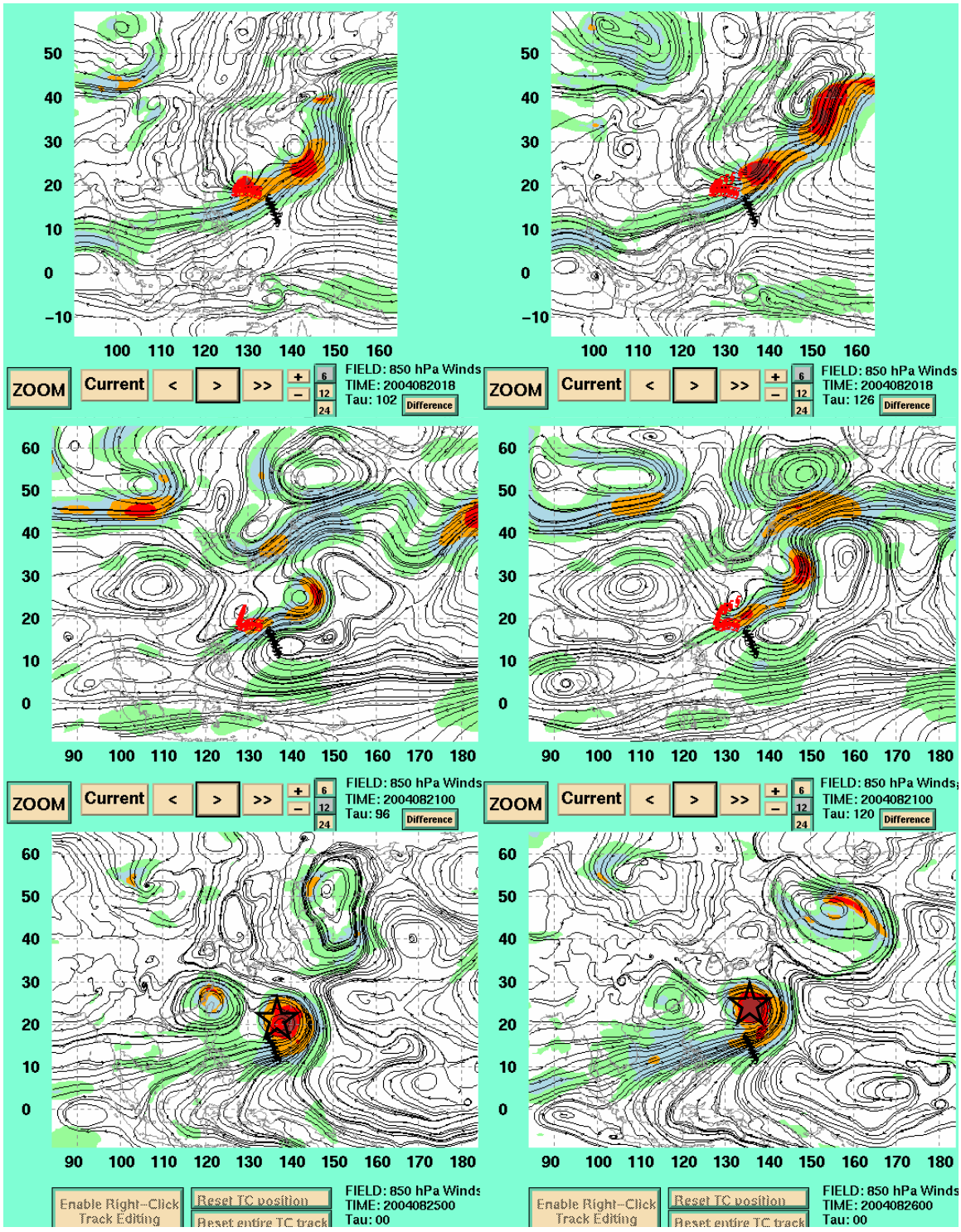

Figure 11. 850-mb streamline and isotach forecast fields for 20W by GFDN (row 1) and NOGAPS (row 2) and verifying 00-h NOGAPS analysis (row 3) for the forecast tau of 1800 UTC of 20 August 2004 (0000 UTC of 21 August 2004) for GFDN (NOGAPS). First column illustrates the 102-h (96-h) forecast fields and the second column illustrates 126-h (120-h) forecast fields for GFDN (NOGAPS). Verifying TC position indicated by star.

In summary, the indications of E-DCI affecting model tracks to 120 h are similar to those found by Carr and Elsberry (2000a) in their review of the 1997 season. These include: (i) CCW rotation of the eastern (western) TC around the adjacent western (eastern) TC; (ii) sudden changes in the temporal progression during the 120-h forecast period; (iii) the western circulation slowed while the eastern circulation accelerated; (iii) formation of a reverse-oriented monsoon trough in the later stage of the forecast as the peripheral anticyclones of the two circulations merged with the subtropical ridge; and (iv) occasional merger of a weak circulation rotating CCW around a much stronger circulation. It was found that streamlines from 850 through 500 mb were most effective in identifying E-DCI for TCs above tropical storm intensity (> 34 kt). For those TCs that were of tropical depression intensity or less (e.g., 31W), mean sea-level pressure fields were the most effective. Mean sea-level pressure fields were also effective in illustrating the melding or merger of two circulations.

Similar to the analysis of the 1997 season by Carr and Elsberry (2000a), a key finding in the analysis of the 2004 season is that actual exaggeration of a naturally occurring DCI event was never observed. All 31 cases of E-DCI in both NOGAPS and GFDN were false representations. The corroborating findings of the 2004 season gives the forecaster further justification to expect any occurrence of DCI in the models to be E-DCI and therefore to eliminate that track forecast from the consensus.

2. Beta Effect Processes

Beta effect processes are the result of an erroneous forecast of the TC size by the model. The error mechanisms that involve the beta effect processes in the 2004 analysis were Insufficient – Beta Effect Propagation (I-BEP) and the Excessive – Reverse Trough Formation (E-RTF). These error mechanisms are associated with the dependence of the propagation and Rossby wave train effect on TC size and motion as outlined by Carr and Elsberry (1997).

a. Insufficient – Beta Effect Propagation (I-BEP)

(1) Description. In the absence of environmental flow, a TC will translate to the west-northwest owing to beta gyres developed by the advection of the latitudinal variation of the Coriolis parameter – beta. Carr and Elsberry (1997) found that an average size TC could self-propagate 129 km/day. The I-BEP error mechanism arises when the outer wind structure of the TC is forecast to be too small. When this occurs, smaller beta gyres are produced and the storm self-propagation will be slower.

When I-BEP is occurring in the dynamical model, the track of the affected model will be slower and south of the actual track, due to the reduction of the west-northwest propagation in the overall motion of the TC. This error will only be readily apparent when the environmental steering flow of the TC is weak. Otherwise, a stronger environmental steering flow will mask the insufficient self-propagation.

(2) Frequency and characteristics. I-BEP occurred only in NOGAPS in the 2004 analysis. It is hypothesized that this occurred because of an overall trend for the TC intensity and horizontal size to be under-forecast in the western North Pacific in 2004. Since the size of the majority of TCs was under-forecast, the potential of insufficient self-propagation existed for each of those TCs. However, this potential was not realized because of the few cases in which the TC was in a region of weak environmental flow. Thus, I-BEP was detectable in only five of the 162 cases of large errors in NOGAPS (Table 3). While five occurrences is only a small percentage of the total NOGAPS large-error cases, this error mechanism is covered because the potential existed for so many more cases to have occurred, if they had not been masked by the environmental flow. These five cases occurred when the TC was in Standard/Tropical Easterly pattern/region, south of the subtropical ridge. The initial intensity of the TCs ranged from 25 knots for 23W to 40-45 knots for 06W and 31W. Since the TCs developed in an area of favorable conditions (SST>26˚C, low vertical wind shear, cyclonic vorticity in the lower levels), it is not

known why the model did not develop the TC, but as will be seen in the case studies below, the TCs struggled to maintain a semblance of a tropical storm.

(3) Case Study. The case of Typhoon Omasis (06W) for the NOGAPS forecast initiated at 0600 UTC 17 May 2004 illustrates the effect I-BEP can have on a track forecast. A scant observation might attribute the large error to a misplaced midlatitude trough since the TC did not make the sudden poleward turn as the best track indicates (Figure 12).

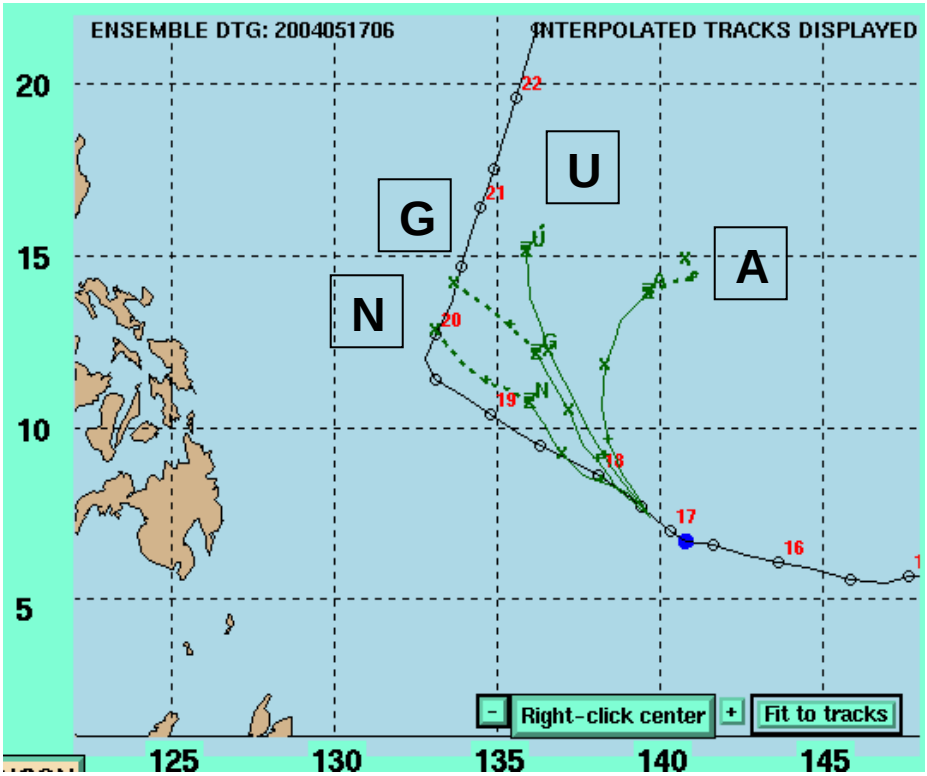

Figure 12. Interpolated forecast tracks for 06W by NOGAPS (N), GFDN (G), UKMO (U), and GFS (A) for the forecast initiated at 0600 UTC 17 May 2004. The solid sections of the forecast tracks represent the 00-h through 72-h forecast while the dashed sections represent the 72-h through 120-h forecast. The solid line with circles and corresponding dates represents the TC best track.

The 24-h forecast fields for NOGAPS (Figure 13, row 2, column 2) illustrate that the Omasis circulation does not extend as far north and south as in the verifying analysis (Figure 13, row 3, column 2). This difference in size would have a negative effect on the magnitude of the beta effect

propagation of the storm that is consistent with the slow bias. The too slow translation over the next three days allows the subtropical ridge to build poleward of the TC after the passage of a midlatitude trough by the 96-h point (Figure 14, row 2, column 1), and this ridge blocks the poleward turn. By 120 h (Figure 14, row 2, column 2) the TC is quickly dissipating. In reality (Figure 14, row 3, column 1), the TC is nearing the axis of the subtropical ridge by 96 h and the approaching trough over Okinawa, Japan further weakens the ridge and allows the TC to move through the axis, which leads to a transition to a Midlatitude/Poleward Flow pattern/region by 120 h (Figure 14, row 3, column 2). The GFDN forecast fields have a similar scenario of I-BEP. However, the 72-h, 96-h and 120-h track forecast errors were not degraded enough to fall in the thresholds set for this study.

A key result is that this error mechanism occurred in less than three percent of all large forecast errors for the 2004 season. Furthermore, it is hypothesized that this error is normally masked by stronger environmental flow. Even in light environmental flow, it is acknowledged that detecting and properly diagnosing I-BEP in the models is a difficult task. To properly diagnose this error mechanism, the forecaster must realize that the model is incorrectly predicting that the TC will not intensify despite being in an area of favorable development, especially when other models are predicting a horizontally larger TC.

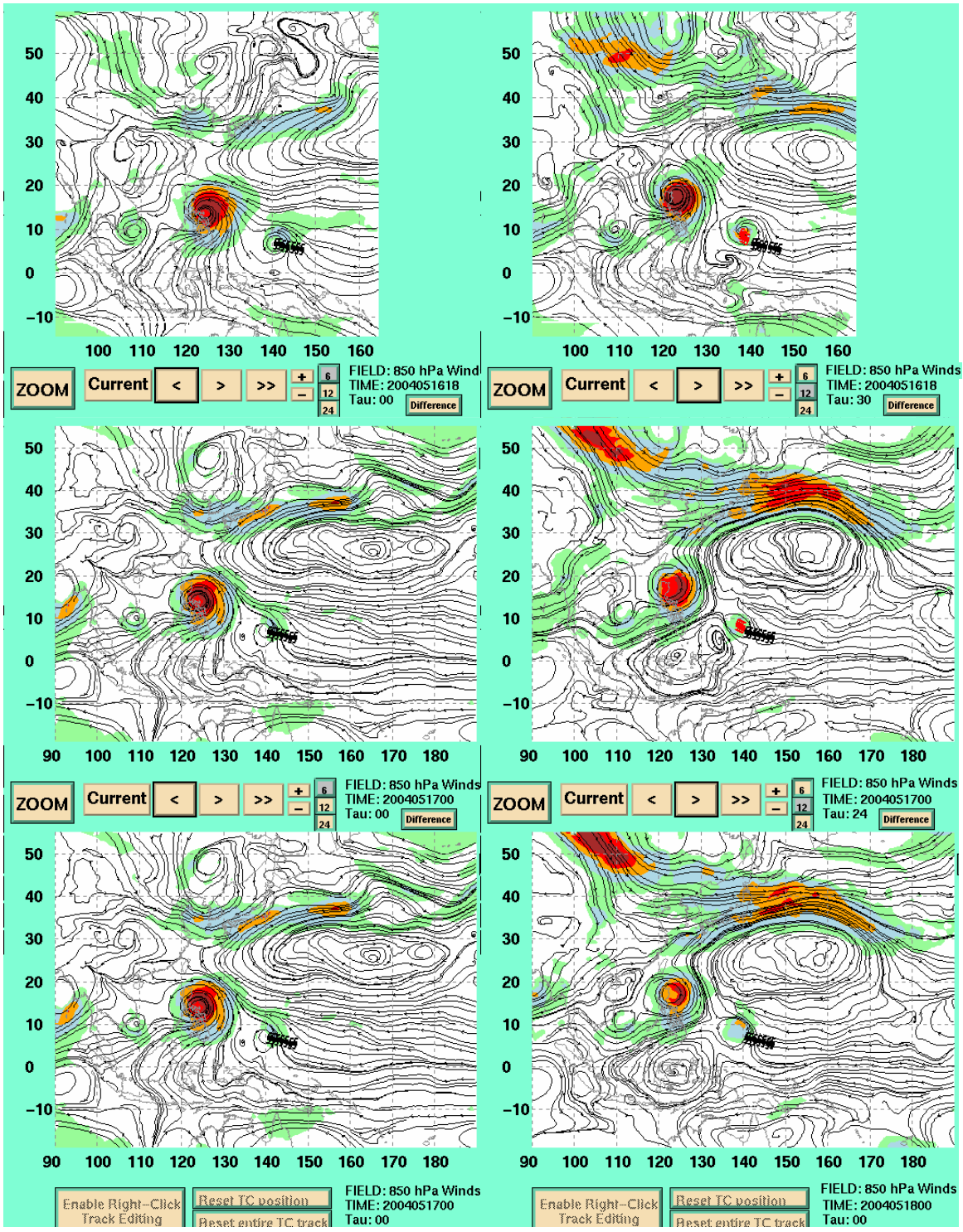

Figure 13. 850-mb streamline and isotach forecast fields for 06W by GFDN (row 1) and NOGAPS (row 2) and verifying 00-h NOGAPS analysis (row 3) for the forecast tau of 1800 UTC 16 May 2004 (0000 UTC 17 May 2004) for GFDN (NOGAPS). First column illustrates the 00-h analysis fields and the second column illustrates 30-h (24-h) forecast fields for GFDN (NOGAPS).

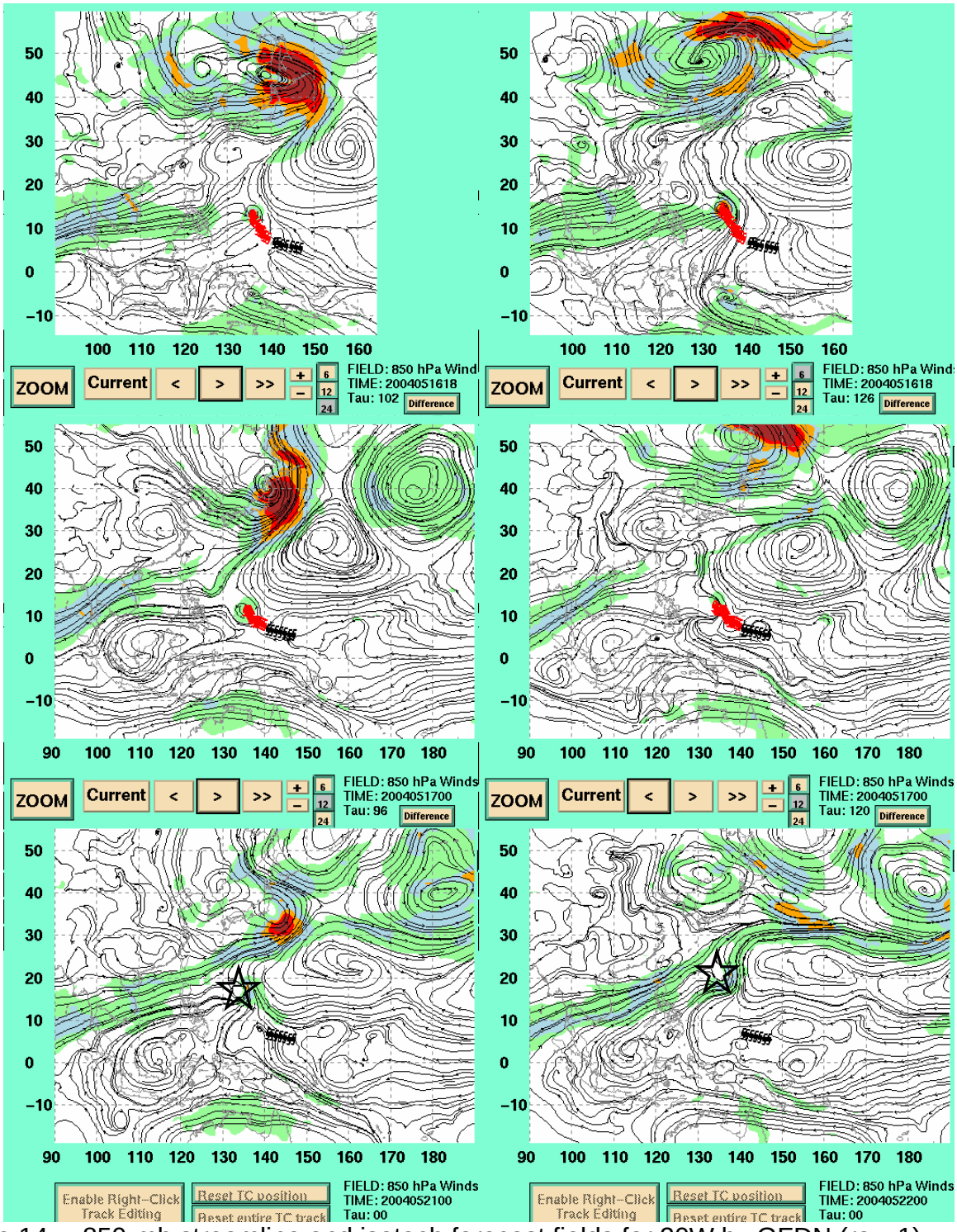

Figure 14. 850-mb streamline and isotach forecast fields for 20W by GFDN (row 1) and NOGAPS (row 2) and verifying 00-h NOGAPS analysis (row 3) for the forecast tau of 1800 UTC 16 May 2004 (0000 UTC 17 May 2004) for GFDN (NOGAPS). First column illustrates the 102-h (96-h) forecast fields and the second column illustrates 126-h (120-h) forecast fields for GFDN (NOGAPS). Verifying TC position indicated by star.

b. Excessive – Reverse Trough Formation (E-RTF)

(1) Description. As described in Carr and Elsberry (2000a), RTF occurs when two TCs are initially oriented east-west along approximately the same latitude such that the peripheral anticyclones of the two TCs can combine to produce one large anticyclone (Figure 15). These peripheral anticyclones may be generated through the Rossby wave train as outlined in Carr and Elsberry (2000a). Once this combined anticyclone forms, both TCs tend to recurve near simultaneously. The potential exists for the model to both excessively or insufficiently predict the formation of the reverse-oriented trough. In the insufficient formation scenario, the Rossby wave dispersion occurs too slowly in the model or not at all, so that the poleward turn of the TC is predicted too late or not at all. In the excessive formation (E-RTF) case, the RTF process occurs too early or falsely in the model and the predicted TC track is poleward compared to reality.

(2) Frequency and occurrence. During the 2004 season, all occurrences of RTF related errors were excessive. However, E-RTF was the primary error mechanism only in three model integrations by GFDN for TC Mindulle (10W). However, E-RTF was evident in an additional 25 model integrations by both NOGAPS and GFDN, two of those additional occurrences were by GFDN for TC Mindulle in which the track errors were less than the prescribed thresholds. In some of the other situations, E-RTF was a secondary error mechanism that led to large errors, e.g., 7 (8) NOGAPS (GFDN) integrations of TC Chaba (19W) and 6 (2) NOGAPS (GFDN) integrations of TC Aere (20W). As discussed in Chapter III.B.1.c, E-DCI in Chaba and Aere was the primary error mechanism that ultimately led to E-RTF. For those E-RTF occurrences by GFDN for 19W and 20W, there was neither a pattern of E-RTF occurring in every simultaneous integration nor a pattern of E-RTF occurring on which GFDN was not centered. As in the 1997 study, the GFDN integrations for two simultaneously occurring TCs predicted very different evolutions of the TCs.

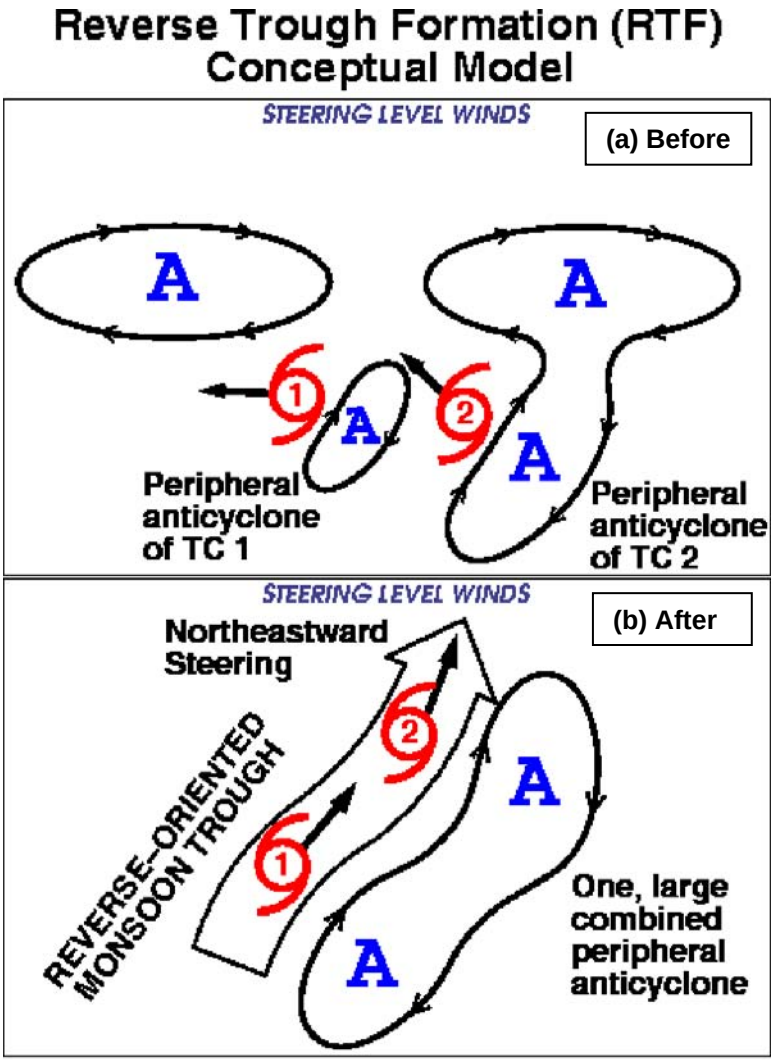

Figure 15. Conceptual model for RTF in which two initially east-west oriented TCs become aligned southwest to northeast in a reverse-oriented monsoon trough with a similarly oriented extensive peripheral anticyclone so that both TCs change to a more poleward track (from Carr and Elsberry 2000a).

(3) Case Study. The GFDN track forecast for TC Mindulle (10W) at 1800 UTC 29 June 2004 is the eastern outlier of the four model tracks and is the result of an E-RTF error (Figure 16). The 700-mb wind fields for the GFDN forecast initiated at 0600 UTC 29 June 2004 (Figure 17) illustrate a transition from Poleward/Poleward Flow pattern/region but the other three models predict a transition to Midlatitude/Poleward Flow pattern/region. The trough that is evident over the Sea of Japan in the 00-h GFDN forecast (Figure 17, row 1, column 1) is predicted to break down the subtropical ridge in

the proceeding time steps allowing 11W, which is initially at 20N, 143E, to the east of 10W, to travel around the axis of the ridge. In the 78-h GFDN forecast (Figure 17, row 1, column 2), a reverse-oriented monsoon trough is evident (note the strong isotach maxima to the southeast of 10W and 11W) that is consistent with the development of peripheral anticyclones illustrated in the RTF conceptual model in Figure 15. The reverse-oriented monsoon trough also concurs with the GFDN prediction of a transition from Standard/Poleward Flow to Poleward/Poleward Flow, while the other models predict a transition from Standard/Poleward Flow to Midlatitude/Poleward Flow. In the NOGAPS 72-h forecast (Figure 17, row 2, column 2) and verifying analysis (Figure 17, row 3, column 2), a trough of similar orientation and intensity also has a similar effect on the subtropical ridge. One difference is in the amount of separation of the TCs in the GFDN forecast compared to the NOGAPS forecast and the verifying analysis. In GFDN, the relatively close TCs disperse energy to the southeast, and the peripheral anticyclones meld with each other and the subtropical ridge to develop one strong peripheral anticyclone through the 78-h forecast. In NOGAPS, the two TCs have a greater separation, and the peripheral anticyclones remain distinct. The peripheral anticyclone of 10W builds between the two TCs and keeps a reverse-oriented monsoon trough from forming. In the 102-h (Figure 18, row 1, column 1) and 126-h (Figure 18, row 1, column 2) GFDN forecasts, the absence of the ridge to impede the progression of 10W allows the cyclone to continue on a poleward track. By contrast, the NOGAPS 96-h forecast (Figure 18, row 2, column 1) and verifying analysis (Figure 18, row 3, column 1) illustrate that substantial ridging continued to occur to the northeast of 10W, which leads to a more northerly track of 10W.

In summary, an E-RTF event can severely degrade a track forecast, especially when the false prediction of a reverse-oriented monsoon trough indicates that the TC will turn poleward and move to the northeast, but the TC actually tracks westward. While E-RTF was the primary error mechanism for large errors in only three integrations of GFDN in 2004, it was a secondary error mechanism that occurred late in the forecast integration and further degraded an

already bad GFDN and NOGAPS forecast. The key factors indicating E-RTF was occurring in the model during the 2004 analysis were similar to the Carr and Elsberry analysis of the 1997 season. Those were: (i) rapid simultaneous amplification of the peripheral anticyclone to the southeast of the eastern and western TC or cyclonic circulation; and (ii) a premature transition from the Standard pattern to the Poleward pattern. This transition, which resulted in an erroneous sharp turn to the northeast, was readily apparent in the track of the western TC/circulation compared to the eastern TC/circulation.

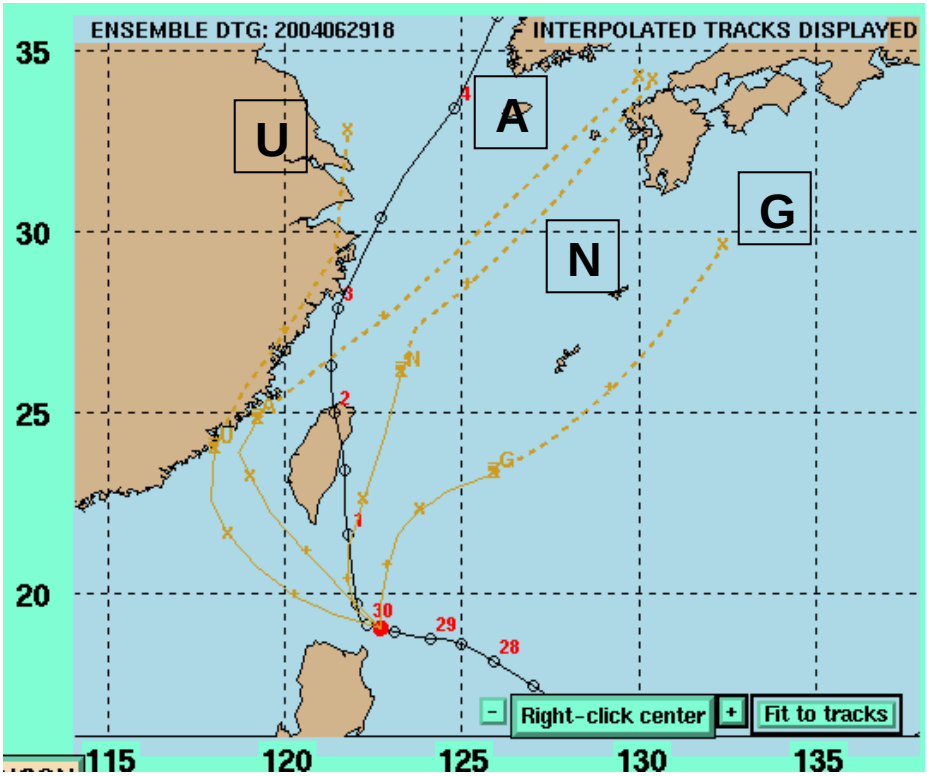

Figure 16. Interpolated forecast tracks for 10W by NOGAPS (N), GFDN (G), UKMO (U), and GFS (A) for the forecast initiated at 1800 UTC 29 June 2004. The solid sections of the forecast tracks represent the 00-h through 72-h forecast while the dashed sections represent the 72-h through 120-h forecast. The solid line with circles and corresponding dates represents the TC best track.

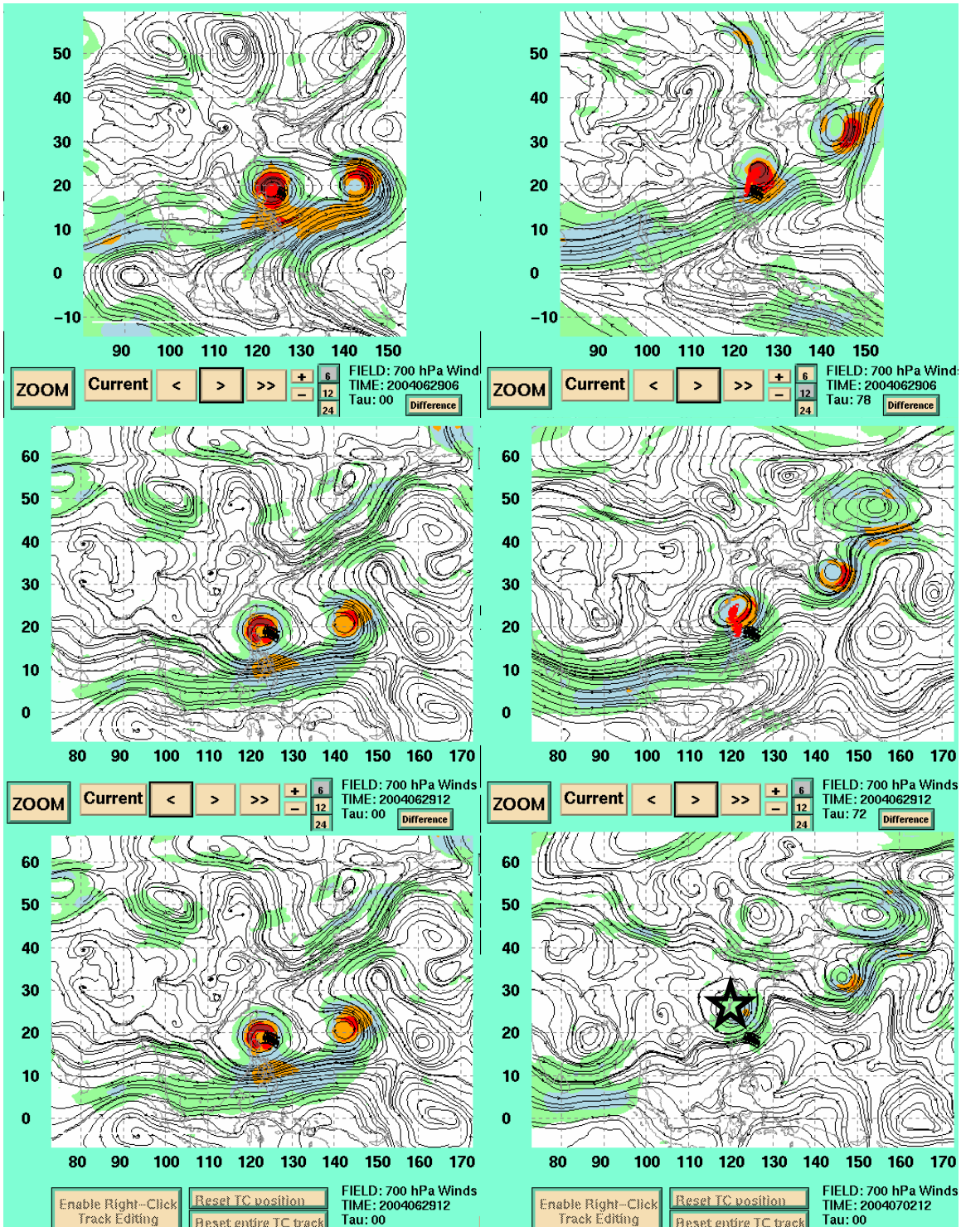

Figure 17. 700-mb streamline and isotach forecast fields for 10W by GFDN (row 1) and NOGAPS (row 2) and verifying 00-h NOGAPS analysis (row 3) for the forecast tau of 0600 UTC 29 June 2004 (1200 UTC 29 June 2004) for GFDN (NOGAPS). First column illustrates the 00-h analysis fields and the second column illustrates 78-h (72-h) forecast fields for GFDN (NOGAPS). Verifying TC position indicated by star.

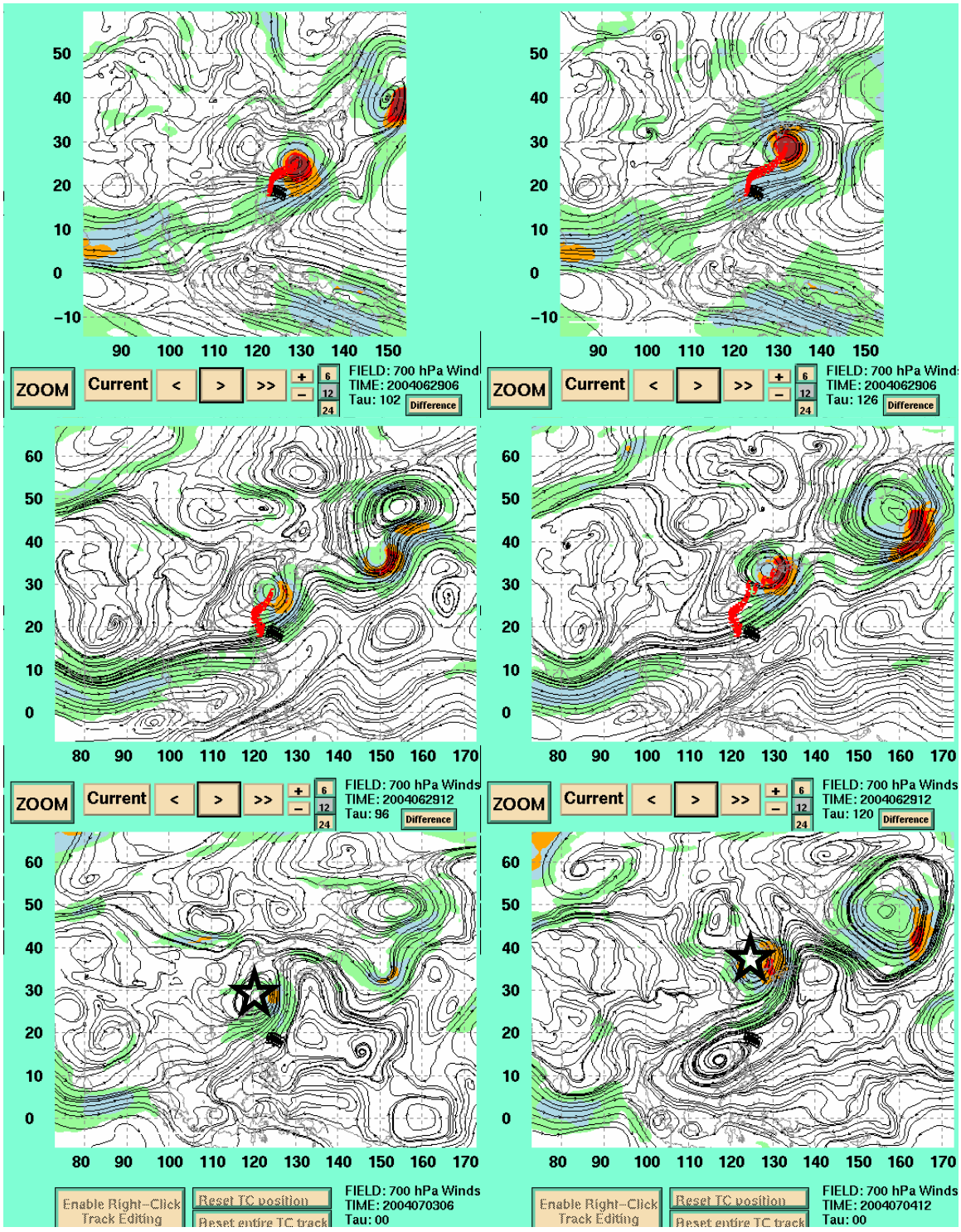

Figure 18. 700-mb streamline and isotach forecast fields for 10W by GFDN (row 1) and NOGAPS (row 2) and verifying 00-h NOGAPS analysis (row 3) for the forecast tau of 0600 UTC 29 June 2004 (1200 UTC 29 June 2004) for GFDN (NOGAPS). First column illustrates the 102-h (96-h) forecast fields and the second column illustrates 126-h (120-h) forecast fields for GFDN (NOGAPS). Verifying TC position indicated by star.

C. MIDLATITUDE INTERACTIONS

As a TC begins moving poleward, the transition from the tropics to the midlatitudes is usually complete within two to three days. Therefore it is no surprise that 75% (72%) of all large errors at 96 h and 120 h in NOGAPS (GFDN) during 2004 were due to midlatitude influences. The errors associated with midlatitude effects occur when the TC is approaching or poleward of the subtropical ridge axis and the environmental flow has a westerly or southerly component or a combination of the two. The most common environmental flow patterns were classified as Standard/Tropical Easterly transitioning into Standard/Poleward Flow, or Midlatitude/Poleward Flow. Because the TC is near or poleward of the subtropical ridge, its motion is directly impacted by midlatitude circulations (cyclones, troughs, anticyclones, or ridges). Therefore, poorly predicted development, dissipation, and/or movement of these midlatitude circulations, which occur independently of the TC, can have a negative impact on predicted TC tracks (Carr and Elsberry 2000b). The forecast track can also be severely degraded when the interaction with a properly diagnosed midlatitude feature is predicted to occur excessively or insufficiently. Large track error mechanisms due to midlatitude influences were Response to Vertical Wind Sheer (RVS), Baroclinic Cyclone Interaction (BCI), Midlatitude Cyclogenesis (MCG), Midlatitude Cyclolysis (MCL), Midlatitude Anticyclogenesis (MAG), Midlatitude Anticyclolysis (MAL), and, added in this study, Direct Cyclone Interaction – midlatitude (DCI-m). These error mechanisms will be prefixed as either occurring excessively (E) or insufficiently (I), or both.

As illustrated in Table 5, E-DCI-m, E-RVS, E-MCG, I-MCG, E-MCL and E-MAG error mechanisms were responsible for the majority of degraded forecasts due to midlatitude influences. Therefore, these will be highlighted in case studies. The E-BCI, I-MAG, E-MAL, and I-MAL error mechanisms only accounted for a total of 6% of all degraded forecasts by NOGAPS and GFDN in 2004 and will therefore not be covered.

Phenomenon name	Acronym	No. of NOGAPS forecasts*	No. of GFDN forecasts*
Direct cyclone interaction (midlatitude)	DCI-m	6-0	5-0
Response to vertical wind sheer	RVS	26-0	0-0
Baroclinic cyclone interaction	BCI	6-0	0-0
Midlatitude cyclogenesis	MCG	6-53	28-46
Midlatitude cyclolysis	MCL	12-0	2-0
Midlatitude anticyclogenesis	MAG	6-0	9-6
Midlatitude anticyclolysis	MAL	2-4	0-0
Total of all degraded forecasts		121	96

Table 5. Number of NOGAPS and GFDN forecast integrations affected by midlatitude influences. Improper midlatitude interactions were responsible for 121 of 162 (96 of 135) degraded NOGAPS (GFDN) forecasts in 2004. *First (second) number indicates excessive (insufficient) occurrence.

1. Direct Cyclone Interaction – midlatitude (DCI-m)

a. Description

The conceptual model of E-DCI-m is the same as that of E-DCI-t. However, the key difference is that the adjacent circulation interacting with the TC is a midlatitude cyclone. This delineation is made because E-DCI-m can have an even greater impact on the forecast track than E-DCI-t. As described in Carr and Elsberry (2000a), the cause of E-DCI-m is overly deep penetration of an upper-level midlatitude circulation into the lower troposphere where it can affect the steering of the TC. The E-DCI-m errors normally occur as the TC is moving into the midlatitude westerlies, and instead of moving to the east in these westerlies, the model incorrectly predicts the TC to rotate CCW around a large midlatitude cyclone. When this occurred during the 2004 season, the largest 120-h errors were over 2000 n mi, which is twice as large as the largest E-DCI-t errors. Thus, correctly identifying and removing models displaying E-DCI-m would reduce the overall error of CONW.

b. Frequency and Characteristics

In the 2004 sample, six occurrences of E-DCI-m were in NOGAPS and five in GFDN for a total of 11 occurrences. The six occurrences in NOGAPS involved only TC Nida (04W) and the five in GFDN involved three TCs: two occurrences in TC Nida, two in TC Dianmu (09W), and one in TC Tingting (11W) (see Table 6, columns 3). The TC environmental structure change during each occurrence was from Standard/Poleward Flow to Midlatitude/Poleward Flow as

the TC was moving through the axis of the subtropical ridge and interacting with the midlatitude westerlies (Table 6, column 4). In each occurrence, the TC was a moderate to strong typhoon ranging from 80-135 knots (Table 6, column 5), which is significant because a moderate vertical structure of the TC is required for it to interact with the overly deep penetration of the midlatitude cyclone into the lower troposphere. As in E-DCI-t, no instances of an exaggeration of an actual DCI event by the model were observed. Rather, every occurrence was falsely predicted to occur. Therefore, the forecaster is once again justified in omitting the model track displaying E-DCI-m from the consensus.

TC No.	Start time of affected model runs	Occurrences NOGAPS (GFDN)	Synoptic environment of affected TC	Intensity before interaction	Nature of second cyclone	Location of second cyclone
04W	0000 UTC 17 MAY - 0600 UTC 18 MAY	6 (2)	S/PF → M/PF	130-135	Midlatitude	NNW
09W	1800 UTC 23JUN - 0000 UTC 24JUN	(2)	S/PF → M/PF	115-120	Midlatitude	NNW
11W	0000 UTC 29JUN	(1)	S/PF → M/PF	80	Midlatitude	NNW

Table 6. Cases of model-predicted E-DCI-m in the western North Pacific in 2004. A total of 11 cases of E-DCI-m occurred in three TCs in 2004.

c. Case Study

In the 0600 UTC 18 May 2004 forecast of TC Nida (04W), three of the four 120-h models available in CONW indicated the TC would recurve to the northwest once it is north of Tokyo, Japan (Figure 19). Notice that the best track has been extended beyond the time JTWC declared the storm to be extratropical to maximize the 96-h and 120-h model verifications. In this post-storm analysis, the extended best track deviates from the official best track beyond 0600 UTC 21 May 2004. In addition to NOGAPS and GFDN, the GFS forecast also predicts a northwest track in the midlatitudes. Whereas the model tracks form a tight cluster up to 72 h, a large spread in the models occurs beyond 72 h.

Both the GFDN (Figure 20, row 1), and NOGAPS (Figure 20, row 2) models appeared to have a good initialization of the TC and deep midlatitude 500 mb trough over eastern Russia and China. By 78 h (72 h) in the GFDN (NOGAPS) forecast, the TC is interacting with the midlatitude trough and has

accelerated to a position just south of Tokyo, Japan (Figure 20, rows 1 and 2, column 2). This forecast position is slow and west of the position in the verifying analysis (Figure 20, row 3, column 2), with 72-h errors greater than 300 n mi (Figure 19). The slow and westward track are rather ambiguous as far as possible error mechanisms, but in the 102-h (96-h) forecast of GFDN (NOGAPS) (Figure 21, rows 1 and 2, column 1), it becomes apparent the TC and midlatitude low are interacting as both models predict a CCW rotation with a TC track to the northwest. By 120 h, the 500 mb circulation of the TC is being absorbed into the midlatitude cyclone in both models (Figure 21, rows 1 and 2, column 2). However, the verifying analyses (Figure 21, row 3, columns 1 and 2) indicate that the TC remnants remained in the westerlies and tracked to the southeast in the Midlatitude/Equatorward Flow pattern/region.

In summary, every occurrence of E-DCI-m during the 2004 season resulted from a false interaction of a TC with a strong midlatitude cyclone to the northwest. While the key indicators of E-DCI-m are the same to those of E-DCI-t, an additional feature to cue the forecaster is a departure from a northeastward track to northwestward track in Midlatitude/Poleward flow. Moreover, there were no occurrences of an exaggeration of an actual DCI event between a TC and deep midlatitude cyclone. The forecaster is therefore justified in omitting the model displaying E-DCI-m from the CONW.

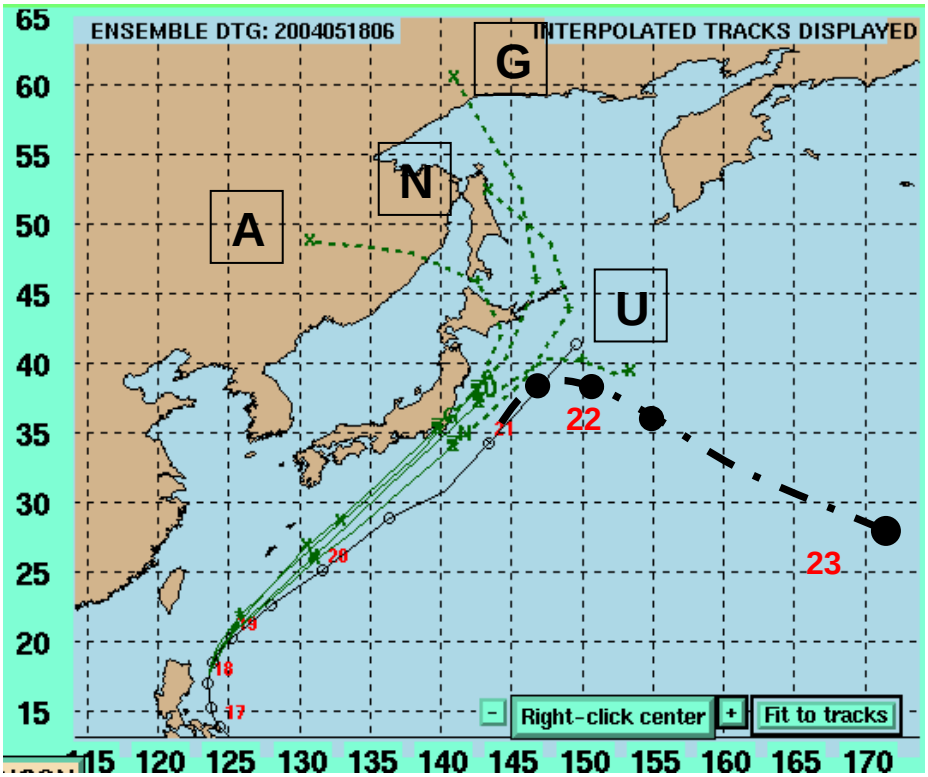

Figure 19. Interpolated forecast tracks for 04W by NOGAPS (N), GFDN (G), UKMO (U), and GFS (A) for the forecast period of 0600 UTC 18 May 2004. The solid sections of the forecast tracks represent the 00-h through 72-h forecast while the thin dashed sections represent the 72-h through 120-h forecast. The solid line with circles and corresponding dates represents the TC best track. The extended best track is represented by the heavy dashed line and solid circles with respective dates.

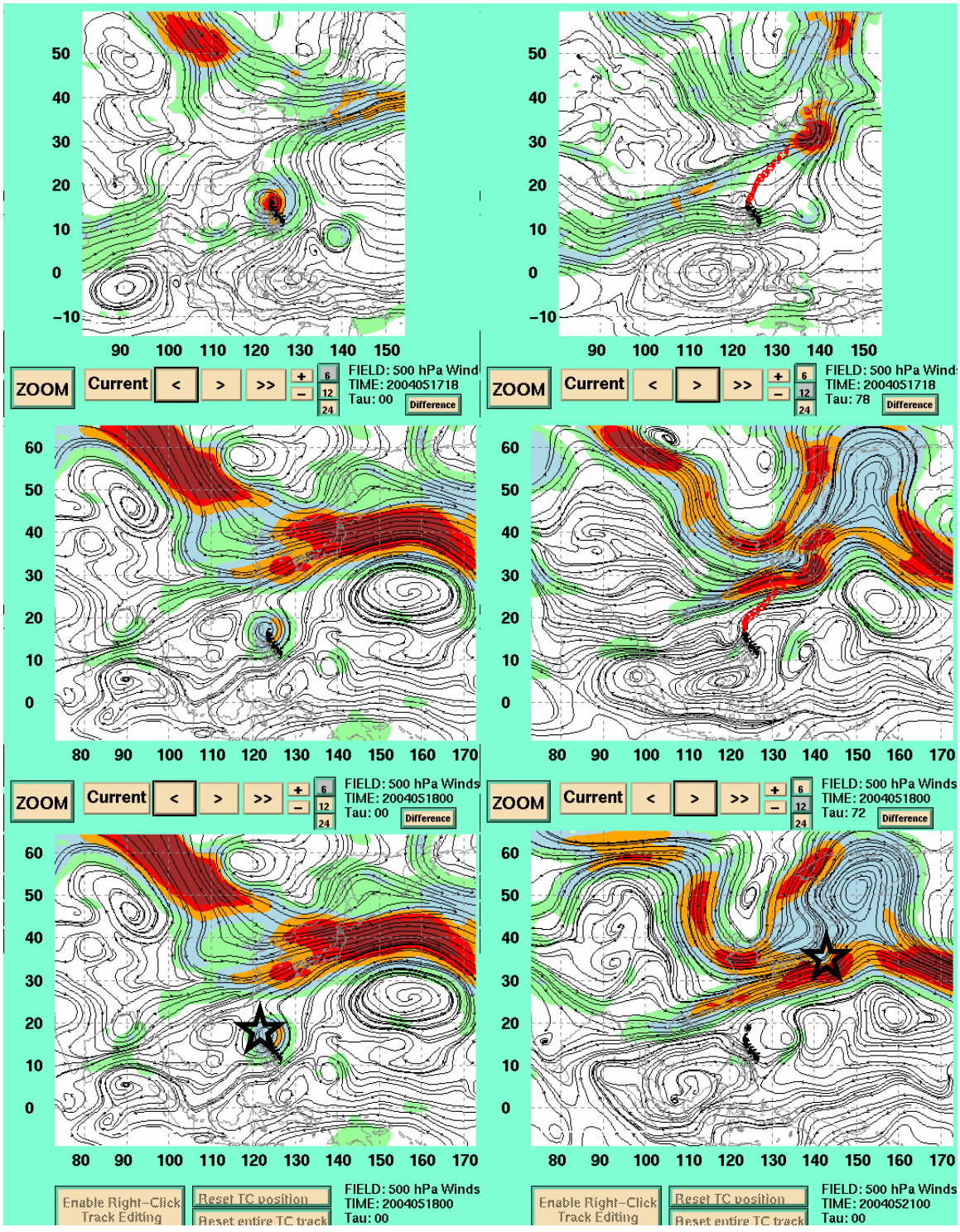

Figure 20. 500-mb streamline and isotach forecast fields for 04W by GFDN (row 1) and NOGAPS (row 2) and verifying 00-h NOGAPS analysis (row 3) for the forecast tau of 1800 UTC 17 May 2004 (0000 UTC 18 May 2004) for GFDN (NOGAPS). First column illustrates the 00-h analysis fields and the second column illustrates 78-h (72-h) forecast fields for GFDN (NOGAPS). Verifying TC position indicated by star.

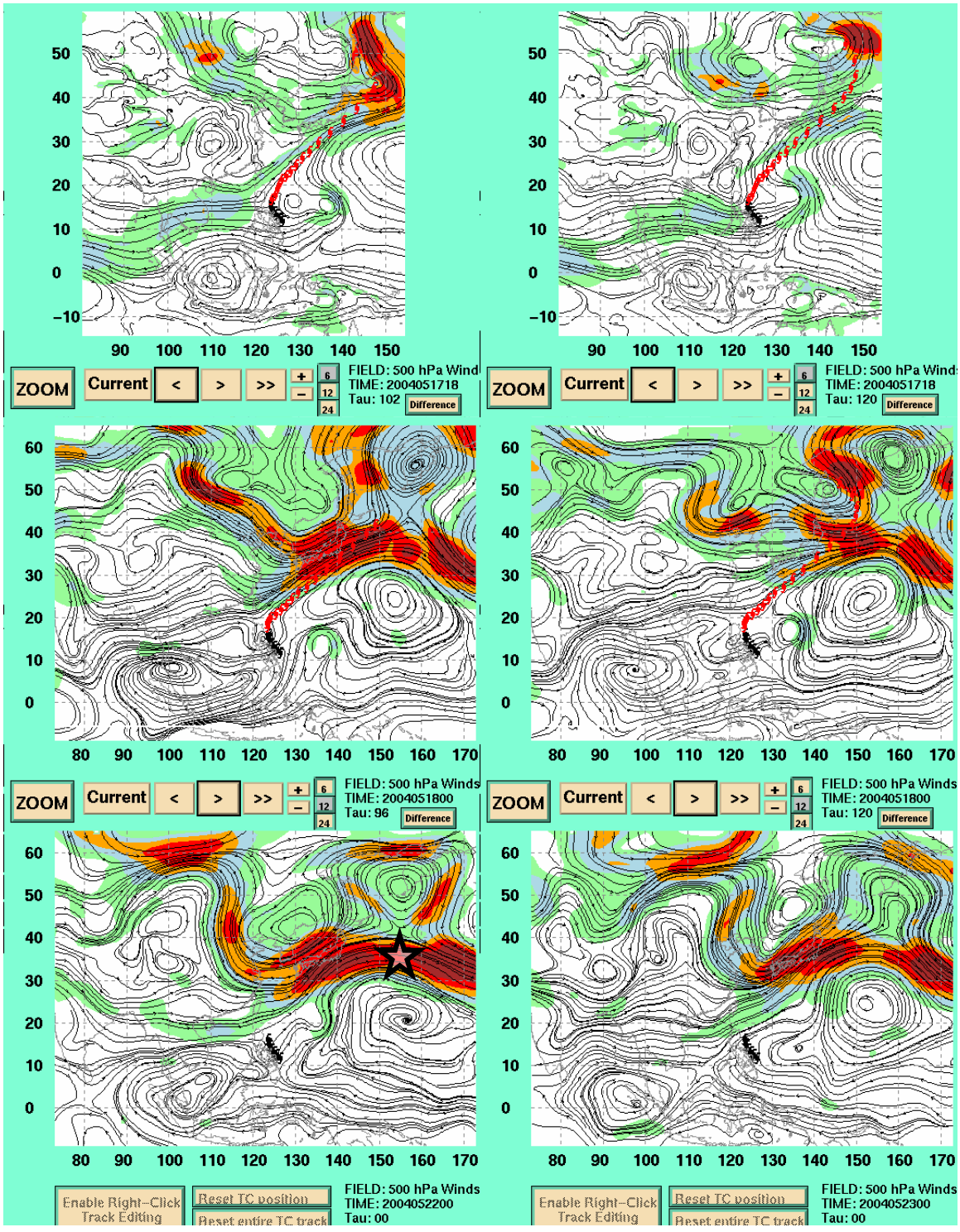

Figure 21. 500-mb streamline and isotach forecast fields for 04W by GFDN (row 1) and NOGAPS (row 2) and verifying 00-h NOGAPS analysis (row 3) for 1800 UTC 17 May 2004 (0000 UTC 18 May 2004) for GFDN (NOGAPS). First column illustrates the 102-h (96-h) forecast fields for GFDN (NOGAPS) and the second column illustrates 120-h forecast. Since 126-h forecast was not available for GFDN, the 120-h forecast is substituted.

2. Midlatitude System Evolutions (MSE)

a. Description

While 75% (72%) of all large 120-h errors by NOGAPS (GFDN) in 2004 were due to midlatitude influences, 52% (65%) of those large errors were due to Midlatitude System Evolutions (MSEs). As described in Carr and Elsberry (2000b), the fundamental idea of MSEs is one of changes to the TC steering flow due to development, dissipation, and/or movement of midlatitude circulations (cyclones, troughs, anticyclones, ridges) that occur essentially independent of the TC. The four conceptual error models that MSEs encompass are: (i) Excessive or Insufficient Midlatitude Cyclogenesis (E-MCG, I-MCG); (ii) Excessive or Insufficient Midlatitude Cyclolysis (E-MCL, I-MCL); (iii) Excessive or Insufficient Midlatitude Anticyclogenesis (E-MAG, I-MAG); and (iv) Excessive or Insufficient Midlatitude Anticyclolysis (E-MAL, I-MAL). A generalized conceptual model of MSEs is presented below (Figure 22).

Before MCG takes place, the TC labeled A in Figure 22a is south of the subtropical ridge axis and is in Standard/Tropical Easterlies pattern/region. During MCG [Figure 22 (a) to (b)], TC A undergoes a transition to the Standard/Poleward Flow pattern/region as the developing midlatitude trough or cyclone breaks the ridge and creates an environment of poleward flow in the vicinity of the TC (Figure 22b). A vigorous MCG event could change the direction of the environmental steering flow and result in a more poleward rather than westward track as depicted by the transition from (a) to (b) in Figure 22. Similarly, TC B is poleward of the subtropical ridge axis (Figure 22a) and moving northeastward in Midlatitude/Poleward Flow. The occurrence of MCG can cause both direction and/or speed changes of the TC. If MCG only alters the translation speed of the TC, then it will remain in a Midlatitude/Poleward Flow. To describe the process of MCL, the reader should simply reverse the order of MCG [i.e., (b) to (a)] depicted in Figure 22 (Carr and Elsberry 2000b).

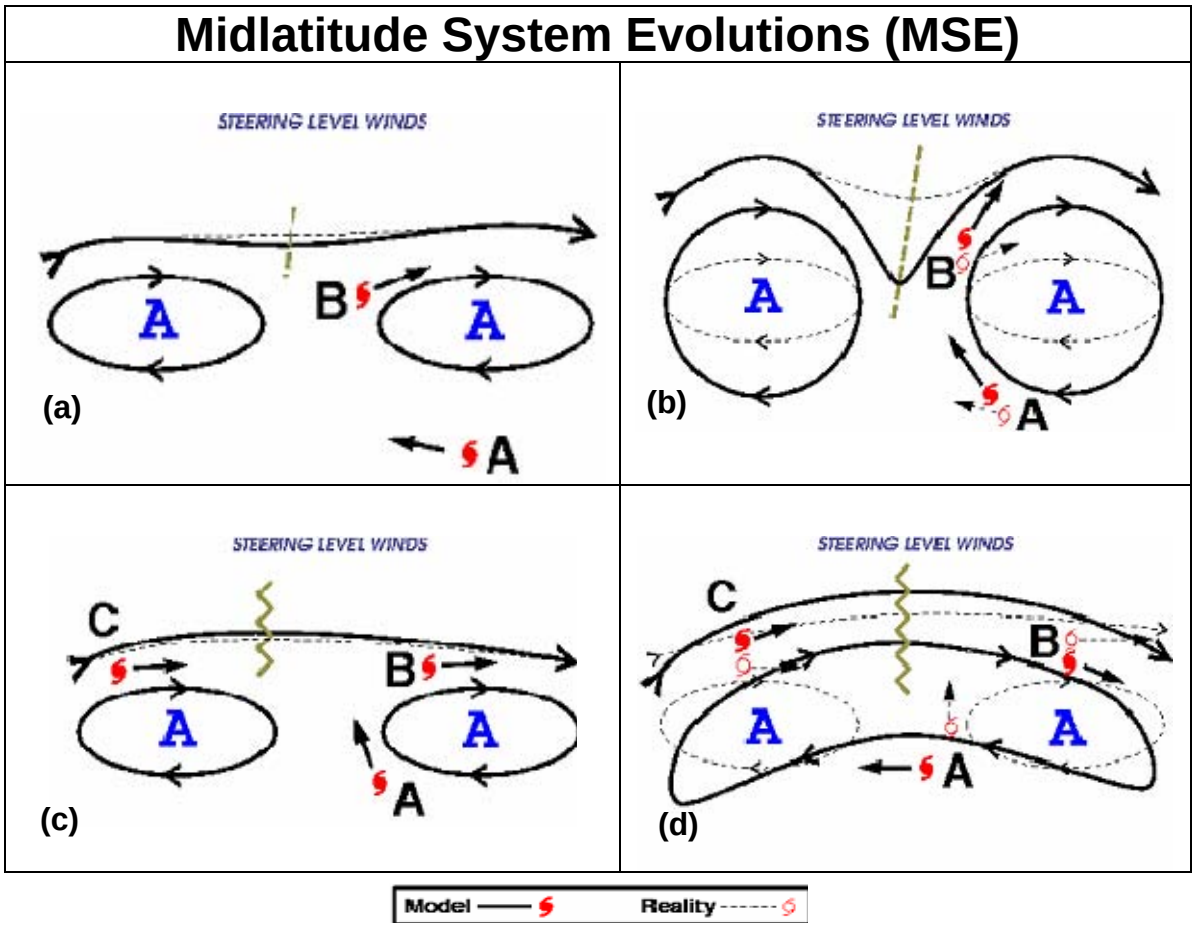

Figure 22. Schematics of the MSEs that may lead to large TC track errors. The deepening of the midlatitude trough from (a) to (b) depicts MCG and the reverse order [(b) to (a)] implies MCL. Similarly, the midlatitude anticyclone change poleward of the TC from (c) to (d) depicts MAG and the reverse order [(d) to (c) implies MAL (from Carr and Elsberry 2000b).

When MAG [Figure 22, (c) to (d)] takes place, a TC labeled A in Figure 22c that has been tracking northward in the Standard/Poleward flow southeast of the col in the subtropical ridge may be turned more westward as the developing midlatitude ridge or anticyclone increases the strength of the subtropical ridge poleward of TC A. If MAG builds the ridge sufficiently, then the TC will undergo a transition to a Standard/Tropical Easterlies or even a Standard/Equatorward Flow pattern/region (see Appendix, Figure 34). A vigorous MAG event could change the direction of the environmental steering flow and result in a more westward or equatorward rather than poleward track as depicted in the transition from (c) to (d) in Figure 22. By contrast, TC B is north

of the subtropical ridge axis and under the influence of Midlatitude/Midlatitude Westerlies flow (Figure 22c). When MAG occurs, TC B may undergo direction and/or speed changes as it did in MCG. If MAG only alters the translation speed of TC B, then it will remain in a Midlatitude/ Midlatitude Westerlies Flow. To describe the process of MAL, the reader should simply reverse the order of MAG [i.e., (d) to (c) depicted in Figure 22] (Carr and Elsberry 2000b).

If any of the MSEs are predicted to occur to a greater (lesser) extent by the model than in reality such that a significant track error results, then the prefix of excessive (E) (insufficient (I)) is assigned to the event. For example, for a TC moving westward in Standard/Tropical Easterlies, if the model depicts the trough to be too weak, and does not break down the subtropical ridge such that it results in the TC remaining on an westward track, then insufficient midlatitude cyclogenesis (I-MCG) has occurred.

It is stressed that the four MSE depictions in Figure 22 are simply an idealized representation of such events. These should be considered flexible templates in that they can be manipulated to fit all of the complex shapes and amplitudes of the midlatitude synoptic circulations.

b. Frequency and Characteristics

As mentioned in the introduction of MSEs, large 120-h errors due to erroneous MSE events accounted for 51% or 83 of 162 (67% or 91 or 135) of all large errors in NOGAPS (GFDN). The most common MSE to occur was I-MCG with 53 (46) occurrences in NOGAPS (GFDN) (Table 7, columns 3 and 4), which accounts for 33% and 34% of all large 120-h errors in NOGAPS and GFDN, respectively. The E-MCG error mechanism was the second most commonly occurring MSE event and accounted for 6 (28) occurrences of large errors in NOGAPS (GFDN). The two-sided nature in GFDN (and to a lesser extent in NOGAPS) is unfortunate in that the forecaster must watch for both variations of the MCG error to occur, unlike the RVS error that only occurs in the excessive state (Table 5). The E-MCL error mechanism accounted for 14 degraded forecasts combined in NOGAPS and GFDN and there were no occurrences of I-MCL The E-MAG mechanism accounted for 6 (9) errors in NOGAPS (GFDN),

while I-MAG accounted for six occurrences in GFDN. The MAL error mechanism only affected NOGAPS with 2 (4) events occurring excessively (insufficiently).

Phenomenon name	Acronym	No. of NOGAPS forecasts*	No. of GFDN forecasts*
Midlatitude cyclogenesis	**MCG**	**6-53**	**28-46**
Midlatitude cyclolysis	**MCL**	**12-0**	**2-0**
Midlatitude anticyclogenesis	**MAG**	**6-0**	**9-6**
Midlatitude anticyclolysis	**MAL**	**2-4**	**0-0**
Total of all degraded forecasts		**83**	**91**

Table 7. Number of NOGAPS and GFDN forecast integrations affected by MSE events. MSE events were responsible for 83 of 162 (91 of 135) degraded NOGAPS (GFDN) forecasts in 2004. First (second) number indicates the excessively (insufficiently) occurring events.

The obvious conclusion that can be drawn from the numerous occurrences of MCG events is that both NOGAPS and GFDN had significant problems both in the development and movement of midlatitude troughs. It is beneficial for the forecaster to know that once the NOGAPS and/or GFDN model started displaying either E-MCG or I-MCG, it normally occurred in successive model integrations and would not switch from excessive to insufficient or visa versa without first correcting the problem in an intermediate integration. That is, the error mechanism would end for at least one model integration before switching to the other variation of the error mechanism.

To draw a more generalized conclusion of the MSE tendencies of NOGAPS and GFDN, the data in Table 7 are divided into two distinct groups. The first group is comprised of I-MCG, E-MCL, E-MAG, and I-MAL events, which are all representative of erroneously predicted environmental flow that is dominated by a ridge. The second group is comprised of E-MCG, I-MCL, I-MAG, and E-MAL events, which are all representative of erroneously predicted environmental flow that is dominated by a trough. These results suggest that regarding MSE events in NOGAPS, they were one-sided in that while the model was indicating the environmental flow of the TC would be dominated by the ridge (Table 8), it was revealed in the retrospective study to be dominated in reality by a trough. Unfortunately, a similar conclusion cannot be drawn for GFDN as the

MSE events in GFDN were two-sided. That is, there were a large number of excessive and insufficient MSE events in GFDN (Table 7).

Phenomenon	No. of NOGAPS forecast	No. of GFDN forecasts
Erroneous prediction of environmental flow dominated by a ridge	**75**	**51**
Erroneous prediction of environmental flow dominated by a trough	**8**	**34**
Total of all degraged forecasts	**83**	**91**

Table 8. Data from Table 7 generalized into two groups. The first group is comprised of I-MCG, E-MCL (trough intensity too weak) and E-MAG, I-MAL (ridge intensity too strong) events, which are all representative of erroneously predicted environmental flow that is dominated by a ridge. The second group is comprised of E-MCG, I-MCL (trough intensity too strong) and I-MAG, and E-MAL (ridge intensity too weak) events, which are all representative of erroneously predicted environmental flow that is dominated by a trough.

Because of the two-sided errors in GFDN, no further conclusions could be drawn as to systematic biases of the GFDN model always over- or under-predicting the amplitude or translation of the midlatitude features. This was true when comparing events occurring with an individual model and even concurrent events between NOGAPS and GFDN. Although a seasonal pattern was also examined, again no pattern was found. A major change in the convective momentum flux parameter in the NOGAPS Emanuel parameterization scheme was made on 8 September 2004 (J. Goerss, NRL—Monterey, personal communication), but the impact of this change in convective momentum flux did not lead to any obvious track error differences for western North Pacific TCs. Thus, a more in-depth study of just the combined total of the 174 falsely predicted events by NOGAPS and GFDN (Table 8) is needed to discover the underlying causes of the errors.

c. Case Studies

(1) I-MCG and E-MCL. The occurrence of I-MCG (E-MCL) by GFDN (NOGAPS) will be illustrated by a case study of the 1800 UTC 17

October 2004 forecast for TC Tokage (27W). The I-MCG (E-MCL) error mechanism was responsible for degrading the GFDN (NOGAPS) forecasts for Tokage over a 2-day period. As illustrated in Figure 23, both the GFDN and NOGAPS track forecasts are undergoing a recurvature with a transition from Standard/Poleward Flow to Midlatitude/Poleward Flow. In comparison to the best track, both have small cross-track errors but very large along-track errors between the 120-h forecast positions and the verifying 120-h position. These along-track errors are due to the slow TC translation speed in each model. The subsequent discussion will be used to explain how: (a) I-MCG is causing the forecast error in GFDN; (b) E-MCL is causing the forecast error in NOGAPS; and then in (c) a brief summary of the forecast period will be given.

(a) I-MCG. This example will demonstrate, for the forecast period of 1800 UTC 17 October 2004, how the most frequently occurring error mechanism, I-MCG, caused the GFDN track forecast error. By 30 h, the trough labeled G1 in the GFDN forecast fields (Figure 24, row 1, column 2) is not nearly as deep and slightly lags the trough (labeled V1) in the verifying analysis (Figure 24, row 3, column 2). By 54 h, the GFDN forecast of trough G1 is still too weak and does not keep the ridge to the northeast of Tokage from building in (Figure 25, row 1, column 1). By 78 h, it has become apparent that the ridge to the northeast of Tokage is the dominant influence on the environmental steering flow, and trough G1 has moved east without “catching” Tokage (Figure 25, row 1 column 2). The verifying analysis for the same time illustrates that Tokage has been caught in the flow of trough V1 (Figure 25, row 3, column 1). At 102 h, a ridge now exists between G1 and Tokage, and the trough labeled G2 is approaching from the west (Figure 26, row 1, column 1). The verifying analysis at 102 h illustrates that Tokage is becoming extratropical as it is interacting with V1 (Figure 26, row 3, column 2). By 126 h in the GFDN forecast (Figure 26, row 1, column 2), Tokage has now merged with the trough of G2, but the verifying 126-h analysis illustrates instead that Tokage has been absorbed into the 700-mb flow of V1. Thus, the I-MCG error mechanism is assigned to the GFDN forecast because it had under-predicted the amplification of the trough V1 and

thus did not move Tokage into the midlatitude westerlies, which resulted in a very large 120-h error (Figure 23). Although the forecast fields for the UKMO model are not available, the similar position (U in Figure 23) would support a similar error.

(b) E-MCL. This example will demonstrate how the E-MCL error mechanism can cause a similar forecast track tendency to I-MCG, but the forecast track error is due to a translation speed of the midlatitude trough that is too fast. By 24 h, the trough labeled N1 in the NOGAPS forecast fields (Figure 24, row 2, column 2) and the same trough labeled V1 in the verifying analysis (Figure 24, row 3, column 2) have approximately the same amplitude and latitudinal extent. Both NOGAPS and the verifying analysis have approximately the same forecast position for Tokage. By 48 h, trough N1 in the NOGAPS forecast has extended southward to approximately 32N and has translated across the Sea of Japan to encroach upon southern Japan (Figure 25, row 2, column 1). However, the same trough V1 in the verifying analysis has translated only as far east as Manchuria and has receded to 40N (Figure 25, row 3, column 1). The faster movement of N1 is causing the trough to move east of Tokage and results Tokage and N1 do not to interact.

By 72 h, it has become apparent that N1 has moved east without “catching” Tokage (Figure 25, row 2, column 2), while the verifying analysis for the same time illustrates that Tokage has been caught in the flow of V1 (Figure 25, row 3, column 2). At 96 h, trough N1 is no longer a major influence on Tokage in the NOGAPS forecast and the trough marked N2 is approaching from the west, while the verifying analysis at 96 h illustrates that Tokage is becoming extratropical after it has interacted with V1 (Figure 26, rows 2 and 3, column 1). By 120 h in the NOGAPS forecast (Figure 26, row 2, column 2), Tokage is now caught up in the flow of trough N2. Whereas the verifying 120-h analysis verifies the presence of N2 (labeled V2), it also illustrates Tokage has now been absorbed into the 700-mb flow of V1 (Figure 26, row 3, column 2).

Because NOGAPS predicted a trough that was too deep, one might think that E-MCG was the error mechanism. However, error

mechanisms describe how poorly-depicted meteorological features affect the environment, steering flow, and track of the TC. In this case, the trough was too deep, but the track error was due to the too fast translation of the trough and caused the TC to encounter a ridge instead of a trough in the middle stage of the forecast integration. The E-MCL error mechanism is therefore assigned to the NOGAPS model. Although NOGAPS does predict recurvature and poleward acceleration it is due to the incorrect interaction with trough N2.

(c) Summary. A key result for the forecaster is that both I-MCG and E-MCL contributed to numerous forecast degradations in both GFDN and NOGAPS. They occurred so frequently that it would behoove the forecaster to investigate how the model in question is representing the midlatitude trough compared to the other models when the NOGAPS and/or GFDN track forecast is an outlier. It is also important for the forecaster to recall that once the error appears, it will likely afflict the model in question for several successive integrations. Thus the forecaster should monitor the track trend display.

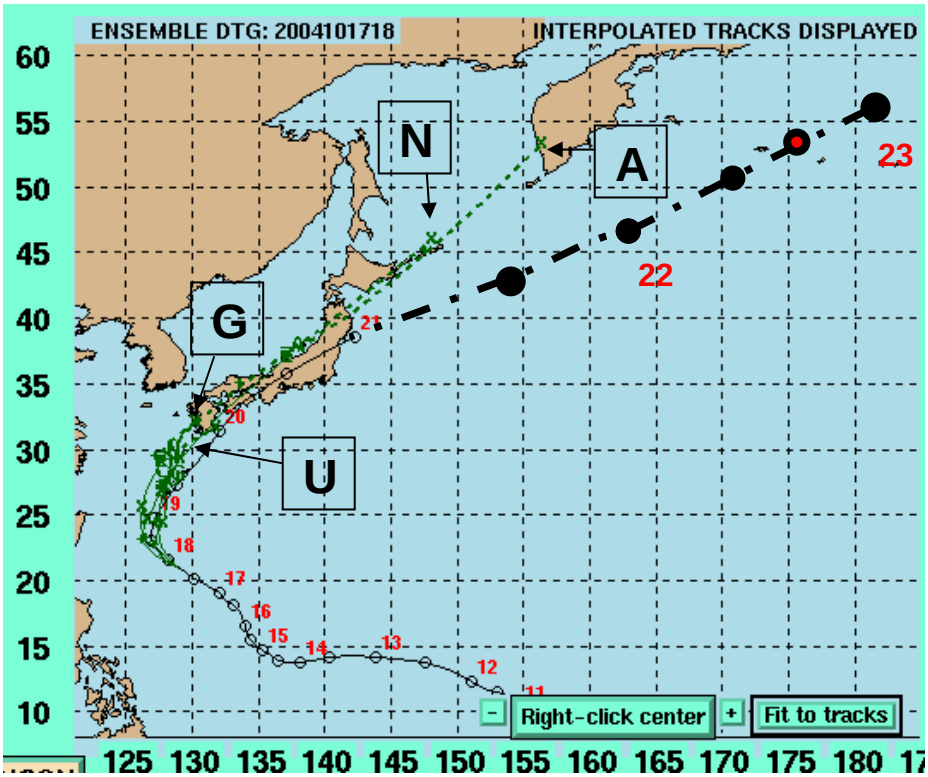

Figure 23. Interpolated forecast tracks for 27W by NOGAPS (N), GFDN (G), UKMO (U) and GFS (A) for the forecast period of 1800 UTC 17 October 2004. The solid sections of the forecast tracks represent the 00-h through 72-h forecast while the thin dashed sections represent the 72-h through 120-h forecast. The solid line with open circles and corresponding dates represents the TC best track. The extended best track verification is represented by the heavy dashed line and solid circles with respective dates. The verifying 120-h position is indicated by the red circle with the heavy black outline.

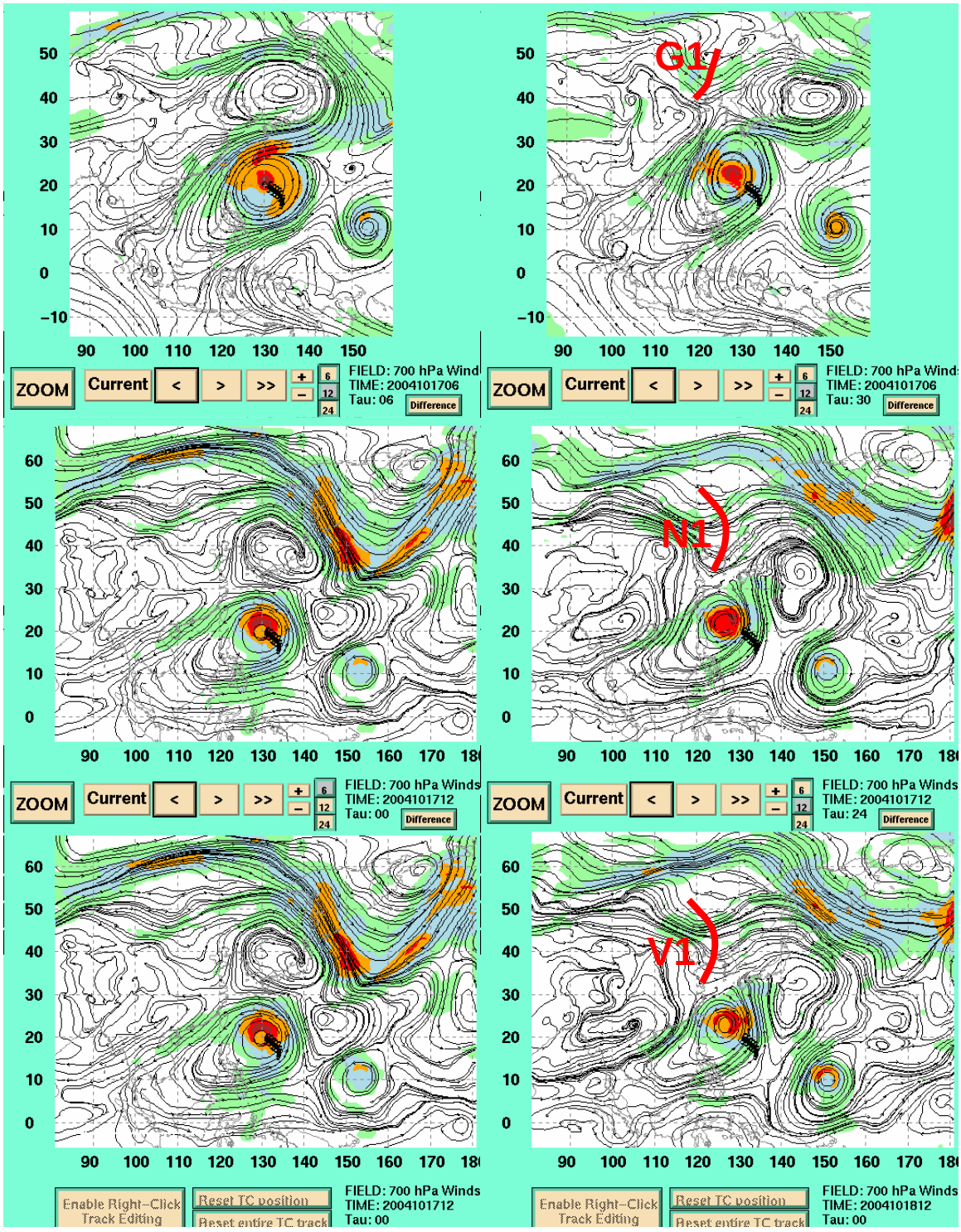

Figure 24. 700-mb streamline and isotach forecast fields for 27W by GFDN (row 1) and NOGAPS (row 2) and verifying 00-h NOGAPS analysis (row 3) for the forecast tau of 0600 UTC 17 October 2004 (1200 UTC 17 October 2004) for GFDN (NOGAPS). First column illustrates the 06-h forecast field for GFDN (00-h analysis fields for NOGAPS) and the second column illustrates 30-h (24-h) forecast fields for GFDN (NOGAPS).

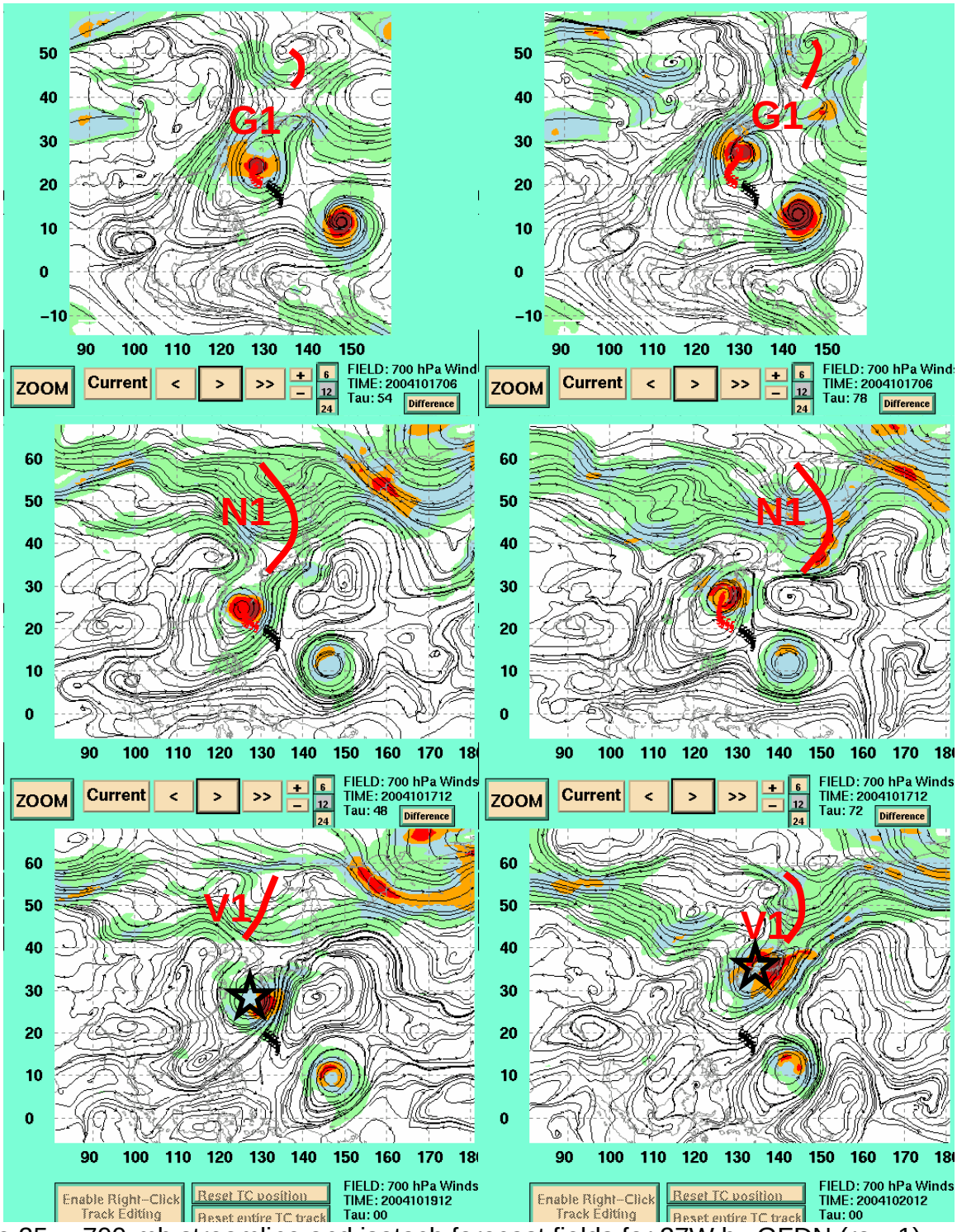

Figure 25. 700-mb streamline and isotach forecast fields for 27W by GFDN (row 1) and NOGAPS (row 2) and verifying 00-h NOGAPS analysis (row 3) for the forecast tau of 0600 UTC 17 October 2004 (1200 UTC 17 October 2004) for GFDN (NOGAPS). First column illustrates the 54-h (48-h) forecast fields and the second column illustrates 78-h (72-h) forecast fields for GFDN (NOGAPS). Verifying TC position indicated by the black star.

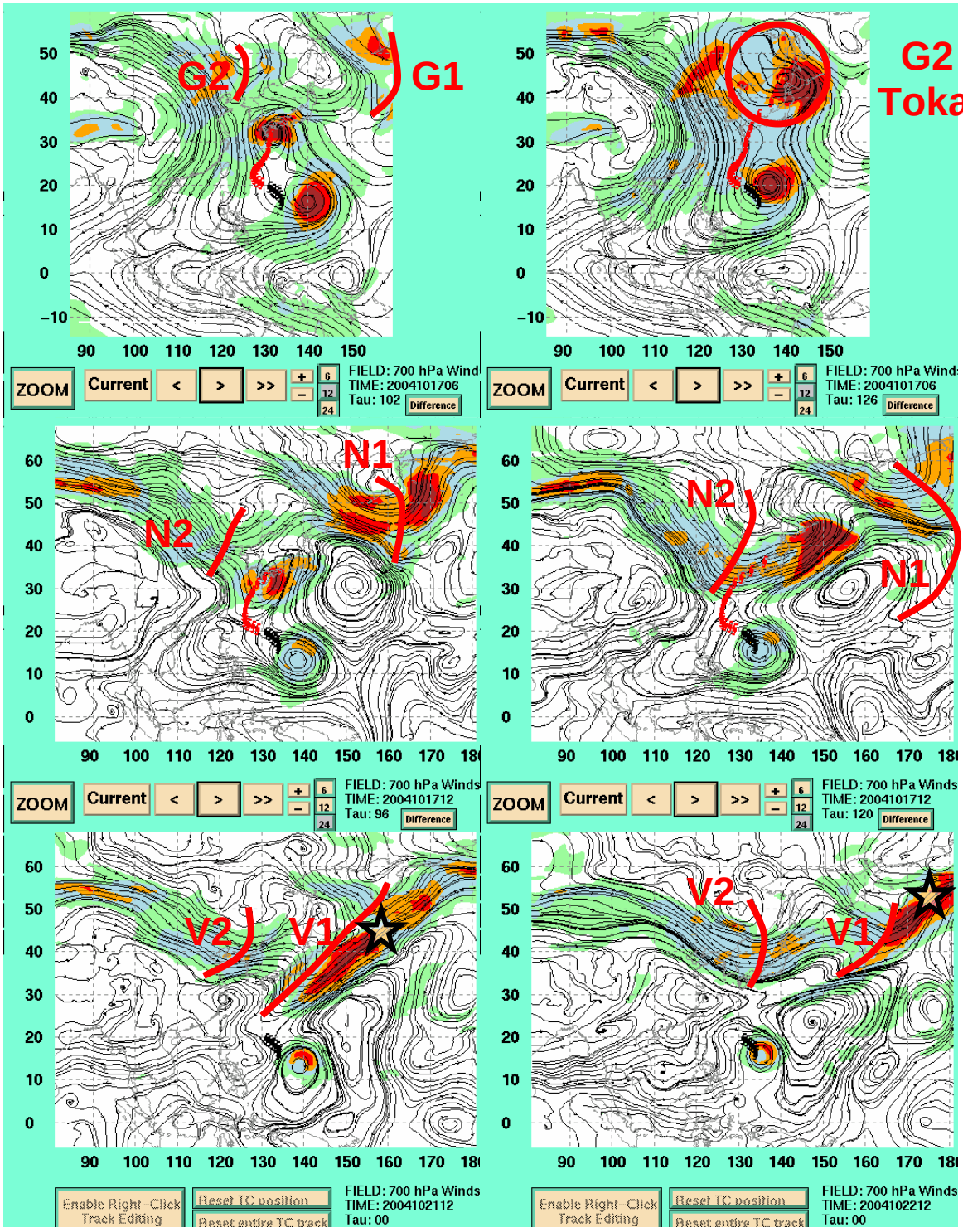

Figure 26. 700-mb streamline and isotach forecast fields for 27W by GFDN (row 1) and NOGAPS (row 2) and verifying 00-h NOGAPS analysis (row 3) for the forecast tau of 0600 UTC 17 October 2004 (1200 UTC 17 October 2004) for GFDN (NOGAPS). First column illustrates the 102-h (96-h) forecast fields and the second column illustrates 126-h (120-h) forecast fields for GFDN (NOGAPS). Verifying TC position indicated by the black star.

(2) E-MCG. The E-MCG error mechanism was the second most frequently occurring error mechanism during the 2004 season and affected 6 (28) forecasts in NOGAPS (GFDN). Because GFDN was more susceptible to E-MCG, a case study of E-MCG in GFDN will be illustrated.

The forecast tracks for the forecast of 1800 UTC 15 May 2004 for TC Nida (04W) indicate that TC Nida is tracking faster in both GFDN and UKMO than in the NOGAPS and GFS (Figure 27). The 6-h forecast of GFDN (Figure 28, row 1, column 1) illustrates that the midlatitude trough over eastern China is well represented compared to the verifying analysis (Figure 28, row 3, column 1).

By 60 h, the trough in GFDN extends further south and is approaching the coast of China (Figure 28, row 1, column 2), whereas the trough in the verifying analysis does not have such a southern extent and is still over central China (Figure 28, row 3, column 2). By 102 h, it has become evident that the TC has merged with the deeper, faster-moving trough in GFDN (Figure 29, row 1, column 1), while the verifying analysis indicates the trough is just now coming of the coast of China, and the TC and trough are still separate entities (Figure 29, row 3, column 1). Finally at 126 h (Figure 29, row1, column 2), the early acceleration of the TC as it became embedded in the flow of the trough has caused the TC to be much farther poleward than in the verifying analysis (Figure 29, row 3, column 2). In essence, the E-MCG mechanism occurs when the model predicts the midlatitude trough to intensify to a greater extent than verifies in reality and causes the TC to recurve sooner than expected.

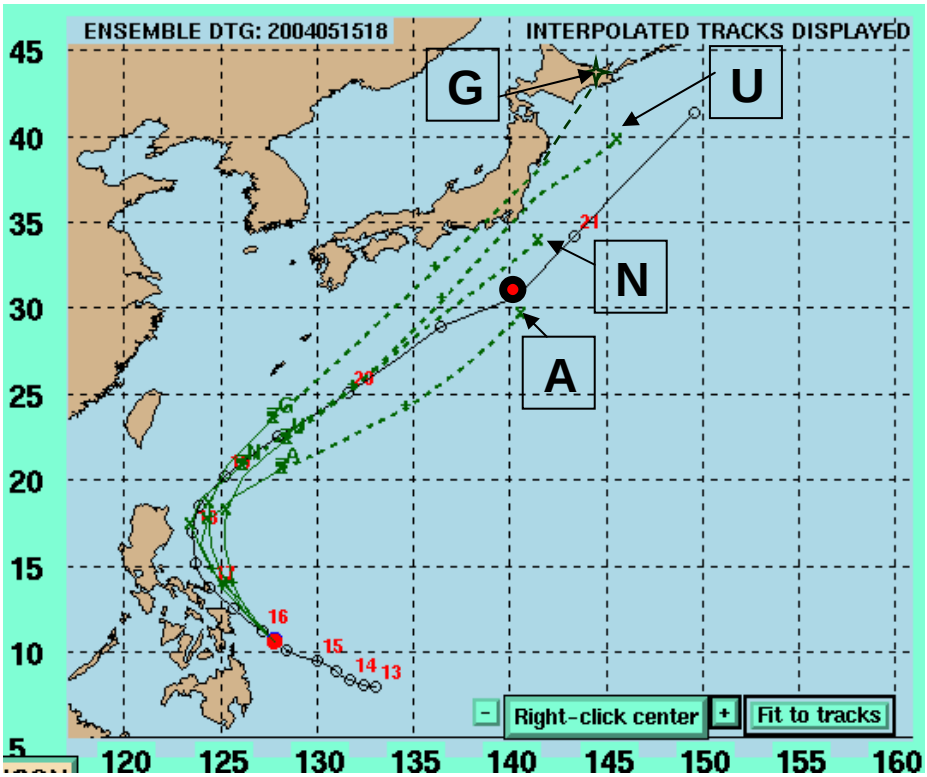

Figure 27. Interpolated forecast tracks for 04W by NOGAPS (N), GFDN (G), UKMO (U), and GFS (A) for the forecast of 1800 UTC 15 May 2004. The solid sections of the forecast tracks represent the 00-h through 72-h forecast while the dashed sections represent the 72-h through 120-h forecast. The solid line with open circles and corresponding dates represents the TC best track. The verifying 120-h position is indicated by the red circle with the heavy black outline.

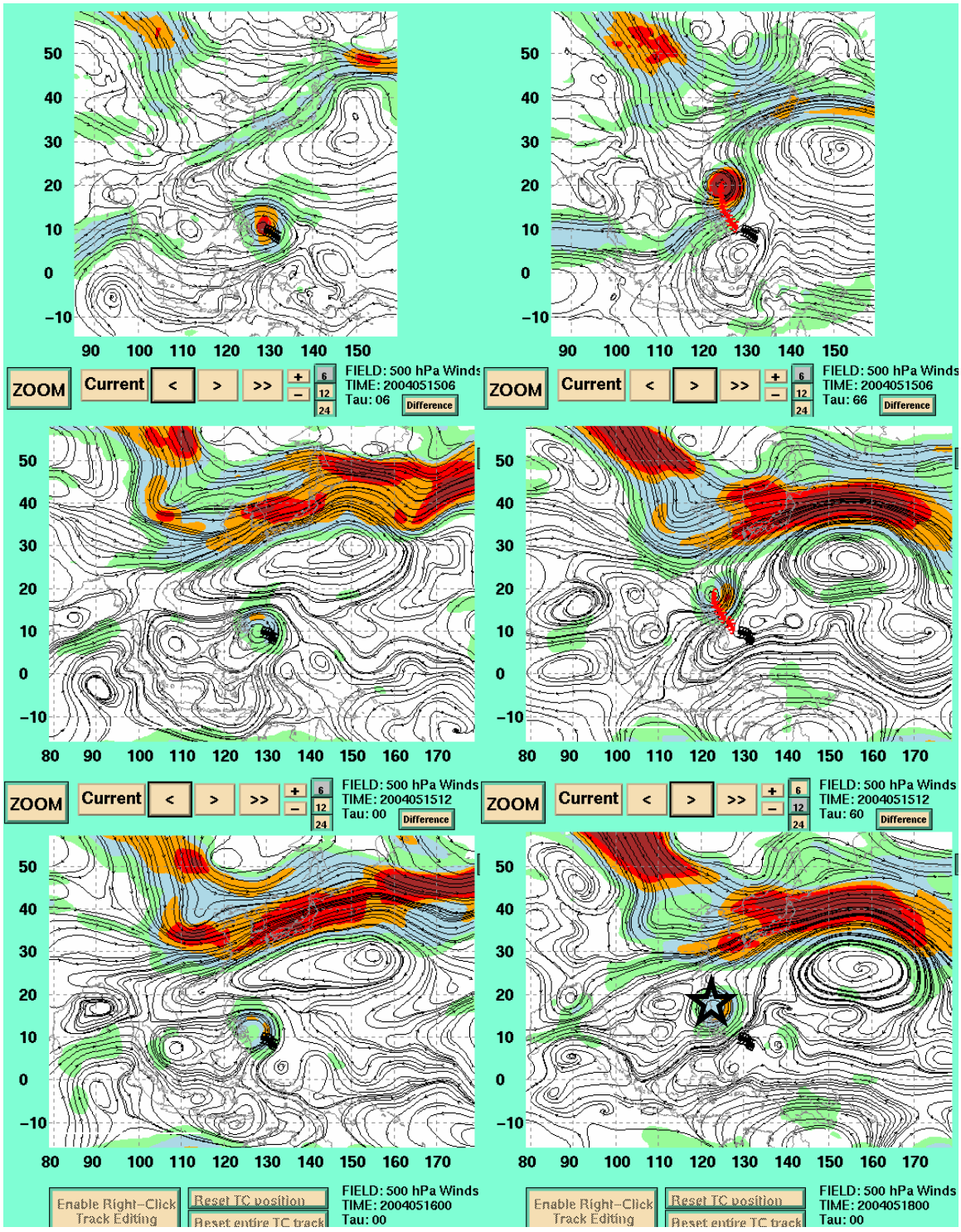

Figure 28. 500-mb streamline and isotach forecast fields for 04W by GFDN (row 1) and NOGAPS (row 2) and verifying 00-h NOGAPS analysis (row 3) for the forecast of 0600 UTC 15 May 2004 (1200 UTC 15 May 2004) for GFDN (NOGAPS). First column illustrates the 06-h forecast (00-h analysis fields) and the second column illustrates 30-h (24-h) forecast fields for GFDN (NOGAPS). Verifying TC position indicated by the star.

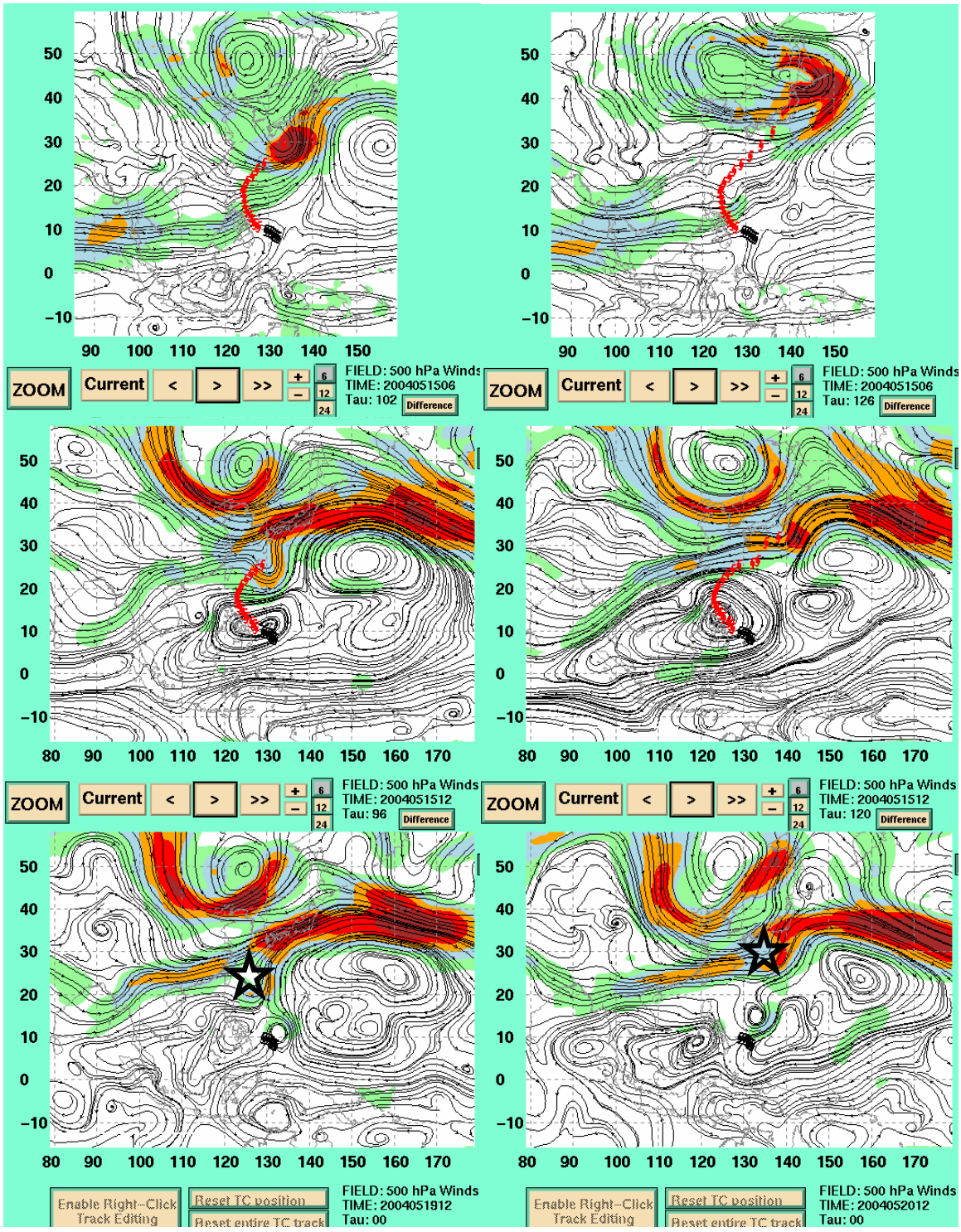

Figure 29. 500-mb streamline and isotach forecast fields for 04W by GFDN (row 1) and NOGAPS (row 2) and verifying 00-h NOGAPS analysis (row 3) for the forecast of 0600 UTC 15 May 2004 (1200 UTC 15 May 2004) for GFDN (NOGAPS). First column illustrates the 102-h (96-h) forecast fields and the second column illustrates 126-h (120-h) forecast fields for GFDN (NOGAPS). Verifying TC position indicated by the star.

(3) E-MAG. The E-MAG error mechanism was the third most frequently occurring error. It affected five separate TCs in the GFDN forecasts during the 2004 season while only one TC had this error in the NOGAPS forecasts. Because GFDN is more susceptible to E-MAG, a case study of E-MAG occurring in GFDN will be illustrated.

The track forecasts for the forecast of 0600 UTC 2 September 2004 for TC Songda (22W) indicate that the GFDN and UKMO tracks are outliers to the far left of the other 120-h tracks (Figure 30). Although the subtropical ridge and midlatitude trough are well represented in the 06-h GFDN forecast (Figure 31, row 1, column 1) compared to the verifying analysis (Figure 31, row 3, column 1), there is already an indication that the midlatitude anticyclone to the northwest of the TC is too strong. By 42 h, this midlatitude anticyclone is predicted in GFDN to develop over the Yellow Sea (Figure 31, row 1, column 2), but this is not substantiated in the verifying analysis (Figure 31, row 3, column 2). This midlatitude anticyclone then translates across the Korean Peninsula and merges with the subtropical ridge to form a substantial ridge to the north of Songda (Figure 32, row 1, column 1), which keeps it on a predicted westward track. The verifying analysis reveals instead that this midlatitude anticyclone is only a ridge at 700 mb and does not add appreciably to the strength of the subtropical ridge. Thus, Songda actually undergoes a transition to a Standard/Poleward Flow pattern/region because the dominant steering current is the subtropical ridge to the east-northeast of the TC (Figure 32, row 3, column 1). By 126 h, (Figure 32, row 1, column 2), the earlier westward and equatorward error in the track forecast has resulted in the 126-h GFDN position that is well south and west of the verifying position (Figure 30). This misplaced TC then has little interaction with the passing midlatitude trough and is instead dominated by another strong midlatitude anticyclone that is not substantiated by the 120-h NOGAPS forecast and the verifying analysis (Figure 32, rows 2 and 3, column 2).

A forecaster examining the model track forecasts of Figure 30 in real-time would see two clusters. The GFDN and UKMO models form a

cluster that implies the TC will remain in a Standard/Tropical Easterlies Flow pattern/region and track westward for the duration of the forecast period. Meanwhile, NOGAPS and GFS predict that Songda will transition to Standard/Poleward Flow pattern/region and turn poleward after 72 h. If GFDN is seriously degraded by an MSE, then the error mechanism must be one involving environmental flow dominated by a ridge. It was found during the 2004 season that there were 57 GFDN forecasts degraded by the erroneous prediction of environmental flow dominated by a ridge (Table 8), so the forecaster should suspect the GFDN model is in error. However, the key to making a good forecast even better is properly diagnosing the NOGAPS forecast too. Because NOGAPS predicts a poleward track, the forecaster should initially suspect that the forecast could be degraded by an MSE involving an environmental flow dominated by a trough. However, during 2004, poor NOGAPS forecasts were overwhelmingly degraded by overly weak troughs (53 occurrences of I-MCG compared to 6 occurrences of E-MCG in Table 7). This results in erroneous track forecasts that remain in the tropics too long of a time. Rarely does NOGAPS predict a track that is too far poleward when an MSE scenario is involved, so the forecaster should know that the NOGAPS forecast is probably a decent forecast compared to the others.

As it turned out, even the poleward-turning NOGAPS was also degraded by the ridge dominated error mechanism E-AG, although not to the extent of GFDN and not enough to be counted as a large error (>500 n mi) at 120 h. By 36 h, the NOGAPS forecast (Figure 31, row 2, column 2) indicates a weaker anticyclone northwest of Songda over Manchuria than depicted in the GFDN forecast (Figure 31, row 1, column 2). However, this NOGAPS-predicted anticyclone was still stronger than the one in the verifying analysis (Figure 31, row 3, column 2). This excessive anticyclone is subtle in NOGAPS, but the result is still a poor NOGAPS forecast, and future inspection of UKMO and GFS fields will likely reveal that they too were degraded by E-MAG.

Although this forecast scenario is difficult in that the actual TC track is to the east of all four model predictions, this bifurcation scenario

between a recurvature track cluster and a westward track cluster is one in which the forecaster can add value over a non-selective consensus track forecast by correctly rejecting the erroneous cluster containing GFDN to create an improved selective consensus. The forecaster can then potentially improve the selective consensus by realizing that the remaining models have a one-sided tendency to falsely predict an environment that is dominated by a ridge (e.g., NOGAPS does not move poleward fast enough). This requires examination of the forecast fields with thorough knowledge of the conceptual model error mechanisms and their frequency.

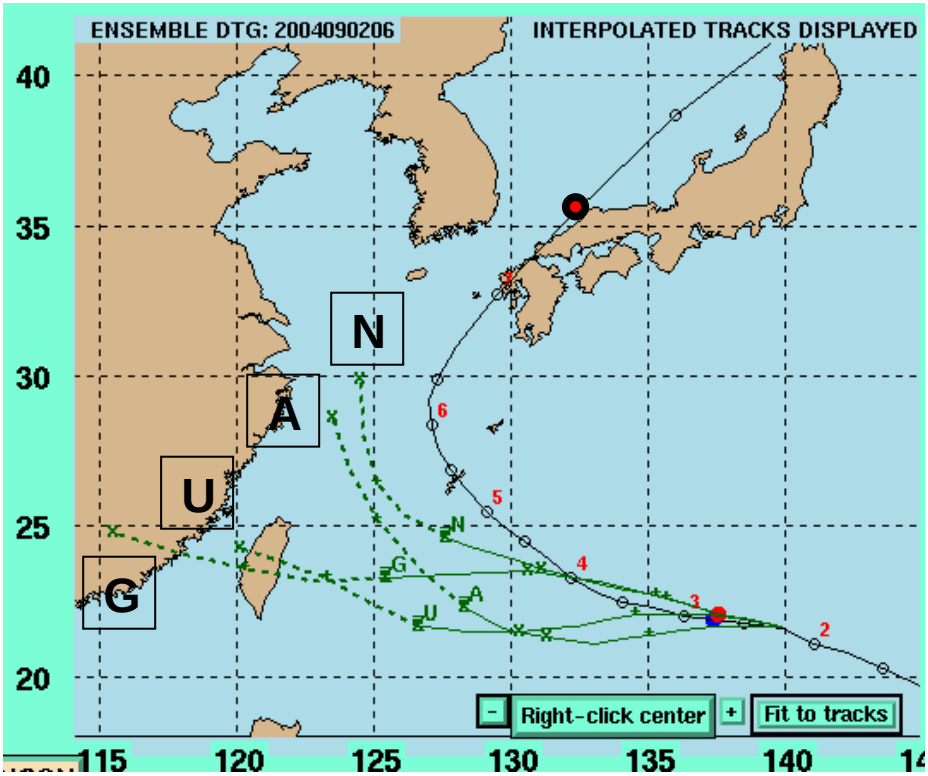

Figure 30. Interpolated forecast tracks for 22W by NOGAPS (N), GFDN (G), UKMO (U), and GFS (A) for the forecast of 0600 UTC 2 September 2004. The solid sections of the forecast tracks represent the 00-h through 72-h forecast while the dashed sections represent the 72-h through 120-h forecast. The solid line with open circles and corresponding dates represents the TC best track. The verifying 120-h position is indicated by the red circle with the heavy black outline.

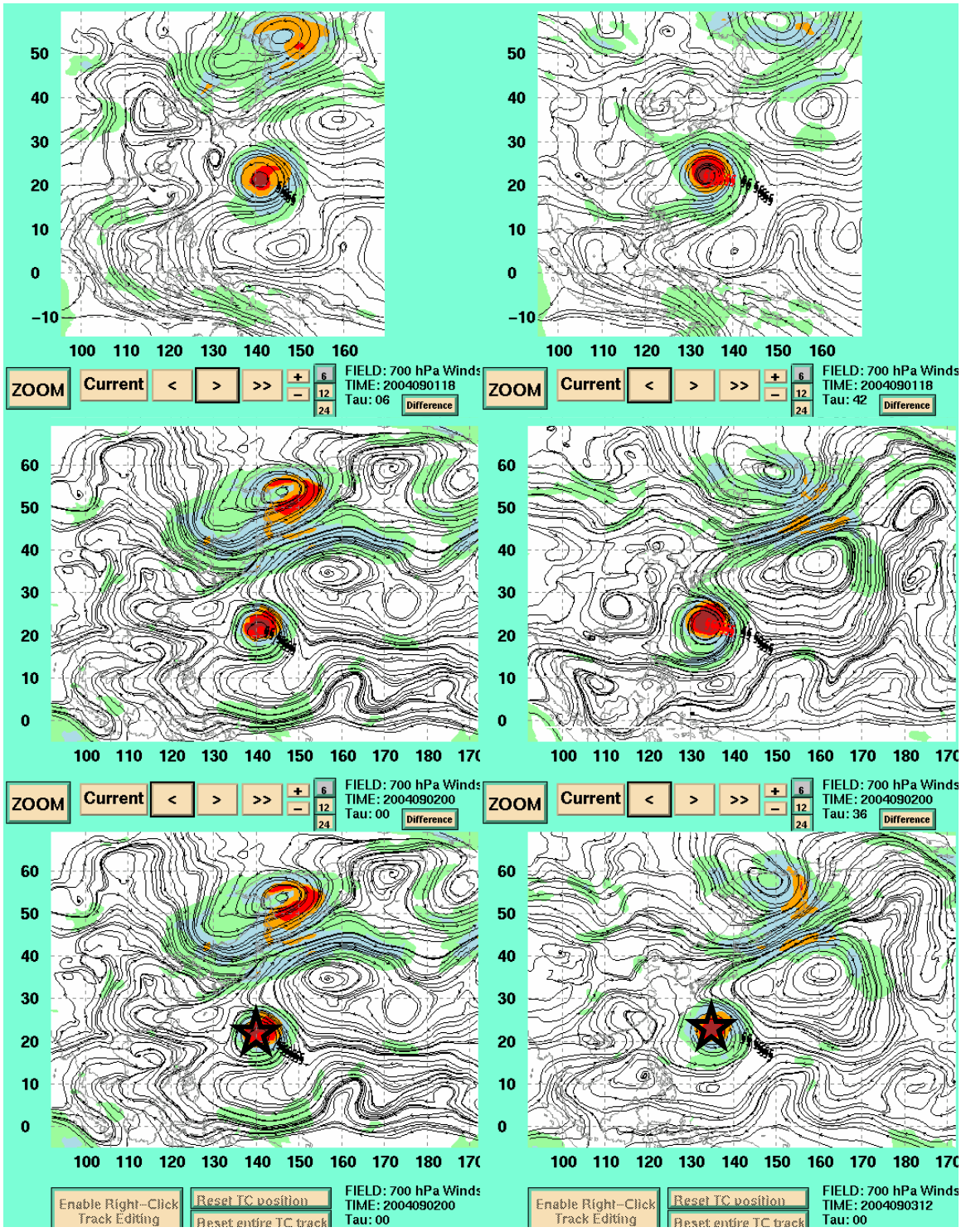

Figure 31. 700-mb streamline and isotach forecast fields for 22W by GFDN (row 1) and NOGAPS (row 2) and verifying 00-h NOGAPS analysis (row 3) for the forecast of 1800 UTC 01 September 2004 (0000 UTC 2 September 2004) for GFDN (NOGAPS). First column illustrates the 06-h forecast (00-h analysis fields) and the second column illustrates 42-h (36-h) forecast fields for GFDN (NOGAPS). Verifying TC position indicated by the star.

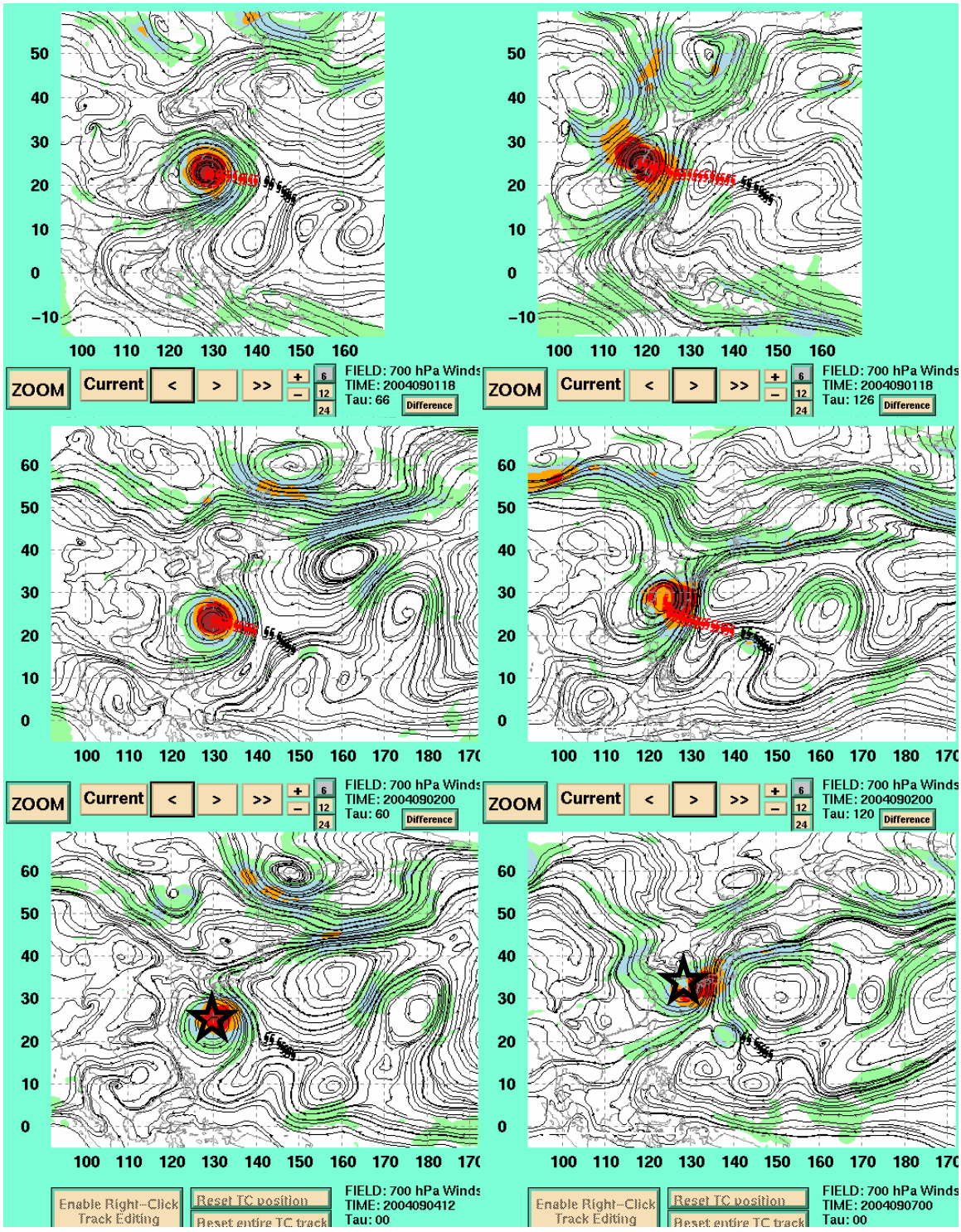

Figure 32. 700-mb streamline and isotach forecast fields for 22W by GFDN (row 1) and NOGAPS (row 2) and verifying 00-h NOGAPS analysis (row 3) for the forecast of 1800 UTC 01 September 2004 (0000 UTC 02 September 2004) for GFDN (NOGAPS). First column illustrates the 66-h (60-h) forecast fields and the second column illustrates 126-h (120-h) forecast fields for GFDN (NOGAPS). Verifying TC position indicated by the star.

3. Response to Vertical Wind Shear (RVS)

a. Description

As discussed in Carr and Elsberry (2000b), the basic assumption of the RVS error conceptual model (Figure 33) is that there is a significant difference in the vertical depth and associated intensity between the actual and model-predicted TC in the presence of a vertically sheared environmental flow. A deeper (less deep) vertical extent of the TC causes the model-predicted TC to have a faster (slower) translation speed (especially in the midlatitude westerlies) than that of the actual TC. Typically, the difference in vertical structure between the model-depicted and actual TC tends to grow with increasing forecast interval, which accentuates the differences in translation speeds, and thus the track errors.

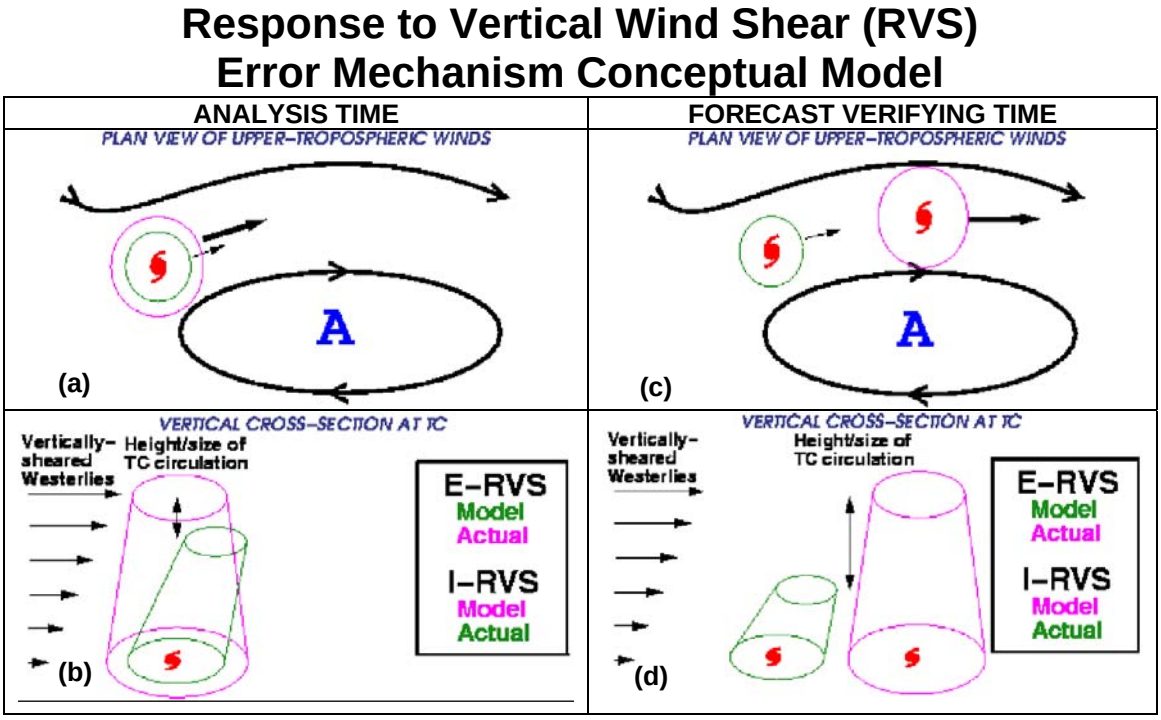

Figure 33. Conceptual model of RVS. (a) Plan view of the 500-mb environmental flow and (b) vertical cross section along the vertical wind shear vector through the TC with different vertical (and presumably horizontal) extents in the model and in nature at analysis time. (c)-(d) Corresponding plan view and vertical cross section at verification time in which E-RVS causes the vortex to be too shallow (d, green) and the track to have a slow bias (c, green). By contrast, an I-RVS error leads to a vortex that is too deep and a fast track bias [magenta lines in (c) and (d)] (from Carr and Elsberry 2000b).

Excessive-RVS (E-RVS) is said to be occurring when the model-depicted TC is too shallow (Figure 33b) and excessively tilted downstream, which will cause the TC to be even more susceptible to vertical shear. When this occurs, the upper (and possibly middle) vortex is sheared from the lower vortex that is then advected by the low-level environmental flow (Figure 30d). Steering by only the low-level flow will then cause a slow bias compared to steering by stronger upper-level flow (Figure 33c). Insufficient-RVS (I-RVS) is said to be occurring when the model-depicted vertical structure of the TC is too deep and upright compared to reality (Figure 33b), which will result in a track forecast that is too fast (Figure 33c).

Carr and Elsberry (2000b) suggested the use of sea-level pressure forecasts to identify either E-RVS or I-RVS. It was found in this study that geopotential heights (not available to Carr and Elsberry in SAFA) at 850, 700, and 500 mb were also a useful tool. Those TCs that had less deep (deeper) vertical structures were found to have less (more) concentric geopotential isopleths at higher isobaric levels. That is, fewer (more) closed geopotential isopleths existed at 500 mb (and 700 mb) for a less deep (deeper) TC.

b. Frequency and Characteristics

The RVS events during the 2004 season were all excessive and occurred only in NOGAPS. These E-RVS events were responsible for 26 degraded forecasts in five TCs during the 2004 season. In all cases, the TC was in the Standard/Poleward Flow or Midlatitude/Poleward Flow with an approaching upper-level midlatitude trough that would provide the vertical wind shear over the TC. A key indication (not included in the Carr and Elsberry (2000b) description) that E-RVS was occurring was when the TC track suddenly switched from a poleward to equatorward track within one-two degrees longitude, which suggested that the upper vortex was being decoupled from the lower vortex. Since the lower vortex was now being steered by the low-level environmental flow, the model predicted a slower and more equatorward track. Carr and Elsberry (2000b) indicated a slow bias once the TC was sheared, but a change

from poleward to equatorward flow of the lower vortex was not noted. This reversal will be illustrated further in the following case study.

c. Case Study

The track forecasts for TC Meari (25W) of 0600 UTC 26 September 2004 have a large spread about the consensus mean with forecast TC positions that imply tracks in all four quadrants of the compass (Figure 34a). The NOGAPS track forecast (Figure 34b) has a sudden reversal from poleward to equatorward flow just south of the Japanese Island of Kyushu, which may indicate E-RVS is a possible error. The GFDN and GFS models also have a reversal of track directions but both have a more arcing track. Post-analysis of the GFDN forecast fields (not shown) indicated the vertical structure of the TC remained intact and the cause of direction reversal was I-MCG. Insufficient trough development in GFDN caused the TC to not be captured by the passing trough and the track of the TC was eventually determined by the steering flow of an approaching midlatitude anticyclone (not shown). It is suspected that the UKMO forecast track was also affected by E-RVS, but no forecast fields were available to investigate further.

The NOGAPS 700-mb geopotential heights forecast fields illustrate that by 72 h the vertical structure of the TC is less deep than in reality (Figure 35, rows 1 and 2, column 2; note fewer concentric isopleths and smaller horizontal scale of the TC). By 96 h, only one closed isopleth is predicted at 700 mb, and it lags behind the midlatitude trough (Figure 36, row 1, column 1). The corresponding 850 mb geopotential heights indicate the TC is coherent with the 700 mb position (not shown). The verifying 96-h analysis shows the TC has actually strengthened even though it is interacting with the midlatitude trough and tracking to the northeast (Figure 36, row 2, column 1). At 120 h, the TC is no longer resolved in the NOGAPS 700-mb field (Figure 36, row 1, column 2). An inspection of the 850-mb streamlines (not shown) from 84 h - 120 h indicates the low-level vortex is embedded in the flow of an approaching anticyclone while the 500-mb streamlines indicate the upper and lower vortex have separated as the 500-mb vortex is displaced to the northeast in the flow of the midlatitude trough.

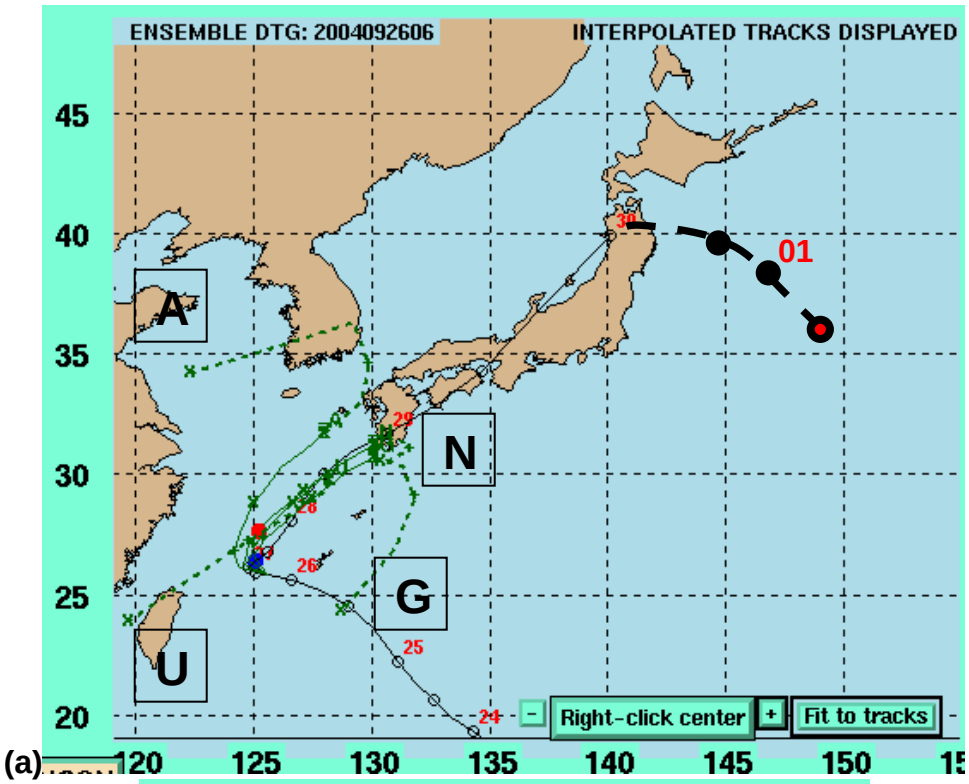

(a)

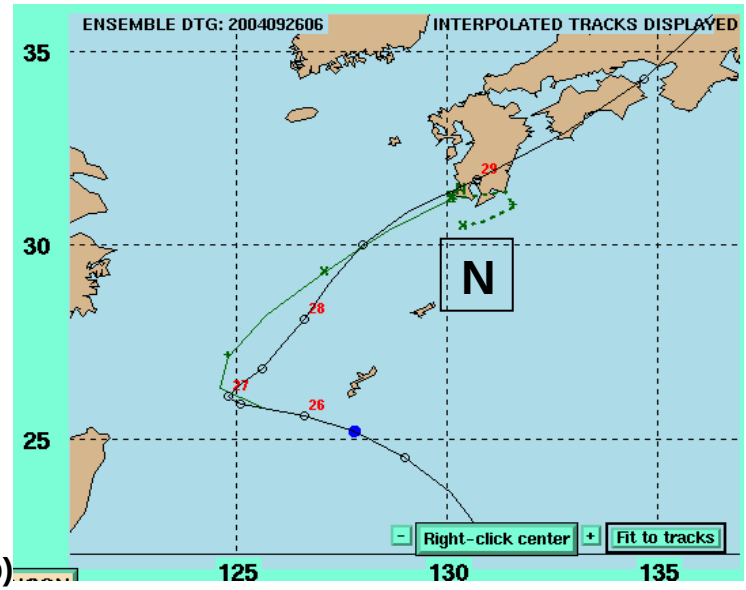

(b)

Figure 34. (a)Interpolated forecast tracks for 25W by NOGAPS (N), GFDN (G), UKMO (U), and GFS (A) for the forecast of 0600 UTC 26 September 2004. The figure legends are the same as those listed in Figure 23. (b) Expanded map of only the NOGAPS forecast track is provided for clarity.

In summary, it is acknowledged that time constraints created by warning schedules and multiple active TCs might not allow the forecaster the

luxury of examining each level previously described. The forecaster can take heed that a reversal in direction of the TC within a few degree longitude can be a clue that the model is suffering from E-RVS. Subsequent inspection of the geopotential height fields could then provide further evidence that the upper levels of the TC are being sheared from the lower levels, as indicated by diminishing numbers of concentric geopotential isopleths at the given isobaric surface. The proper identification and removal of the NOGAPS track forecast displaying E-RVS could then provide a selective CONW that is more accurate than CONW. However, in the 0600 UTC 26 September 2004 forecast for TC Meari, all four forecast TC tracks are outliers and therefore eliminating NOGAPS would go against the rules set forth in SAFA.

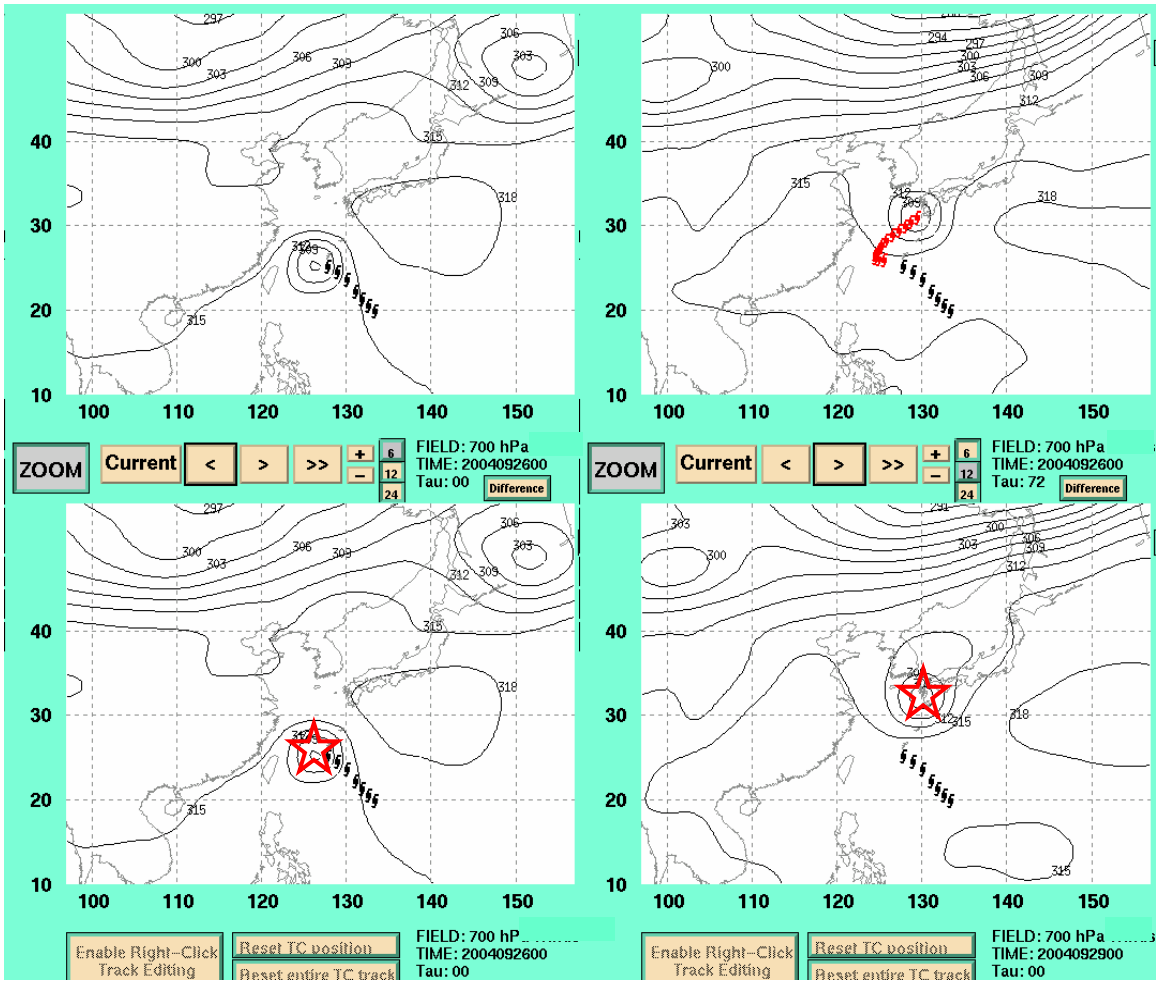

Figure 35. Initial analysis and forecast of 700-mb geopotential height fields for 25W by NOGAPS (row 1) and verifying NOGAPS analyses (row 2) for the forecast of 0000 UTC 26 September 2004. Note: GFDN fields are not included due to lack of archived geopotential height fields. Verifying TC position indicated by red star.

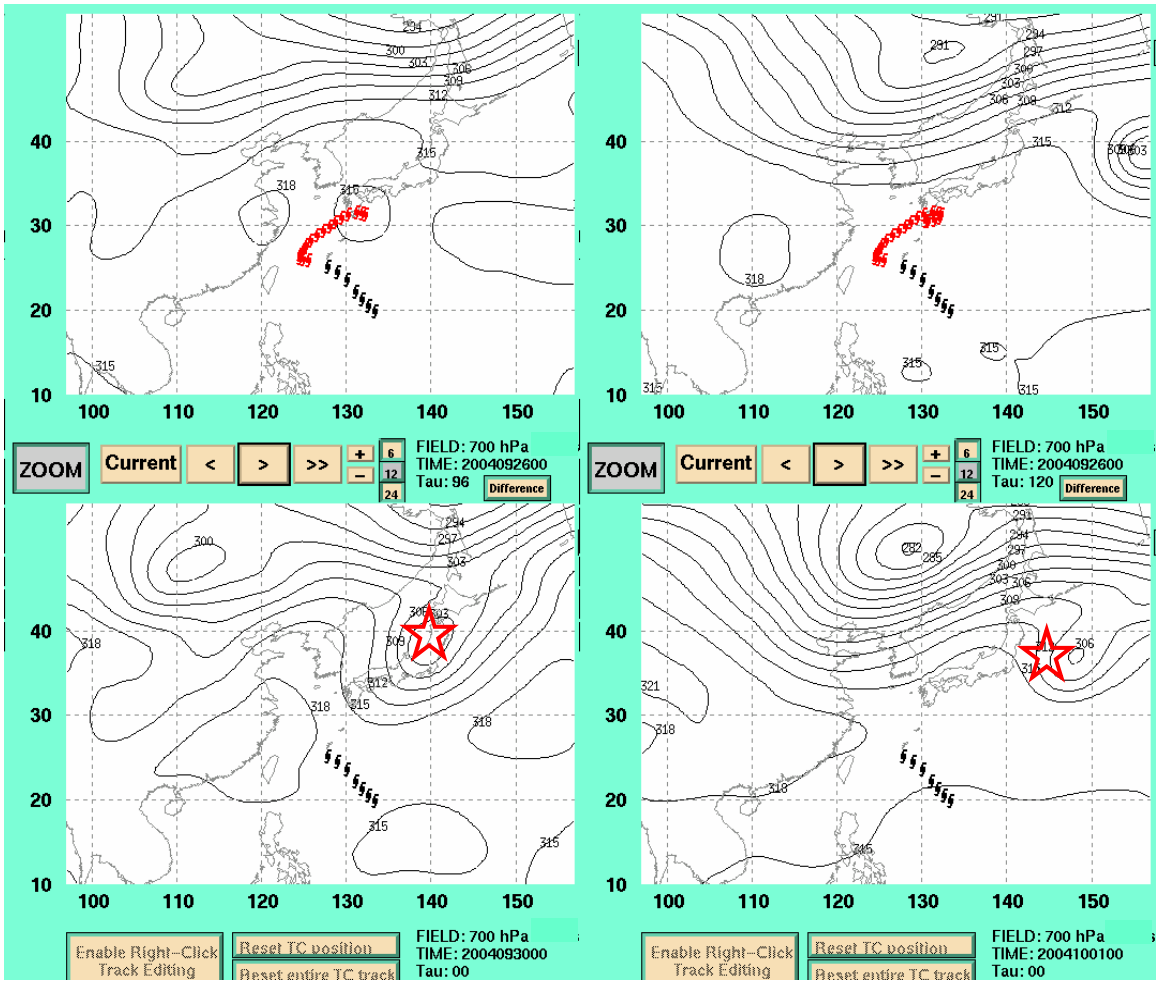

Figure 36. Forecast of 700-mb geopotential height fields for 25W by NOGAPS (row 1) and verifying NOGAPS analysis (row 2) for the forecast of 0000 UTC of 26 September 2004. First (second) column illustrates the 96-h (120-h) forecast fields. Note: GFDN fields are not included due to lack of archived geopotential height fields. Verifying TC position indicated by red star.

THIS PAGE INTENTIONALLY LEFT BLANK

IV. SUMMARY AND CONCLUSIONS

A. SUMMARY

The objective of this study was the extension of the error mechanism conceptual models (Carr and Elsberry 2000a,b) from 72 h to 120 h for NOGAPS and GFDN. This extension was achieved through an in-depth retrospective analysis of tropical cyclone track forecasts over the western North Pacific Ocean to identify characteristic tropical and midlatitude wind, sea-level pressure, and geopotential height patterns that were associated with large 120-h model track errors. Conceptual models of these 120-h model error characteristics were then integrated into known 72-h error mechanisms and case studies of frequently occurring 120-h large-errors were then given to highlight identification techniques that forecasters may use in considering elimination of model tracks from the consensus.

The approach was to first identify and analyze cases in which large track errors (300 n mi at 72, 400 n mi at 96 h, or 500 n mi at 120 h) occurred in NOGAPS and GFDN in the western North Pacific during 2004 (Figures 3 and 4). Of the four dynamical models available to 120 h, only these two model analyses and forecasts were available in entirety to search for explanations of large track errors.

In addition to the standard JTWC evaluations of 120-h track errors, this study maximized the number of 120-h forecast verifications for both NOGAPS and GFDN by manually extending the best-track positions beyond the point of extratropical declaration using mean sea-level pressure analyses. This extension was considered valid since the hazards associated with the wind, precipitation, and waves accompanying a TC do not suddenly diminish at the time it is declared extratropical. By following these procedures, an increase of nearly 28% (24%) in large 120-h forecast errors was realized for NOGAPS (GFDN) (Table 2).

In the 2004 season, a total of 354 (422) 120-h (96-h) NOGAPS forecasts were made in the western North Pacific. For GFDN in the same year, 262 (318) 120-h (96-h) forecasts were available for the same basin (Table 2). Of those forecasts, 162 (135) cases for NOGAPS (GFDN) had a large forecast error at 72, 96, and/or 120 h. To identify the causes of these large errors, both the predicted and verifying analysis fields of the winds and geopotential heights at 200, 500, 700, and 850 mb and the mean sea-level pressures were utilized. The geopotential heights from 850 through 500 mb were found to be most beneficial in diagnosing the cause of the large track forecast error when midlatitude synoptic features were affecting the steering current for the TC. If vertical wind shear effects were suspected of causing the error, the vector difference in winds between 500 mb and 850 mb as well as the 200 mb was vital. When a large TC was actively contributing to its propagation, the mean sea-level pressure fields were found to be most effective in detecting the cause of the error.

The retrospective analysis of the 2004 season found that the conceptual error mechanisms that affect tropical cyclone 120-h track forecasts were classified into two categories: i) large track errors due to tropical influences; and ii) large track errors due to midlatitude influences. Large track error mechanisms due to tropical influences were Direct Cyclone Interaction – tropical (DCI-t), Reverse-oriented monsoon Trough Formation (RTF) and Beta Effect Propagation (BEP). Those error mechanisms due to midlatitude influences were Direct Cyclone Interaction – midlatitude (DCI-m), Response to Vertical Wind Shear (RVS), Baroclinic Cyclone Interaction (BCI), Midlatitude Cyclogenesis (MCG), Midlatitude Cyclolysis (MCL), Midlatitude Anticyclogenesis (MAG), and Midlatitude Anticyclolysis (MAL). A slight departure was made from the conceptual error mechanisms outlined by Carr and Elsberry (2000a, b) to delineate DCI occurring in the tropics from those occurring in the midlatitudes. While the physical process of the two was the same, the large track errors associated with E-DCI-m were twice as large as those due to E-DCI-t.

The NOGAPS (GFDN) forecasts were affected by tropical influences in 25 of 162 or 15% (14 of 135 or 10%) of large-error cases at 72 h, 96 h, and/or 120 h

and by midlatitude influences in 121 of 162 or 75% (95 of 135 or 70%) of its large-error cases (Table 3). As expected, these percentages indicated that the proper prediction of the amplitude, scales, and transition of midlatitude synoptic features is a critical component to 120-h TC track forecasting.

The tropical error mechanisms that occurred with the most frequency were E-DCI-t and E-RTF, which accounted for 31 and 3 track errors, respectively (Table 3). However, E-RTF was frequently a secondary error mechanism in an additional 25 model integrations by both NOGAPS and GFDN and was therefore worthy of a case study in this analysis.

The indications of E-DCI-t or E-RTF affecting model tracks to 120 h during the 2004 season were similar to the Carr and Elsberry (2000a, b) analysis of the 1997 season. The indications of E-DCI-t included: (i) CCW rotation of the eastern (western) TC around the adjacent western (eastern) TC; (ii) sudden changes in the temporal progression during the 120-h forecast period; (iii) the western circulation slowed while the eastern circulation accelerated; (iii) formation of a reverse-oriented monsoon trough in the later stage of the forecast as the peripheral anticyclones of the two circulations merged with the subtropical ridge; and (iv) occasional merger of a weak circulation rotating CCW around a much stronger circulation. Another key finding in the analysis of E-DCI-t was that actual exaggeration of a naturally occurring DCI event was never observed. All 31 cases of E-DCI-t in both NOGAPS and GFDN were false representations. The key factors indicating E-RTF was occurring in the model during the 2004 analysis were: (i) rapid simultaneous amplification of the peripheral anticyclone to the southeast of two east-west oriented TCs or cyclonic circulations; and (ii) a premature transition from Standard to Poleward pattern. This transition is readily apparent in the track of the western TC/circulation compared to the eastern TC/circulation.

The I-BEP error mechanism, while not occurring with great frequency in 2004, was presented as a case study due to the tendency in the NOGAPS model to under-predict the intensity and horizontal extent of tropical storms during the

2004 season. This too small horizontal extent is the root of the dynamics that causes the I-BEP error mechanism.

Those error mechanisms due to midlatitude influences accounted for 121 of 162 or 75% (96 of 135 or 71%) of all large errors in the NOGAPS (GFDN) model during the 2004 western North Pacific typhoon season. Those error mechanisms that occurred with the most frequency were E-DCI-m, E-RVS, E-MCG, I-MCG, E-MCL and E-MAG, which accounted for 68% of all large errors occurring in both NOGAPS and GFDN models.

Every occurrence of E-DCI-m during the 2004 season resulted from a false interaction of a TC with a strong midlatitude cyclone to the northwest. While the key indicators of E-DCI-m are the same as those of E-DCI-t, an additional feature to cue the forecaster is a direction change in the track forecast from northeastward to northwestward while the TC is under the influence of Midlatitude/Poleward Flow. As in the E-DCI-t, there were no occurrences of an exaggeration of an actual DCI event between a TC and deep midlatitude cyclone. The forecaster is therefore justified in omitting the model displaying E-DCI-m from CONW.

The obvious conclusion that can be drawn for MSE events is that both NOGAPS and GFDN had significant problems both in the development and movement of midlatitude troughs. It is beneficial for the forecaster to know that once the NOGAPS and/or GFDN model started displaying either E-MCG or I-MCG, it normally occurred in successive model integrations and would not switch from excessive to insufficient or visa versa without first correcting the problem in an intermediate integration. That is, the error mechanism would end for at least one model integration before switching to the other variation of the error mechanism.

To draw a more generalized conclusion of the MSE tendencies of NOGAPS and GFDN, the data in Table 7 are divided into two distinct groups. The first group is comprised of I-MCG, E-MCL, E-MAG, and I-MAL events, which are all representative of erroneously predicted environmental flow that is

dominated by a ridge. The second group is comprised of E-MCG, I-MCL, I-MAG, and E-MAL events, which are all represented of erroneously predicted environmental flow that is dominated by a trough. These results suggest that regarding MSE events in NOGAPS, they were one-sided in that while the model was indicating the environmental flow of the TC would be dominated by the ridge (Table 8), it was revealed in the retrospective study to be dominated in reality by a trough. Unfortunately, a similar conclusion cannot be drawn for GFDN as the MSE events in GFDN were two-sided. That is, there were a large number of excessive and insufficient MSE events in GFDN (Table 7).

The case study identifying E-RVS was acknowledged as being more in-depth than what the time constraints created by the warning schedule and multiple active TCs might allow the forecaster. However, the reversal in direction of the TC within a few degrees longitude was offered as a diagnostic clue to quickly identify E-RVS occurring in the model. The subsequent inspection of the geopotential height fields could then provide further evidence that the upper levels of the TC were being sheared from the lower levels, as indicated by a decrease in the number of concentric geopotential isopleths at the given isobaric surface.

These conceptual models were presented so that the proper identification and removal of the model track forecast displaying a conceptual error mechanism could provide a selective CONW that is more accurate than CONW. As outlined in Carr and Elsberry (2000a, b), this would require the availability and the capability to display the analysis and forecast fields from the model. Such tools that could accommodate these requirements are SAFA and ATCF software programs. Application of the conceptual models presented and the symptoms to detect the potential error require either the streamlines/isotachs, the sea-level pressures, or the geopotential heights. A universal symptom indicating the presence of a systematic error mechanism in the model is the sudden deviation from the previous track guidance, which can be easily detected by examining a sequence of past track forecasts relative to the actual track. When a significant

deviation occurs, it should alert the forecaster to search for the cause. Such a deviation is especially noteworthy if it is also a track outlier from the other guidance.

Removing even one of the four 120-h model tracks that comprise CONW does raise concerns about the accuracy of the remaining three-model consensus. In a 2002 report from JTWC, it is noted that the consensus forecasts were more accurate if more than three track forecasts were available (Jeffries and Fukada 2002). Even so, a dilemma with CONW occurs when one of the four 120-h models has a highly erroneous track, which may cause the consensus to be seriously degraded. Therefore the potential exists to improve upon CONW by eliminating the positively identified erroneous track through the conceptual error models outlined in this study.

B. FUTURE RESEARCH

The first step to further extending the 120-h conceptual error mechanisms is to obtain a complete set of analyses and forecasts for the other two 120-h models that comprise CONW: the GFS and UKMO models. It is believed that the analysis of these two models will further validate the 120-h conceptual error mechanisms found in this study, because when the NOGAPS or GFDN tracks were outliers, they were often accompanied by the GFS and/or UKMO tracks.

Another item of interest is to investigate and compare the accuracy of CONW to a selective consensus (S-CONW) that would be derived by applying the new summary of 120-h error mechanisms. If the source of this error could be reliably identified using these 120-h conceptual models, the subsequent elimination of this highly erroneous track from CONW to create S-CONW could provide a marked improvement to the official track forecast, even though that would have reduced the number of models below the desired threshold of four models in the consensus defined as accurate by Jeffries and Fukada (2002). Ultimately, the use of S-CONW would allow the forecaster in those cases to add value to a forecast essentially based on CONW. Looking forward, S-CONW

would be beneficial in probability forecasts by removing an erroneous track that would cause the probability area to be wider than a non-selective consensus would.

Given the CONW forecast tracks, a S-CONW can be derived by removing the identified large-error track forecast from the consensus. The procedure would be to apply the newly defined 120-h error mechanisms in all cases in which one can confidently identify the source of the large error and then eliminate that erroneous track from CONW. Even though this error mechanism is applied retrospectively, this S-CONW could indicate the potential improvement to the official track forecast.

Because of the two-sided errors MCG in GFDN, no further conclusions could be drawn as to systematic biases of the GFDN model always over- or under-predicting the amplitude or translation of the midlatitude features. This was true when comparing events occurring with an individual model and even concurrent events between NOGAPS and GFDN. Although a seasonal pattern was also examined, again no pattern was found. A major change in the convective momentum flux parameter in the NOGAPS Emanuel parameterization scheme was made on 8 September 2004 (J. Goerss, NRL—Monterey, personal communication), but the impact of this change in convective momentum flux did not lead to any obvious track error differences for western North Pacific TCs. Thus, a more in-depth study of just the combined total of the 174 falsely predicted events by NOGAPS and GFDN (Table 8) is needed to discover the underlying causes of the errors.

THIS PAGE INTENTIONALLY LEFT BLANK

APPENDIX

The following is extracted from the 2002 masters thesis by R. A. Spollen.

A. ENVIRONMENT STRUCTURE

Environment structure is used in the Systematic Approach to describe the general environmental synoptic features related to tropical cyclone motion, such as the subtropical ridge, monsoon trough, and midlatitude flow. The environment structure is then divided into synoptic patterns and synoptic regions. A synoptic pattern describes the orientation of the dominant cyclones and anticyclones relative to the tropical cyclone. The synoptic region describes the position of the TC in relation to the predominant flow regime within the pattern. A pattern and region combination then defines the environment structure that is the first-order effect on tropical cyclone motion. Prior studies have demonstrated that each pattern/region combination has a characteristic track orientation, and each transition from one pattern/region combination to another implies a corresponding track change. Carr and Elsberry (1999), Boothe (1997), Boothe et al. (2000), and Reader et al. (1999) have identified three common patterns (Standard, Poleward, and Midlatitude – in Figure 37 to be described below) that exist in the western North Pacific, central and eastern North Pacific, Atlantic, and Southern Hemisphere Oceans, respectively.

1. Standard Pattern

The Standard (S) pattern (Figure 37) is the most common synoptic pattern that occurs 60%, 84%, 48%, 64%, and 35% of the time in the western North Pacific, eastern/central North Pacific, Atlantic, South Indian and South Pacific Oceans, respectively (Figure 38). The S pattern is characterized by two extensions of a predominantly zonal subtropical anticyclone with equatorial buffer cells (cyclonic or anticyclonic) to the south (north) in the Northern (Southern) Hemisphere. When an equatorial or monsoon trough is at least 8-10 deg. latitude from the equator, equatorial westerlies occur between the monsoon trough and the buffer cells. Between the monsoon trough and subtropical anticyclone are the

tradewind easterlies. The S pattern contains four synoptic regions where the TC motion is determined by the predominant flow around the subtropical anticyclone and the equatorial or monsoon trough. For example, the Tropical Easterlies (TE) region is south (north) of the subtropical anticyclone in the Northern (Southern) Hemisphere. Most TC tracks within this TE region are straight-runners moving westward, generally parallel to the subtropical ridge axis. In the Poleward Flow (PF) and Equatorward Flow (EF) synoptic regions of the S Pattern (Figure 34), the TC is being steered by the flow on the southwestern and southeastern (Northern Hemisphere) flanks of the subtropical anticyclone, respectively. The TC is moving toward (away from) a col between the subtropical anticyclone cells in the PF (EF) regions. The col may have been created as the anticyclone was weakened by advection of positive vorticity by the TC, by a midlatitude cyclone on the poleward side, or by a combination of both. Given these steering flows, the TC tracks tend to be toward the northwest in a PF region and toward the southwest in an EF region. At times, the TC track may have a “stair-step” characteristic in which westward motion in the TE region is followed by poleward motion in the PF region, and then a return to a more westward track after a transition to the EF region. Such a PF to EF transition will occur as the steering flow exerted by the eastern (western) subtropical anticyclone cell weakens (strengthens). Thus, the TC translation speed will decrease, and the TC may remain nearly stationary until the western subtropical anticyclone gains steering control, which will then advect the TC toward the west-southwest.

As shown in Figure 37, equatorial westerlies occur with cross-equatorial flow in response to the displacement of the monsoon trough away from the equator. A TC in the Equatorial Westerlies (EW) region is then steered by the flow between the equatorial buffer cells and the monsoon trough. Tropical cyclones in this EW region tend to move eastward for only a short time in the Northern Hemisphere before they cross the monsoon trough axis and are advected toward the west by the tropical easterly flow. This is an example of an EW-to-TE region transition within the S pattern that exhibits a track change from eastward to westward motion.

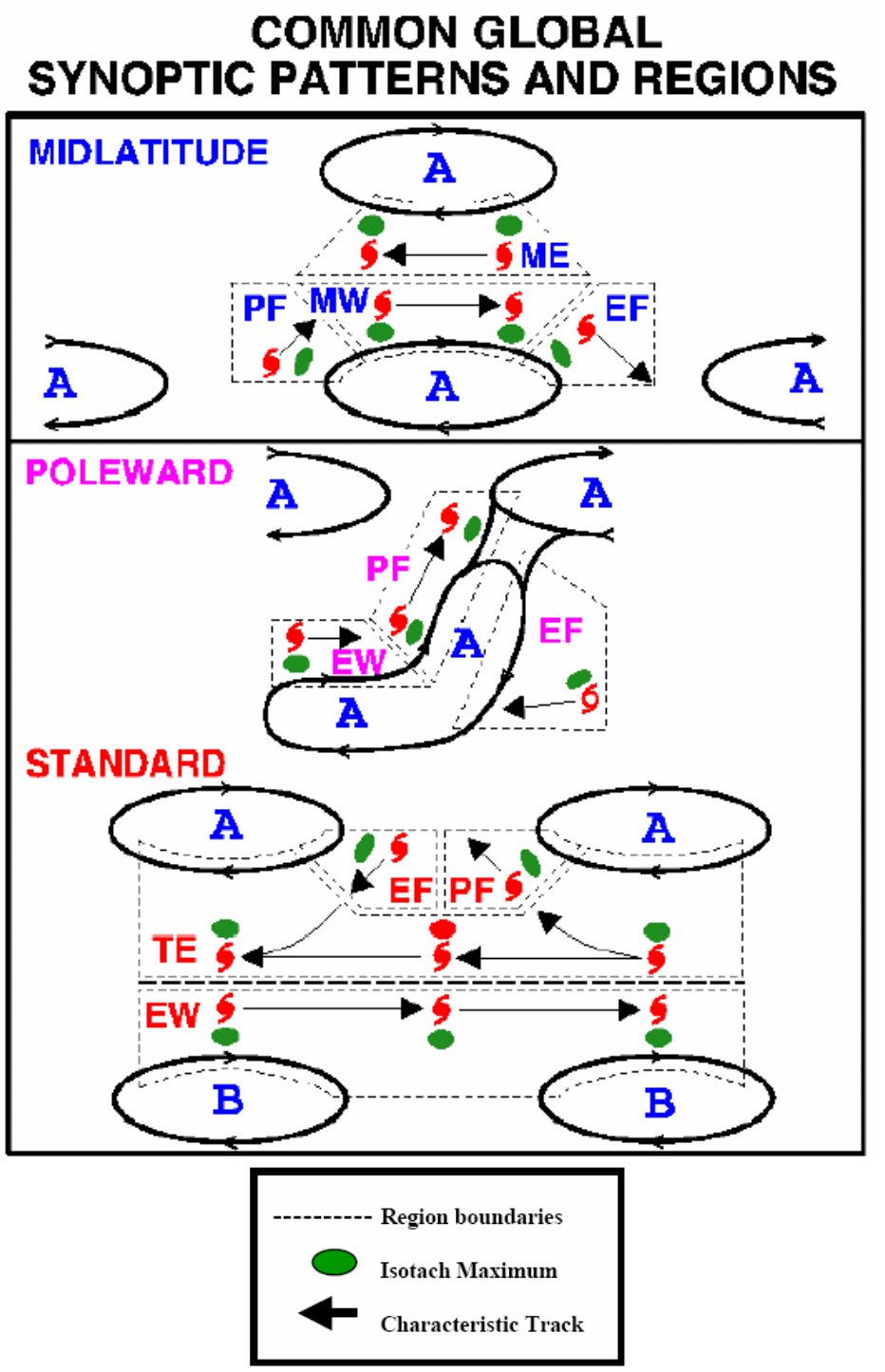

Figure 37. Common synoptic pattern and region conceptual models in the Systematic Approach TC Motion Meteorology Knowledge Base for tropical cyclone basins relative to adjacent anticyclones (A) and buffer (B) circulations. Key to region abbreviations: EW = equatorial westerlies; TE = tropical easterlies; PF = poleward flow; EF = equatorward flow; MW = midlatitude westerlies; ME = midlatitude easterlies (from Spollen 2002).

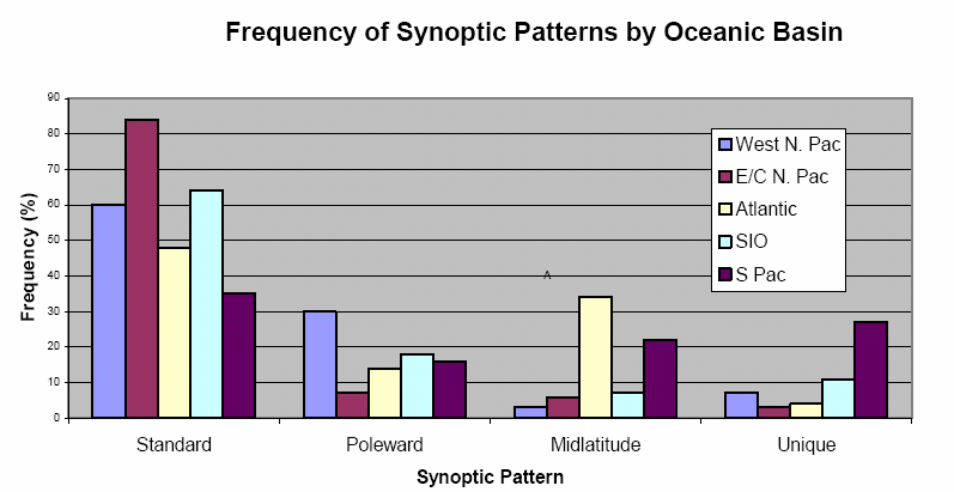

Figure 38. Frequency of occurrence for the common (Standard, Poleward, and Midlatitude) and the unique patterns in different tropical cyclone basins (from Spollen 2002).

2. Poleward Pattern

The second-most common synoptic pattern is the Poleward (P) pattern (Figure 38). This pattern is characterized by a meridionally-oriented trough/anticyclone, which typically forms as a result of Rossby wave dispersion from a large TC, but may also form with a "digging" midlatitude trough to the northwest (Northern Hemisphere). This P pattern is more common with the large TCs in the western North Pacific, whereas the smaller storms in the central and eastern North Pacific do not typically build a strong "peripheral anticyclone" via Rossby wave dispersion. When the peripheral anticyclone in this Rossby wake connects with the subtropical anticyclone, a TC moving westward in the TE region may have a sharp turn to a northwestward or north-northeastward track on the western side of the peripheral anticyclone. A TC in this region of the Poleward pattern is therefore in the Poleward Flow (PF) region. A TC in the Equatorial Westerlies (EW) region of the P pattern is often at a lower latitude and is steered by the westerly flow between the monsoon trough and the equatorial buffer cells. The typical transition from the EW region in the P pattern is into the PF region as the monsoon trough changes from an east-west orientation to a meridional orientation. The tropical cyclone then becomes steered by the flow between the poleward-oriented (or reverse-oriented) monsoon trough and the

peripheral anticyclone. As in the EW region of the S pattern, a TC typically remains in this (EW) region of the P pattern for only a short time before a transition occurs to another pattern/region. Thus, the track changes from eastward to north-northeastward, as long as the P pattern persists. When a second TC is present to the southeast of a Rossby wave train associated with a TC, the track of the second TC will be steered primarily by the northerly flow on the eastern side of the peripheral anticyclone. This region is thus termed the Equatorward Flow (EF) region. A TC in the EF region typically will experience a transition from a westward track (Northern Hemisphere) toward a more equatorward track as it comes under the steering influence of the southeastern flank of the peripheral anticyclone. However, this is a transient situation, and the tracks in the EF region of the P pattern tend to be short.

3. Midlatitude Pattern

The least frequent of the common patterns in every global region (Figure 38) is the Midlatitude (M) pattern. A TC is considered to have entered the M pattern once it has tracked poleward of the subtropical anticyclone axis. A TC typically is decreasing in intensity in this pattern because: (i) it is at higher latitudes, the sea-surface temperature drops, vertical shear of horizontal wind increases, and conditional instability decreases; and (ii) extratropical transition begins. In other words, the TC is nearing the end of its life cycle by the time it enters the midlatitude flow associated with this pattern. Four synoptic regions are associated with the M pattern. A typical track scenario is first in the PF region with a transition to the Midlatitude Westerlies (MW) region, and then perhaps to the EF region through simple advection of the TC around the poleward half of the subtropical anticyclone. The Midlatitude Easterlies (ME) region is formed when a midlatitude anticyclone is formed poleward of the subtropical anticyclone. A TC in the ME region is steered toward the west (Spollen 2002).

THIS PAGE INTENTIONALLY LEFT BLANK

LIST OF REFERENCES

Boothe, M.A., 1997: Extension of the Systematic Approach to Tropical Cyclone Track Forecasting in the eastern and central North Pacific. M.S. Thesis, Naval Postgraduate School, Monterey, CA 93943, 134 pp.

Boothe, M.A., R.L. Elsberry, L.E. Carr, III, 2000: Atlantic application of the Systematic Approach to Tropical Cyclone Track Forecasting: Part I: Environmental structure characteristics. NPS Tech. Rep. NPS-MR-00-003, Naval Postgraduate School, Monterey, CA 93943-5114, 77 pp.

Carr, L.E., III, and R.L. Elsberry, 1994: Systematic and Integrated Approach to Tropical Cyclone Forecasting. Part I. Approach, overview and description of meteorological basis. NPS Tech. Rep. NPS-MR-94-002, Naval Postgraduate School, Monterey, CA 93943-5114, 273 pp.

Carr, L.E., III, and R.L. Elsberry, 1997: Models of tropical cyclone wind distribution and beta-effect propagation for application to tropical cyclone track forecasting. *Mon. Wea. Rev*., **125**, 3190-3209.

Carr, L.E., III, and R.L. Elsberry, 1999: Systematic and Integrated Approach to Tropical Cyclone Track Forecasting. Part III: Traits Knowledge Base for JTWC Track Forecast Models in the Western North Pacific. Tech. Rep. NPS-MR-99-002, Naval Postgraduate School, Monterey, CA 93943-5114, 227 pp.

Carr, L.E., III, and R.L. Elsberry, 2000a: Dynamical tropical cyclone track forecast errors. Part I: Tropical region errors. *Wea. Forecasting,* **15**, 641-661.

Carr, L.E., III, and R.L. Elsberry, 2000b: Dynamical tropical cyclone track forecast errors. Part II: Midlatitude circulation influences. *Wea. Forecasting,* **15**, 662-681.

Carr, L.E., III, R.L. Elsberry, and J.E. Peak, 2001: Beta test of the systematic approach expert system prototype as a tropical cyclone track forecasting aid. *Wea. Forecasting,* **16**, 355-368.

Elsberry, R.L., and L.E. Carr, 2000: Consensus of dynamical tropical cyclone track forecasts — error versus spread. *Mon. Wea. Rev.*, **128**, 4131-4138.

Goerss, J., 2000: Tropical cyclone track forecasts using an ensemble of dynamical models. *Mon. Wea. Rev.*, **128**, 1187-1193.

Jeffries, R. A., and E.J. Fukada, 2002: Consensus approach to track forecasting. Paper TP3.2, *Extended Abstracts*, *Fifth International Workshop on Tropical Cyclones,* Cairns, Australia, World Meteorological Organization (Geneva).

Reader, G., M.A. Boothe, R.L. Elsberry, and L.E. Carr, III, 1999: Southern Hemisphere Application of the Systematic Approach to Tropical Cyclone Track Forecasting. Part III. Updated Environmental Structure Characteristics. Tech. Rep. NPS-MR-99-004, Naval Postgraduate School, Monterey, CA 93943-5114, 73 pp.

Spollen, R. A. 2002: Meteorological and model traits knowledge bases for North Indian Ocean tropical cyclones. M.S. thesis, Dept. of Meteorology, Naval Postgraduate School, 140 pp.

INITIAL DISTRIBUTION LIST

1. Defense Technical Information Center
   Ft. Belvoir, Virginia

2. Dudley Knox Library
   Naval Postgraduate School
   Monterey, California

3. Air Force Institute of Technology
   Wright-Patterson Air Force Base, OH

4. Director, Joint Typhoon Warning Center
   Naval Pacific Meteorology and Oceanography Center
   Pearl Harbor, Hawaii

5. Office of Naval Research
   Arlington, Virginia

6. R. L. Elsberry
   Naval Postgraduate School
   Monterey, California

7. M. A. Boothe
   Naval Postgraduate School
   Monterey, California

8. R. M. Kehoe
   Joint Typhoon Warning Center
   Pearl Harbor, Hawaii